TAMPEREEN TEKNILLINEN YLIOPISTO
TAMPERE UNIVERSITY OF TECHNOLOGY
Julkaisu 785 • Publication 785

Mikko Routimo

Developing a Voltage-Source Shunt Active Power Filter for Improving Power Quality

Tampere 2008

Tampereen teknillinen yliopisto. Julkaisu 785
Tampere University of Technology. Publication 785

Mikko Routimo

Developing a Voltage-Source Shunt Active Power Filter for Improving Power Quality

Thesis for the degree of Doctor of Technology to be presented with due permission for public examination and criticism in Rakennustalo Building, Auditorium RG202, at Tampere University of Technology, on the 12th of December 2008, at 12 noon.

Tampereen teknillinen yliopisto - Tampere University of Technology
Tampere 2008

ISBN 978-952-15-2085-3 (printed)
ISBN 978-952-15-2117-1 (PDF)
ISSN 1459-2045

Abstract

Active filters are controlled current or voltage sources that can be used, for example, to compensate current harmonics, interharmonics and reactive power. They offer a wide and/or selectable filtering bandwidth and they are small in size. In addition, active filters can solve almost all the problems that exist with conventional passive filters.

This thesis is concerned with developing a digitally controlled three-phase voltage-source shunt active power filter. First, the current compensation characteristic of the active power filter is studied and methods to improve this by compensating and minimizing effects caused by control system delays are investigated and proposed. Computational and prediction-based delay compensation methods are presented. Also, two methods in which the effect of the processing delay is eliminated by applying current-sensorless control and modified main circuit structure are proposed. Both the theoretical study and the experimental results presented show that all the studied methods provide effective compensation characteristics.

The use of the LCL-type supply filter in an active power filter is studied by comparing an active and a passive resonance damping method and by assessing the suitability of each for the active power filter application. The results presented show that both of the damping methods provide the fast dynamic responses required in using the active power filter as well as efficient current ripple attenuation. In addition, the results obtained show that the passive damping method increases the power losses only slightly. In contrast, the active damping requires several current sensors and more complicated control than the passively damped system.

The power loss profile of the active filter is determined and the effect of replacing the antiparallel silicon diodes in the IGBT bridge with their silicon carbide (SiC) counterparts is studied. The calculation and measurement results show that SiC diodes provide a reduction in the semiconductor power losses of the active filter. The reduction is important, since this would make it possible to reduce the cooling or to increase the switching frequency. The higher switching frequency would enable the use of smaller filter chokes.

A comparison of the digitally controlled and vector-modulated voltage-source and current-source active power filters is presented. The main circuit configurations and space-vector modulation techniques used are discussed as well as the load current detection -based control systems. In addition, the filtering characteristics, power loss distributions, and efficiencies of both systems are studied and compared in various operating points.

Finally, a case study in which a combined active and passive compensator is applied to mitigate the voltage flicker problem caused by a resistance spot welding process is presented. The compensation characteristic of the solution is considered comprehensively, using simulations and practical measurements. Furthermore, the resulting flicker severity indices are assessed. The results show that the compensator offers a great reduction of the voltage drops causing the flicker.

Preface

This work was carried out in the Institute of Power Electronics at Tampere University of Technology during the years 2002 – 2008. The research was funded by Tampere University of Technology, the Graduate School in Electrical Engineering, Tekes (Finnish Funding Agency for Technology and Innovations), the Academy of Finland, and industrial partners (Fingrid Oyj, Nokian Capacitors Oy, Paneliankosken Voima Oy, Ratahallintokeskus, Tampereen Sähköverkko Oy, Trafomic Oy, Verteco Oy). I am also very grateful for the financial support in the form of personal grants from Tekniikan edistämissäätiö (Finnish Foundation for Technology Promotion) and Ulla Tuomisen säätiö (the Ulla Tuominen foundation)

I express my gratitude to Professor Heikki Tuusa for supervising and guiding my thesis work and providing an excellent research environment. I am very grateful also to Dr. Mika Salo for his valuable guidance and ideas. In addition, I owe gratitude to Antti Mäkinen, Lic. Tech., for research co-operation in the flicker mitigation study. I thank also Technician Pentti Kivinen and Perttu Parkatti, M.Sc., for designing and implementing the calorimeter used in the power loss studies. I am very thankful to all colleagues at the Institute of Power Electronics during the years 2000 – 2008. Special thanks go to Dr. Matti Jussila and Dr. Tero Viitanen, for numerous constructive and fruitful conversations related to power electronics, but also to other topics. I thank also Juha Turunen, Lic. Tech., Dr. Matti Eskola, Jarno Alahuhtala, M.Sc., Panu Lauttamus, Lic. Tech., and Sami Pettersson, M.Sc., for their advice and friendship.

I am very thankful to J.D. Donoghue, who proofread my manuscript and made some improvements to the language. In addition, I thank Professor Frede Blaabjerg and Dr. Pekka Koponen for their constructive comments and for the pre-examination of this thesis.

Finally, I thank my parents for their encouragement and support in the past.

Espoo, October 2008

Mikko Routimo

Contents

List of Publications

This thesis consists of a summary and the following publications:

[P1] Routimo M., Salo M., Tuusa H. (2003) "A control delay compensation method for voltage source active power filter," *Proceedings of the Ninth European Power Quality Conference*, *PCIM 2003 Europe*, Nuremberg, Germany, May 20 – 22, pp. 93 – 97.

[P2] Routimo M., Salo M., Tuusa H. (2004) "A novel simple prediction based current reference generation method for an active power filter," *Proceedings of the IEEE 35th Annual Power Electronics Specialists Conference*, *PESC'04*, Aachen, Germany, June 20 – 25, vol. 4, pp. 3215 – 3220.

[P3] Routimo M., Salo M., Tuusa H. (2007) "Voltage-source active power filter with a current sensorless control," *International Review of Electrical Engineering (I.R.E.E.)*, vol. 2, no. 3, pp. 346 – 358, May-June 2007.

[P4] Routimo M., Salo M., Tuusa H. (2006) "Control method to improve the transient performance of a current sensorless active power filter," *Proceedings of the Nordic Workshop on Power and Industrial Electronics*, *NORPIE/2006*, Lund, Sweden, June 12 – 14, 6 p.

[P5] Routimo M., Tuusa H. (2007) "LCL type supply filter for active power filter – comparison of an active and a passive method for the resonance damping," *Proceedings of the IEEE 38th Annual Power Electronics Specialists Conference*, *PESC07*, Orlando, FL, USA, June 17 – 21, pp. 2939 – 2945.

[P6] Routimo M., Tuusa H. (2007) "Effect of SiC diodes on power losses of the voltage-source shunt active power filter," *International Review of Electrical Engineering (I.R.E.E.)*. vol. 2, no. 6, pp. 803 – 813, November-December 2007.

[P7] Routimo M., Salo M., Tuusa H. (2007) "Comparison of voltage-source and current-source shunt active power filters," *IEEE Transactions on Power Electronics*, vol. 22, no. 2, pp. 636 – 643, March 2007.

[P8] Routimo M., Mäkinen A., Salo M., Seesvuori R., Kiviranta J., Tuusa H., "Flicker mitigation with a hybrid compensator," *IEEE Transactions on Industry Applications*, vol. 44, no. 4, pp. 1227 – 1238, July-August 2008.

The Author has been the main author in all the Publications included. He has written all the Publications with help and guidance from Professor Heikki Tuusa. In Publications [P1] – [P4] and [P7] – [P8], help and guidance were also provided by Dr. Mika Salo, who also designed

and implemented the prototype of the current-source shunt active power filter used in Publication [P7]. The Author designed and implemented the prototypes of the voltage-source active filter, planned and conducted the tests, and analyzed the results presented in Publications [P1] – [P7].

Publication [P8] was written by the Author. Antti Mäkinen, Lic.Tech, performed flicker index calculations, wrote the text relating to flicker assessment, and helped in refining the final manuscript. The test setup was designed and the tests were planned by the Author in co-operation with Antti Mäkinen, Lic.Tech., Dr. Mika Salo, Reino Seesvuori, B.Sc, and Janne Kiviranta, M.Sc. The Author was responsible for modeling, simulations, measurements, and analysis.

Related Publications

The following publications relate to the topic, but are not included in the thesis:

[RP1] Routimo M., Salo M., Tuusa H. (2002) "Experimental results of a voltage source shunt active power filter," *Proceedings of the 2002 Nordic Workshop on Power and Industrial Electronics (NORPIE/2002)*, Stockholm, Sweden, August 12 – 14, 6 p.

[RP2] Routimo M., Salo M., Tuusa H. (2003) "A novel control method for wideband harmonic compensation," in *Proceedings of the Fifth IEEE International Conference on Power Electronics and Drive Systems (PEDS 2003)*, Singapore, November 17 – 20, pp. 799 – 804.

[RP3] Routimo M., Salo M., Tuusa H. (2004) "Wideband harmonic compensation with a voltage-source hybrid active power filter," in *Proceedings of the Nineteenth Annual IEEE Applied Power Electronics Conference and Exposition (APEC'04)*, Anaheim, CA, USA, February 22 – 26, vol. 1, pp. 191 – 196.

[RP4] Routimo M., Salo M., Tuusa H. (2004) "Improving the active power filter performance with a prediction based reference generation," in *Proceedings of the Nordic Workshop on Power and Industrial Electronics (NORPIE/2004)*, Trondheim, Norway, June 14 – 16, 6 p.

[RP5] Routimo M., Salo M., Tuusa H. (2005) "Current sensorless control of a voltage source active power filter," in *Proceedings of the 20th Annual IEEE Applied Power Electronics Conference and Exposition (APEC'05)*, Austin, Texas, USA, March 6 – 10, vol. 3, pp. 1696 – 1702.

[RP6] Pettersson S., Routimo M., Salo M., Tuusa H. (2006) "A simple prediction based current reference generation method for a four-wire active power filter," in

Proceedings of the 12th International Power Electronics and Motion Control Conference (EPE-PEMC 2006), Portorož, Slovenia, August 30 – September 1, pp. 1648 – 1653.

[RP7] Alahuhtala J., Virtakoivu J., Viitanen T., Routimo M., Tuusa H. (2007) "Space vector modulated and vector controlled Vienna I rectifier with active filter function," in *Proceedings of the Fourth Power Conversion Conference (PCC '07)*, Nagoya, Japan, April 2 – 5, pp. 62 – 68.

Symbols and Notations

Abbreviations

ac	alternating current
AD	analog to digital
APF	active power filter
CDC	control delay compensation
CSAPF	current-source active power filter
CT	current transformer
dc	direct current
DSP	digital signal processor
EMC	electromagnetic compatibility
EMI	electromagnetic interference
ESR	equivalent series resistance
FFT	fast Fourier transform
Filt.	filter
FPGA	field programmable gate array
GaAs	gallium arsenide
GaN	gallium nitrate
GTO	gate turn-off thyristor
IEC	International Electrotechnical Committee
IEEE	Institute of Electrical and Electronics Engineers
IEV	International Electrotechnical Vocabulary
IGBT	insulated gate bipolar transistor
LV	low voltage
MOSFET	metal-oxide-silicon field effect transistor
MV	medium voltage
pcc	point of common coupling
p.u.	per unit
PI	proportional-integral
PID	proportional-integral-derivative
PLL	phase-locked loop
PWM	pulse width modulation
RB-IGBT	reverse blocking IGBT
rms	root mean square
Si	silicon
SiC	silicon carbide
STATCOM	static synchronous compensator

THD	total harmonic distortion
TSC	thyristor switched capacitor
UPS	uninterruptible power supply
VSAPF	voltage-source active power filter

Symbols

$\underline{a}$	$e^{j2\pi/3}$
C	capacitance, capacitor
c	coefficient
e	error
G	transfer function
I	root mean square of current i
i	current
j	imaginary unit
k	discrete-time variable
L	inductance, inductor
m	variable
P	proportional gain
p	instantaneous power, positive integer
Plt	long-term flicker severity index
Pst	short-term flicker severity index
Q	fundamental three-phase reactive power
q	instantaneous imaginary power
R	resistance, resistor
sw	switching function
T	time period
t	time
U	root mean square of voltage u
u	voltage
x	arbitrary variable
Z	impedance
Δ	unit delay
φ	alignment angle of a space vector
ω	angular speed
θ_{fi}	alignment angle of the i^{th} switching vector
θ_s	alignment angle of the synchronous reference frame
θ_{ua}	angle of the phase-a voltage
τ	time constant, time variable

Subscripts

a, b, c	phase quantities
ac	ac circuit quantity, alternating quantity

ad	active damping
appr.	approximated
c	compensation, capacitor
cc	current control
CDC	control delay compensation
D	derivative
d	damping
d, q	real and imaginary components of a space vector in synchronous reference frame
dc	dc circuit quantity, dc quantity
f	active filter related quantity
ff	filter side quantity in the LCL filter
fs	supply side quantity in the LCL filter
f*i*	quantity relating to the switching vector *i*
h	harmonic, distortion
in	inflow
I	integration
L	filter-coil-related quantity
l	load-related quantity
LV	low voltage
max	maximum
meas	measured
mod	modified
MV	medium voltage
out	outflow
pd	passive damping
pred.	prediction
s	supply-related quantity
semic	semiconductor
sf	quantity related to the supply filter of the modified main circuit structure
sum	sum
sw	carrier
sync	synchronization
v	voltage
z	zero sequence component
1 – 6	serial numbers of switching states
0	fundamental frequency component in synchronous reference frame, zero state
α, β	real and imaginary components of a space vector in stationary reference frame
Δ	delay
+	upper switch in a phase
–	lower switch in a phase

Other Notations

$\underline{x}$	space vector
$\lvert\underline{x}\rvert$	length of the space vector
$\underline{x}^{s}$	space vector in synchronous reference frame
$\underline{x}^{*}$	complex conjugate of the space vector, reference vector
$\underline{x}_{(n)}$	n^{th} harmonic component of the space vector
$\mathrm{Re}\{\underline{x}\}$	real part of the space vector
$\mathrm{Im}\{\underline{x}\}$	imaginary part of the space vector
$x_{(x,y)}$	x_x and x_y
$\hat{x}$	magnitude of x
$X(s)$	Laplace transform of $x(t)$

1. Introduction

The generation and transmission of electrical energy usually take place at certain nominal voltage and frequency levels. However, utilization of the energy often relies on controlled voltage and/or frequency, and hence the interface between transmission and utilization requires power conversion. From the electrical transmission system point of view, devices such as power electronic circuitry used for power conversion can often be identified as non-linear loads. (Arrillaga and Watson, 2003)

In an ideal three-phase system, the phase-to-phase voltages are continuous single-frequency sine waves with a rated constant frequency and amplitude. Furthermore, the phase angles between the phase-to-phase voltages are equal and the phase order is as defined. Phase currents drawn by a non-linear load connected to ideal three-phase voltages via a transmission network are not sinusoidal but consist of various frequency components, i.e. harmonics and interharmonics. Harmonic is a sinusoidal component of a periodic wave and its frequency is an integral multiple of the fundamental frequency (IEEE Std. 519-1992, 1993), while interharmonic refers to any continuous signal element with a frequency which is not an integer multiple of the fundamental frequency (IEEE Interharmonic Task Force and the Cigré 36.05/CIRED 2 CC02 Voltage Quality Working Group, 1997; Halpin and Singhvi, 2007). Because of the network impedances, the distorted currents cause non-sinusoidal voltage drops and as a result the network voltages become distorted.

Examples of such non-linear elements causing distortion are power electronic converters, consumer electronics, electric arc furnaces, arc welders, and electric discharge lamps. In addition, transformers and motors may also cause distortion due to their non-ideal characteristics. Although non-linear loads have existed for decades, the number of them has increased substantially in the last decades. Not only the high-power industrial equipment but also the increased number of low-power consumer electronics cause severe current and voltage distortion. Although a single low-power application does not give rise to notable distortion compared to e.g. an electric arc furnace, several low-power devices operating simultaneously may cause a severe problem. Simultaneously with the increased number of power electronic systems connected to mains, the systems have also become more sensitive to supply voltage disturbances. (Bollen, 2000; Stones and Collinson, 2001; Arrillaga and Watson, 2003; Bendre et al., 2006)

Distorted voltages and currents have several harmful effects. For example, they may excite resonances between the supply network inductances and capacitances, leading to overcurrents and overvoltages. In motors and generators, harmonics and interharmonics cause additional losses, torque pulsations, or a reduction and variation in angular velocity. Since distortion

increases the effective current, also the losses in power transmission and distribution increase. In transformers, distorted currents cause heating and mechanical vibrations, which further lead to thermal and mechanical insulation stresses. Distortion reduces the accuracy of various measuring instruments and degrades the operating characteristics of power system protection, thus causing malfunctions and faults. In addition, communication system circuits and consumer electronics may be disturbed or damaged due to distortion. (Bollen, 2000; Arrillaga and Watson, 2003; Akagi et al., 2007a; IEEE Std. 519-1992, 1993)

Large, rapidly changing, or varying industrial loads, such as electric arc furnaces, welding machines, alternators, rolling mills, and motors may also give rise to supply voltage fluctuations (Ashmole and Amante, 1997; Zhang et al. 2001; Morcos and Gomez, 2002) which may further cause tripping of equipment. In some cases, a single tripping of equipment may require a complete restarting of the process, leading to interrupted production lasting for hours (Bendre et al., 2006). Voltage fluctuations may also give rise to significant illumination changes in lighting equipment (IEEE Std. 1453-2004, 2005). This "unsteadiness of visual sensation induced by a light stimulus whose luminance or spectral distribution fluctuates with time" as defined in International Electrotechnical Vocabulary (IEV 161-08-13) is called flicker. The frequency of the voltage fluctuations causing the flicker is much less than the supply frequency. However, the flicker phenomenon becomes annoying if it exceeds a certain threshold and the annoyance can increase very rapidly, depending on the amplitudes of the fluctuation.

1.1. Power Quality

The term power quality is commonly used to define interactions between power system and load (Bollen, 2000). However, there is no generally accepted definition for the term, and hence various definitions can be found in the literature. For example, the IEEE standard (IEEE Std. 100-2000, 2000) defines power quality as: "The concept of powering and grounding electronic equipment in a manner that is suitable to the operation of that equipment and compatible with the premise wiring system and other connected equipment." Instead, according to Heydt (1998), the definition is "...the provision of voltages and system design so that the user of electric power can utilize electric energy from the distribution system successfully, without interference or interruption. A broad definition of power quality borders on system reliability, dielectric selection in equipment and conductors, long-term outages, voltage unbalance in three-phase systems, power electronics and their interface with the electric power supply, and many other areas. Narrower definition focuses on issues of waveform distortion."

Issues similar to those in (Heydt, 1998) can be found in (Kazmierkowski et al., 2002): "Power quality is measured in terms of such things as line interruptions, sags, brown-outs, flicker, transients, phase unbalance, and distortion. For all devices in the grid there is a general issue of immunity and emission regarding all these power quality parameters." Kazmierkowski et

al. furthermore point out that the term power quality relates also to non-technical issues, such as business issues between distribution companies and end users.

Bollen (2000) summarizes terms related to interactions between power system and load: From the technical point of view *power quality* can be defined using *voltage quality* and *current quality*. Voltage quality concerns deviations from the ideal, continuous single-frequency sine wave with a rated constant frequency and amplitude. Correspondingly, current quality concerns the deviations from the ideal, single-frequency sine wave with a constant frequency and amplitude that is in phase with the supply voltage. Power quality is the result of the combination of the previous concepts. In addition, *electromagnetic compatibility* (EMC) has to do with mutual interaction between equipment and with interaction between equipment and supply. The non-technical aspects covering the interaction between the customer and the utility are included in the terms *quality of supply* and *quality of consumption*.

This thesis concentrates on power quality and the improving of power quality from the point of view of filtering current distortion [P1] – [P7]. In addition, a case study examining mitigation of interharmonics causing voltage flicker is presented [P8].

Standards for Current Harmonics

National and international organizations have set standards to limit current distortion in the power systems. For example, standard IEC 61000-3-2 specifies limits of current harmonic components produced by low-voltage equipment with rated current lower than 16 A, and standard IEC 61000-3-12 to low-voltage equipment with the rated current between 16 A and 75 A. Current distortion is discussed also in IEEE standard 519-1992, where limits for harmonics in general distribution and transmission systems are defined. IEC 61000-3-2 defines limits with absolute values, but IEC 61000-3-12 specifies relative values which depend on the ratio between the short-circuit power of the power system at the point of common coupling and the rated power of the equipment. The larger the ratio the higher are the harmonics allowed. The latter approach is used also in IEEE 519-1992, but instead of the ratio of the powers, the ratios between short-circuit currents and rated currents are defined.

For future, new standards and/or technical reports are currently being drafted. For example, will define limits for interharmonics (IEC 61000-3-9) and emission limits for frequency range 2 – 9 kHz (IEC 61000-3-10) will apply to equipment with input current lower than 16 A. In addition, IEC 61000-3-14 will assess emission limits for the connection of disturbing installations to low-voltage power systems.

1.2. Solutions to Harmonics-Related Problems

Voltage and current distortions have been problems in power system design from the beginning of ac transmission (Arrillaga and Watson, 2003). Owen (1998), for example, mentions that a harmonics-related motor problem was reported as early as 1893 and that the first long-distance electric power transmission system was installed at Portland, Oregon,

USA, in 1890. Conventional solutions for reducing current harmonic distortion have been passive shunt filters consisting of one or more tuned LC circuits. Their operating principle is to prevent harmonics from propagating to the supply network by providing low impedance paths for the current harmonics. However, the filtering characteristics of passive filters are dependent on the ratio between the source and the filter impedances. If the source impedance is not accurately known or it varies depending on the system configuration, this affects considerably the characteristics of the shunt filter. Harmonics from the source may flow into the passive shunt filter and in the worst case the passive filter falls in series resonance with the source impedance. Furthermore, the parallel resonance circuit formed by the passive filter and other system impedances may cause amplification of harmonic currents. In addition, several capacitors or filters installed in the same distribution system may cause detuning of the passive filters. After installation, passive filters are rigidly in place and neither the tuned frequency nor the size of the filter can easily be changed. (Akagi, 1994; Das, 2004)

A new method for eliminating harmonic currents was proposed in the 1970's. The idea was to compensate the harmonics actively by means of power amplifier. In 1971, Sasaki and Machida proposed the compensator shown in Fig. 1.1. The principle of the proposed system was to detect harmonics in a transformer secondary current and to draw the harmonics in opposite phases with the compensator. Consequently, the currents drawn from the mains are sinusoidal. The compensator was connected in parallel with the load and this was done using transformer tertiary winding. The authors presented operating principles and a detailed analysis of the constraints regarding the harmonic current detection circuit (denoted as 'Filt.' in Fig. 1.1) and the amplifier producing the compensating current. Several years later, in 1974, Sasaki and Machida proposed a further improved control system and presented simulation results concerning the harmonic cancellation characteristics in the case of changing load (Sasaki and Machida, 1974).

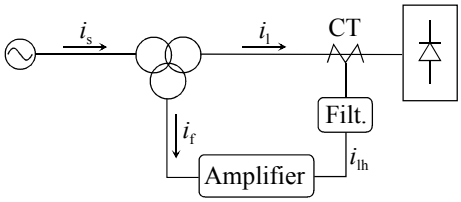

Fig. 1.1. Harmonic current compensator (Sasaki and Machida, 1971).

Gyugyi and Strycula (1976) proposed various topologies for active harmonic compensation. Their concepts were based on pulse-width-modulated inverters using power transistors and the proposed systems were named *active power filters*. Figure 1.2(a) – (d) shows the practical circuit realizations they proposed. The shunt ripple current generator presented in Fig. 1.2(a) supplies harmonic currents needed by the load. An externally identical filter is shown in Fig. 1.2(b), which operates as a fundamental voltage generator and through this the load current harmonics circulate. In contrast, circuit configurations shown in Fig. 1.2(c) and (d) are connected in series with the supply and they are used to filter the supply voltage harmonics. Moreover, Gyugyi and Strycula presented measurement results obtained with the laboratory model of the circuit shown in Fig. 1.2(a).

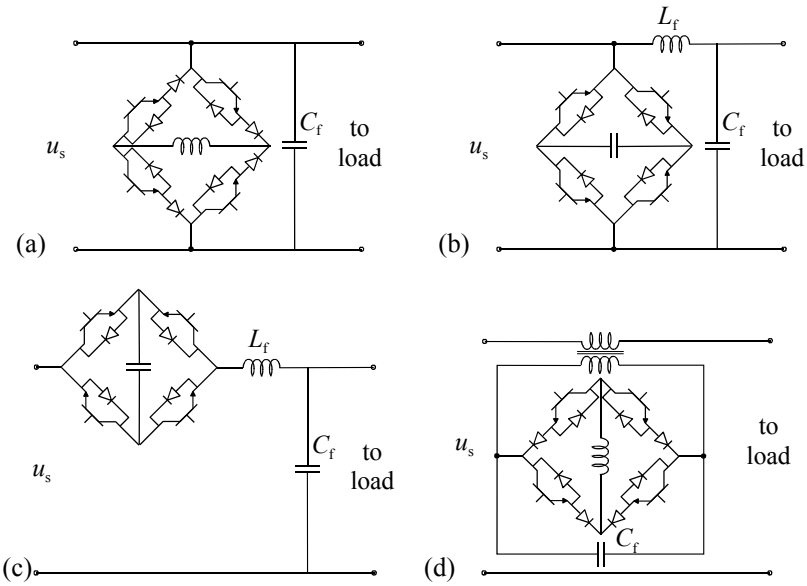

Fig. 1.2. Active power filter circuits proposed by Gyugyi and Strycula (1976). (a) Shunt ripple current generator. (b) Shunt fundamental voltage generator. (c) Series ripple voltage generator. (d) Series ripple voltage generator using ripple current generator.

In 1976, also Harashima et al. proposed a control system for reducing instantaneously both reactive and harmonic current components in single-phase circuits. The compensator used was called a "regulated reactive power source" and this was connected in parallel with the load as illustrated in Fig. 1.3. The proposed control system was based on calculating so-called instantaneous reactive power that consisted of harmonic current components and the displacement of fundamental current component. The authors presented also some experimental results obtained.

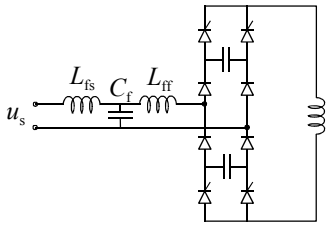

Fig. 1.3. Compensator for harmonics and fundamental reactive power (Harashima et al., 1976).

Although the principles for active filters were developed in the 1970's, they remained at the laboratory level until the 1980's, because power semiconductor device technology did not make practical implementations possible. According to Akagi (1994), the first shunt active conditioner was put into practical use for harmonic compensation in 1982. The compensator was rated for 800 kVA and it consisted of current-source inverters using GTO thyristors. Since the 1980's, improvements in power semiconductor devices, microprocessors, and digital signal processors have spurred also research and development in active power filters. Development has made it possible to implement active power filters at higher power levels and with higher switching frequencies than before. Nowadays, active power filters are in commercial operation. The main circuit is commonly implemented using voltage-source topology (Akagi et al., 1984; Akagi et al. 2007), shown in Fig. 1.4(a), but the use of current-

source topology shown in Fig. 1.4(b) is also possible (Kawahira et al., 1983; Choe and Park, 1988; Itoh and Fukuda, 1988; Hayashi et al., 1991; Salo, 2002).

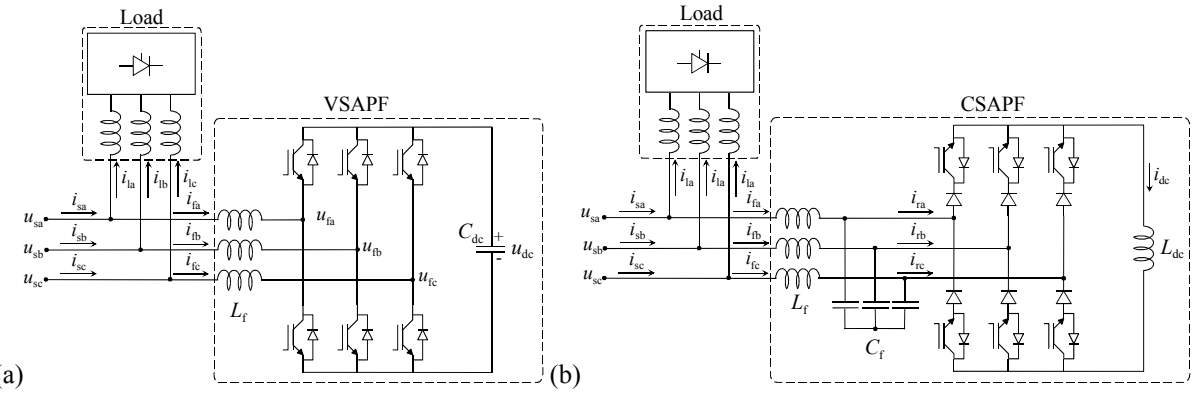

Fig. 1.4. Main circuit of a three-phase (a) voltage-source shunt active power filter and (b) current-source shunt active power filter.

A shunt active power filter can be used to compensate load current harmonics and interharmonics, but also to operate as a fundamental reactive power compensator or generator, see e.g. (Akagi et al., 1984; Takeda et al. 1988). In addition, it is possible to attenuate harmonic resonances and to mitigate system voltage disturbances, see e.g. (Akagi et al., 1999; Bongiorno and Svensson, 2007). Features depend on the compensation strategy selected.

Algorithms for extracting distorting components and generation of the active filter compensating reference have been popular topics in research, and various methods have been proposed and analyzed over the years. The methods can be divided into time and frequency domain methods (Grady et al., 1990; González et al., 2007). The first group consists of instantaneous reactive power theory or ‘pq-theory’ based methods, presented e.g. by Akagi et al. (1984), Itoh and Fukuda (1988), and Chaoui et al. (2007), of rotating reference frame methods, presented e.g. by Takeda et al. (1987), Xie et al. (2006), Tong et al. (2007), and Wang et al., (2007), and of stationary frame methods utilizing different filters, such as a notch-filter (Newman et al., 2002), or optimization technique, see e.g. (George and Agarwal, 2007). The other group consists basically of various Fourier transformation based methods, see e.g. (Williams and Hoft, 1991; Huaijun et al., 2005; Sozanski and Jarnut, 2005; Borisov et al., 2007; González et al., 2007), but also include the wavelet approach (Liu et al., 2006). Also, methods utilizing neural network have been proposed, see e.g. (Pecharanin et al., 1994; Nishida et al., 2005; Nascimento et al., 2007). Various previously published reference generation methods and their characteristics have been analyzed and compared, e.g. by Maza Ortega et al. (2005) and Asiminoaei et al. (2007b).

Conventional control methods used with the active filters rely on hysteresis control, as in (Akagi et al., 1984), on linear PI or PID control, see e.g. (Mendalek et al., 2000), or on variations of them, see e.g. (Malesani et al., 1996; Newman et al., 2002). Other possibilities have also been proposed, for example dead-beat current control (Malesani et al., 1998a;

Malesani et al. 1999; Mattavelli, 2001), predictive control (Mendalek et al. 2002b), repetitive control (Mattavelli and Marafão, 2004; García-Cerrada et al., 2007; Griño et al. 2007), sliding mode control (Radulovic and Sabanovic, 1994; Saetieo et al., 1995; Mendalek et al., 2002a), robust control (Marconi et al., 2003; Bajnica and Naunin, 2005), and fuzzy control (Dixon et al., 1999).

In addition to research efforts connected with the control issues in recent years, various active filter topologies have also been examined and proposed. For example, active filtering function applied to the operation and control of a three-phase voltage-source line-converter is examined e.g. in (Cichowlas et al., 2005; Tarkiainen, 2005), topology consisting of two shunt active filters connected in parallel in (Asiminoaei et al., 2007a), and a hybrid filter that is connected in series with a passive shunt filter in (Srianthumrong and Akagi, 2003; Akagi et al., 2003; Akagi, 2007b). In addition to the conventional two-level PWM bridge topologies, there has been an increasing interest in multi-level topologies, e.g. a three-level shunt active filter (Aburto et al., 1997; Gutiérrez et al., 2006; Munduate et al., 2006), a three-level hybrid filter (Tangtheerajaroonwong et al., 2007), and a shunt connected 81-level voltage-source converter operating as a harmonic compensator (Ortúraz et al., 2006). Furthermore, Oum et al. (2007) apply a fuel cell supplied Z-source converter as an active power filter and Itoh and Tamada (2007) use a combination of a matrix converter and a permanent magnet generator to compensate various power quality problems.

1.3. Objectives and Outline of Research

In this thesis, a digitally controlled three-phase three-wire voltage-source shunt active power filter is examined. The main aim of the research is to develop the active power filter and its control for improving power quality. This thesis studies the problem through five objectives, which are:

1. *to improve the current compensation characteristic of the voltage-source shunt active power filter*. The current compensation behavior of the voltage-source shunt active power filter is highly dependent on the delays caused by performing the digital control algorithm and sampling the measurement signals. The objective is to compensate and to minimize effects caused by the delays. Computationally light microcontroller implementation is required.
2. *to compare an active and a passive method for LCL filter resonance damping and to assess their suitability for active power filter application*. The use of the LCL filter is challenging in active power filter applications because of the resonance phenomenon and hard dynamic response requirements for the control system. In addition, the control delays and phase errors caused by the supply filter significantly impair the filtering behavior.
3. *to determine the active filter power loss profile and to examine possible benefits resulting from the use of silicon carbide (SiC) based power diodes in the active filter main circuit*.

4. *to compare voltage-source and current-source active power filters from the point of view of power circuit, modulation, control system, and harmonic filtering and to determine the power loss profiles*. The voltage-source shunt active power filter is the most commonly used active filter topology, but it is also possible to implement the system on the basis of current-source technology. In the literature, current-source technology has been claimed to have several drawbacks compared to voltage-source systems, but no in-depth comparison has been published recently.
5. *to examine voltage flicker mitigation obtained using shunt active power filter*.

This thesis consists of a summary and eight Publications [P1] – [P8] which are arranged to form a progressive presentation of the scientific contribution. The harmonics-producing load used in Publications [P1] – [P7] is a three-phase diode rectifier, which supplies either a series connection of a dc choke and a resistor or a parallel connection of a dc capacitor and a resistor. The ac mains currents produced by the loads characterize a typical dc-motor drive and voltage-source frequency converter, respectively. The supply is assumed to comprise symmetric sinusoidal three-phase voltages, with constant amplitude and frequency. Furthermore, in Publications [P1] – [P7] short-circuit power of the mains is assumed to be so great compared to the power of the load that the currents drawn by the load do not affect the supply voltages at the point of common coupling. The effect of disturbances in the mains voltages on the active filter characteristics are beyond the scope of this thesis.

The introduction in Chapter 1 is followed in Chapter 2 by a presentation of basic principles of modeling and control of the voltage-source shunt active power filter. Chapter 3 presents literature overview covering methods proposed to improve active power filter current distortion compensation characteristics. This is followed by a summary of the methods examined and proposed by the Author in [P1] – [P4]. Chapter 4 examines the use of an LCL-type supply filter in an active power filter and presents a comparison between an active and a passive resonance damping methods. This is based on Publication [P5]. Active power filter power loss profile is studied in Chapter 5 [P6]. Chapter 6 compares voltage-source and current-source shunt active power filters and assesses their power losses [P7]. Application of the voltage-source active power filter to mitigate the voltage flicker problem is examined in Chapter 7. This is based on Publication [P8]. Finally, Chapter 8 summarizes the scientific contribution of Publications [P1] – [P8] and presents the final conclusions of the thesis.

1.4. Summary of Scientific Contributions

The main contributions of the thesis are:

- Methods for compensating the delays caused by the digital control algorithm are analyzed and developed [P1], [P2].
- Current-sensorless control of the voltage-source active filter is proposed, analyzed, and tested in [P3] and [P4].
- An active and a passive method for LCL filter resonance damping are compared and their suitability for active power filter application is assessed [P5].

- The power loss profile of the voltage-source active power filter is presented and the distribution of the conduction and switching losses in the active filter semiconductor bridge is estimated. The application of SiC -based semiconductor devices is also examined. [P6]
- State-of-the-art voltage-source and current-source shunt active power filters with similar compensation algorithms are compared [P7]. Furthermore, detailed estimates for power loss distributions between the main circuit components in both of the active filter topologies are presented.
- A simulation model for evaluating flicker indices resulting from installing an active compensator is developed and validated [P8]. In addition, application issues concerning flicker mitigation using an active compensator and a fixed detuned filter as well as stability analysis of the system are presented [P8].

The contributions of Publications are presented separately and more precisely in Chapter 8.

2. Shunt Active Power Filter

This chapter presents an introduction to the operation and control of the voltage-source shunt active filter illustrated in Fig. 2.1. First in this chapter, space-vector theory used in modeling and analysis is briefly introduced. Next, the space-vector model of the main circuit is presented and the control principles are considered. Finally, the test setups used in Publications [P1] – [P8] are presented.

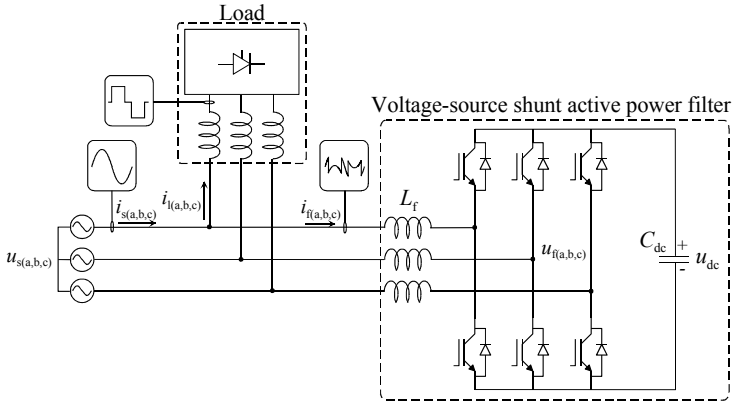

Fig. 2.1. Main circuit and operation principle of a voltage-source shunt active power filter connected to power system to compensate the current distortion caused by a non-linear load.

2.1. Space Vectors

Space-vector theory provides a useful tool for analyzing and modeling three-phase systems. Originally it was developed to model the dynamical behavior of ac machines (Kovács and Rácz, 1959), but since then space vectors have been applied to various electrical systems, such as power converters and ac motor drives, as presented e.g. by Akagi et al. (1984), Pfaff et al. (1984), Vas (1992), and Novotny and Lipo (1996). Space vectors are closely related to the two-axis theory of electrical machines presented e.g. by Park (1929), but the simplicity and compactness of space-vector equations can be considered advantages (Vas, 1998).

According to space-vector theory, arbitrary time-variant three-phase quantities can be represented with a single vector in the complex plane and a zero-sequence component. From the mathematical point of view, the calculation using the space vectors corresponds to the vector calculus. However, the space vectors should not be confused with complex phasors normally used to represent sinusoidally alternating quantities in steady state.

Space vector $\underline{x}$ for arbitrary time-variant three-phase quantities is defined using the phase quantities x_a, x_b, and x_c and a complex unit vector $\underline{a} = e^{j2\pi/3}$ in the stationary coordinate system as (Kovács and Rácz, 1959):

$$\underline{x}(t)=\frac{2}{3}\left[x_{\mathrm{a}}(t)+\underline{a}\,x_{\mathrm{b}}(t)+\underline{a}^{2}x_{\mathrm{c}}(t)\right]. \tag{2.1}$$

If the sum of the phase quantities does not equal zero, the zero-sequence component has to be calculated (Kovács and Rácz, 1959):

$$x_{\mathrm{z}}(t)=\frac{1}{3}\left[x_{\mathrm{a}}(t)+x_{\mathrm{b}}(t)+x_{\mathrm{c}}(t)\right]. \tag{2.2}$$

Figure 2.2(a) illustrates the space vector $\underline{x}$ constructed with the phase quantities x_{a}, x_{b}, and x_{c}. In the following, the space vectors and the phase quantities denoted with lower case italic letters express the time-varying functions, but for the sake of simplicity the time variable t has been omitted.

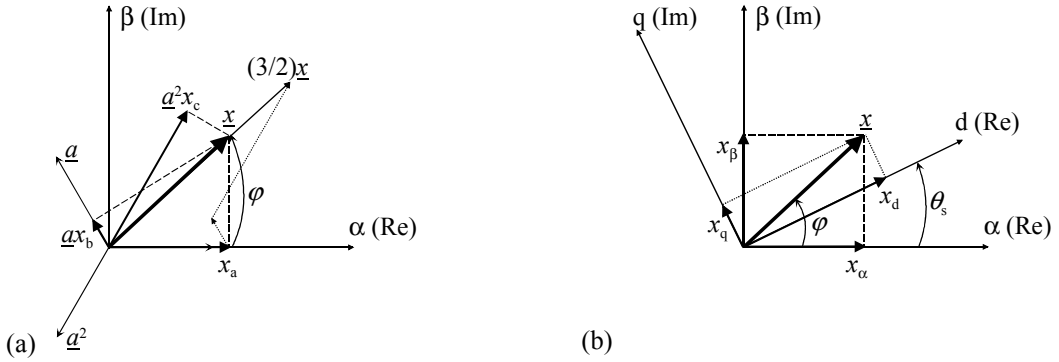

Fig. 2.2. (a) Illustration of the complex space vector $\underline{x}$ for three-phase quantities x_{a}, x_{b} and x_{c} in the complex plane. (b) Transformation from the stationary reference frame to the synchronous frame.

Equation (2.1) is called a non-power invariant (Vas, 1992) or amplitude invariant definition of the space vector: If the zero-sequence component does not exist, the phase quantities x_{a}, x_{b}, and x_{c} can be obtained as the projections of the space vector on the corresponding 'phase axis', i.e. the axis oriented parallel to the unit vectors $\underline{a}^{0}$, $\underline{a}$, and $\underline{a}^{2}$, respectively. This can be seen in Fig. 2.2(a). As a consequence, in the case of a symmetrical sinusoidal three-phase system, in steady state the length of the space vector equals the amplitude of the phase quantity. (Vas, 1992) Instead of the non-power invariant form presented, the so-called power invariant form would also be possible. In this case, coefficients $\sqrt{2/3}$ and $\sqrt{1/3}$ were used in (2.1) and (2.2) instead of 2/3 and 1/3. Hence, the power equations presented in the space-vector form would not need any additional coefficients (Novotny and Lipo, 1996; Vas, 1998).

The space vectors are usually presented using the real and the imaginary axis -oriented, so-called two-axis components. In the stationary reference frame, space vector $\underline{x}$ can be expressed as

$$\underline{x} = x_{\alpha} + \mathrm{j}\, x_{\beta}, \tag{2.3}$$

where x_{α} and x_{β} correspond to the real and imaginary -axis oriented components respectively. The two-axis components and the zero-sequence component can be calculated with three phase quantities as

$$\begin{bmatrix} x_\alpha \\ x_\beta \\ x_z \end{bmatrix} = \frac{2}{3}\begin{bmatrix} 1 & -1/2 & -1/2 \\ 0 & \sqrt{3}/2 & -\sqrt{3}/2 \\ 1/2 & 1/2 & 1/2 \end{bmatrix}\begin{bmatrix} x_a \\ x_b \\ x_c \end{bmatrix} \tag{2.4}$$

and inversely

$$\begin{bmatrix} x_a \\ x_b \\ x_c \end{bmatrix} = \begin{bmatrix} 1 & 0 & 1 \\ -1/2 & \sqrt{3}/2 & 1 \\ -1/2 & -\sqrt{3}/2 & 1 \end{bmatrix}\begin{bmatrix} x_\alpha \\ x_\beta \\ x_z \end{bmatrix}. \tag{2.5}$$

Sometimes it is convenient to present space vectors in the reference frame rotating with an arbitrary angular velocity. In the stationary frame we can write

$$\underline{x} = |\underline{x}|\, e^{j\varphi}, \tag{2.6}$$

where $|\underline{x}|$ refers to the length and φ to the displacement angle of the vector at time instant t (Fig. 2.2(b)). In the rotating frame, which rotates with angular velocity ω_s and a displacement angle of which at the same time instant t is θ_s, the space vector presented in (2.6) can be expressed as

$$\underline{x}^s = |\underline{x}|\, e^{j(\varphi-\theta_s)} = |\underline{x}|\, e^{j\varphi} e^{-j\theta_s} = \underline{x}\, e^{-j\theta_s}, \tag{2.7}$$

Conversely, the space vector presented in the rotating frame can be transformed back into the stationary frame using

$$\underline{x} = \underline{x}^s e^{j\theta_s}. \tag{2.8}$$

In the rotating frame, the frequency components which have the same angular velocity as the co-ordinate system are seen as dc components. With controlled PWM rectifiers and active power filters, a so-called synchronous reference frame is often used. The real axis of the synchronous frame is tied to the mains voltage vector. In the following, superscript s used with the space vectors refers to the synchronous frame and the vectors without superscript to the stationary frame representation.

Transformation from the stationary to the synchronous reference frame and the corresponding inverse transformation derived using (2.7) and (2.8) can be given in matrix notation:

$$\begin{bmatrix} x_d \\ x_q \\ x_z \end{bmatrix} = \begin{bmatrix} \cos\theta_s & \sin\theta_s & 0 \\ -\sin\theta_s & \cos\theta_s & 0 \\ 0 & 0 & 1 \end{bmatrix}\begin{bmatrix} x_\alpha \\ x_\beta \\ x_z \end{bmatrix} \tag{2.9}$$

$$\begin{bmatrix} x_\alpha \\ x_\beta \\ x_z \end{bmatrix} = \begin{bmatrix} \cos\theta_s & -\sin\theta_s & 0 \\ \sin\theta_s & \cos\theta_s & 0 \\ 0 & 0 & 1 \end{bmatrix}\begin{bmatrix} x_d \\ x_q \\ x_z \end{bmatrix}, \tag{2.10}$$

where x_d and x_q refer to the real and imaginary axis -oriented components of the space vector presented in the synchronous reference frame, respectively. The dependencies between the reference frame transformations are illustrated in Fig. 2.2(b). The components of the space vector presented in the synchronous reference frame can be calculated directly from the phase quantities as

$$\begin{bmatrix} x_\mathrm{d} \\ x_\mathrm{q} \\ x_\mathrm{z} \end{bmatrix} = \frac{2}{3} \begin{bmatrix} \cos\theta_\mathrm{s} & \cos(\theta_\mathrm{s} - 2\pi/3) & \cos(\theta_\mathrm{s} - 4\pi/3) \\ -\sin\theta_\mathrm{s} & -\sin(\theta_\mathrm{s} - 2\pi/3) & -\sin(\theta_\mathrm{s} - 4\pi/3) \\ 1/2 & 1/2 & 1/2 \end{bmatrix} \begin{bmatrix} x_\mathrm{a} \\ x_\mathrm{b} \\ x_\mathrm{c} \end{bmatrix}. \tag{2.11}$$

This is also known as Park's transformation (Kovács and Rácz, 1959; Vas, 1992). The corresponding inverse transformation is:

$$\begin{bmatrix} x_\mathrm{a} \\ x_\mathrm{b} \\ x_\mathrm{c} \end{bmatrix} = \begin{bmatrix} \cos\theta_\mathrm{s} & -\sin\theta_\mathrm{s} & 1 \\ \cos(\theta_\mathrm{s} - 2\pi/3) & -\sin(\theta_\mathrm{s} - 2\pi/3) & 1 \\ \cos(\theta_\mathrm{s} - 4\pi/3) & -\sin(\theta_\mathrm{s} - 4\pi/3) & 1 \end{bmatrix} \begin{bmatrix} x_\mathrm{d} \\ x_\mathrm{q} \\ x_\mathrm{z} \end{bmatrix}. \tag{2.12}$$

2.1.1 Electrical Power

In *three-phase three-wire systems*, instantaneous power which describes the total instantaneous energy flow per time unit between two electrical subsystems can be expressed as

$$p = u_\mathrm{a} i_\mathrm{a} + u_\mathrm{b} i_\mathrm{b} + u_\mathrm{c} i_\mathrm{c}. \tag{2.13}$$

This can be written in terms of the voltage and current space vectors $\underline{u}$ and $\underline{i}$, respectively (Kovács and Rácz, 1959; Vas, 1992):

$$p = \frac{3}{2} \mathrm{Re}\{\underline{u}\,\underline{i}^*\}, \tag{2.14}$$

where $\underline{i}^*$ denotes the complex conjugate of the current vector $\underline{i}$. Equation (2.14) can be expressed with space-vector components as

$$p = \frac{3}{2}\left(u_\alpha i_\alpha + u_\beta i_\beta\right) = \frac{3}{2}\left(u_\mathrm{d} i_\mathrm{d} + u_\mathrm{q} i_\mathrm{q}\right). \tag{2.15}$$

In the early 1980's, Akagi et al. proposed a control method for active power filters that was based on determining the instantaneous power p and the instantaneous imaginary power q (Akagi et al., 1984). The latter is calculated with space vectors as

$$q = \frac{3}{2}\left(u_\beta i_\alpha - u_\alpha i_\beta\right). \tag{2.16}$$

Akagi et al. (1984) originally defined q as negation of (2.16) and with space vectors presented in the power invariant form. Based on Akagi et al. (2007a), the instantaneous imaginary power can be expressed also as

$$q = \frac{3}{2} \mathrm{Im}\{\underline{u}\,\underline{i}^*\} = \frac{3}{2}\left(u_\mathrm{q} i_\mathrm{d} - u_\mathrm{d} i_\mathrm{q}\right) \tag{2.17}$$

and with three-phase variables as

$$q = \frac{1}{\sqrt{3}}\left[i_\mathrm{a}(u_\mathrm{b} - u_\mathrm{c}) + i_\mathrm{b}(u_\mathrm{c} - u_\mathrm{a}) + i_\mathrm{c}(u_\mathrm{a} - u_\mathrm{b})\right]. \tag{2.18}$$

The instantaneous imaginary power cannot be dealt with as a conventional electrical quantity, as pointed out by Akagi et al. (1984). This is because of the terms in (2.16) and (2.17) that are products of the instantaneous voltage in one axis and the instantaneous current in another axis, the terms $u_\beta i_\alpha$ and $u_\alpha i_\beta$ in (2.16), for example. However, in steady-state with balanced and

symmetric sinusoidal voltages and balanced, symmetric currents, the average of the instantaneous imaginary power q over the voltage period T has the same numerical value as the conventional fundamental three-phase reactive power definition, as discussed in Ferrero and Superti-Furga (1991) and Akagi et al. (2007a). This can be written

$$\frac{1}{T}\int_0^T q\,dt \hat{=} Q = 3\,UI_1\sin(\varphi_1)\,, \tag{2.19}$$

where U, I_1, and φ_1 are the rms value of the phase-to-neutral voltage, the rms value of the fundamental frequency component of the phase current, and the phase displacement between the fundamental voltage and the fundamental current, respectively. In power electronic vector control systems when the three-phase three-wire systems without zero-sequence mains current component are considered, the instantaneous imaginary power q is frequently called instantaneous reactive power.

The instantaneous reactive power theory a.k.a. “pq-theory” has given rise to a debate in scientific publications and its physical meaning is subjected to doubt e.g. by Czarnecki (2004; 2006). He has shown that when used as a power theory, the pq-theory is not capable of explaining all power phenomena and properties in electrical systems. Results which demonstrate that there are contradictions between the pq-theory and some common power definitions are shown in (Czarnecki, 2004; Czarnecki, 2006). However, Czarnecki (2006) also states: “These deficiencies could be considered as irrelevant when the pq-theory is used as the fundamental for a switching compensator control algorithm…”.

Because of its applicability to real-time control, in this thesis the instantaneous imaginary power q is used in the control systems to calculate the current component that carries the fundamental frequency reactive power. This is done taking into account the assumptions made for (2.19). Furthermore, in Publication [P8] instantaneous imaginary power is also used to visualize rapidly varying reactive power.

2.2. Space-Vector Model of the Voltage-Source Active Power Filter

The main circuit of the voltage-source shunt active power filter is presented in Fig. 2.3. It is constructed with a supply filter, controllable bridge, and energy storage element. The PWM bridge consists of six controllable switches with antiparallel diodes. In Fig. 2.3, insulated gate bipolar transistors (IGBTs) are used as the switching devices. The purpose of the supply filter is to enable control of the filter currents using the voltage-source bridge, but also to limit the switching ripple current. Usually, the filter has either first-order (L) or third-order (LCL) structure. In the dc link, there is an electrolytic capacitor with a dc voltage u_{dc} as a voltage source and an energy storage. The dc-link voltage should be so high that the filter currents can be controlled to draw the load current distortion components through the supply filter. In the following, a space-vector model of the voltage-source active filter is presented.

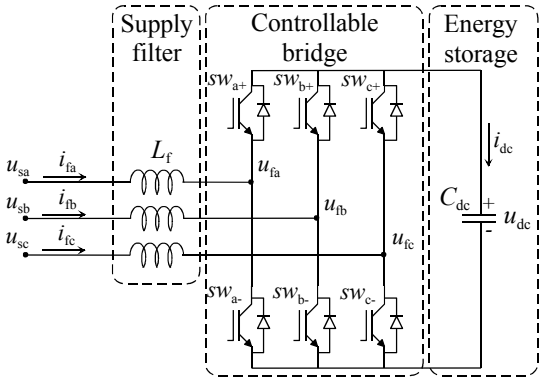

Fig. 2.3. Main circuit of the voltage-source shunt active power filter.

2.2.1. PWM Bridge and Space-Vector Modulation

Pulse width modulation comprises the methods of producing the desired short-term average output voltage of the controlled bridge, i.e. the methods of controlling the relative on-times of the active switches. A form of pulse width modulation called space-vector modulation was proposed in the 1980s, e.g. by Pfaff et al. (1984), and further developed by van der Broeck et al. (1988) (Kazmierkowski et al., 2002; Holmes and Lipo, 2003). The method can be used to determine the pulse widths for the bridge directly from the space-vector form voltage references by means of the space-vector calculus. Space-vector modulation is easy to implement fully digitally using e.g. a DSP or microcontroller. Moreover, it offers the possibility for the explicit identification of the pulse placements which can be exploited to modify the harmonic performance of the voltage produced (Holmes and Lipo, 2003) and the switching losses in the bridge.

Figure 2.3 presents the two-level PWM bridge used in the voltage-source active filters examined in this thesis. Each of the switches (sw_{a+}, sw_{b+}, sw_{c+}, sw_{a-}, sw_{b-}, sw_{c-}) can be either turned on or off, corresponding to the value 1 or 0, respectively. If we use the virtual middle point of the dc link as a reference, we can define the switching functions for each of the phases as (Ollila, 1993):

$$sw_a = \frac{1}{2}\left(sw_{a+} - sw_{a-}\right) \tag{2.20a}$$

$$sw_b = \frac{1}{2}\left(sw_{b+} - sw_{b-}\right) \tag{2.20b}$$

$$sw_c = \frac{1}{2}\left(sw_{c+} - sw_{c-}\right). \tag{2.20c}$$

Normally, the ideal voltage-source converter is controlled so that at every time instant, one of the two switches in each of the phases is in on-state at a time. Thus, the phase switching functions can have values ±1/2, depending on the state of the switches. Assuming that one of the switches in every phase is in on-state at every time instant, commutation of the current between switches is infinitely fast and the voltage drops in the switches are neglected, we can write the phase to mid-point voltages produced with the bridge (Ollila, 1993):

$$u_{fa} = sw_a u_{dc} \tag{2.21a}$$

$$u_{\mathrm{fb}}=sw_{\mathrm{b}}u_{\mathrm{dc}} \tag{2.21b}$$

$$u_{\mathrm{fc}}=sw_{\mathrm{c}}u_{\mathrm{dc}}, \tag{2.21c}$$

where u_{dc} is the dc-link voltage.

The switching vector $\underline{sw}$ can be defined according to the definition (2.1)

$$\underline{sw}=\frac{2}{3}\left(sw_{\mathrm{a}}+\underline{a}\,sw_{\mathrm{b}}+\underline{a}^{2}sw_{\mathrm{c}}\right). \tag{2.22}$$

Taking into account all the switching states allowed, we have in total eight vectors. Two of these correspond to a short circuit of the phase outputs and they are called zero vectors. The other six can be considered to form non-zero vectors of magnitude 2/3. They are called active vectors and can be expressed as

$$\underline{sw}_i = 2/3e^{\mathrm{j}(i-1)\pi/3}, \text{ where } i = 1\ldots6 \tag{2.23}$$

Correspondingly, (2.21) can be written in space-vector form as

$$\underline{u}_{\mathrm{f}} = \underline{sw}\,u_{\mathrm{dc}}\,. \tag{2.24}$$

Figure 2.4 shows the allowed switching combinations and the corresponding voltage vectors produced with the PWM bridge. In the figure, '+' refers to the on-state of the upper switch and '–' to the on-state of the lower switch. Since there is no neutral conductor in the three-phase three-wire system presented in Fig. 2.3, the zero-sequence current may not exist and thus the possible zero-sequence component of the voltage does not affect the power flow in the system. Therefore, the zero-sequence components have been omitted.

state i	a	b	c	$\underline{u}_{\mathrm{f}i}=\underline{sw}_i u_{\mathrm{dc}}$
1	+	–	–	$2/3u_{\mathrm{dc}}$
2	+	+	–	$2/3e^{\mathrm{j}\pi/3}u_{\mathrm{dc}}$
3	–	+	–	$2/3e^{\mathrm{j}2\pi/3}u_{\mathrm{dc}}$
4	–	+	+	$2/3e^{\mathrm{j}\pi}u_{\mathrm{dc}}$
5	–	–	+	$2/3e^{\mathrm{j}4\pi/3}u_{\mathrm{dc}}$
6	+	–	+	$2/3e^{\mathrm{j}5\pi/3}u_{\mathrm{dc}}$
7	+	+	+	0
8	–	–	–	0

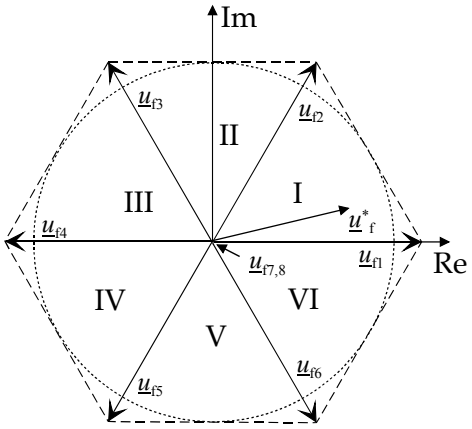

Fig. 2.4. The allowed switching combinations and the corresponding voltage vectors produced with the PWM bridge.

In the space-vector modulation, an arbitrary reference vector $\underline{u}_{\mathrm{f}}^{*}$ is formed by the summation of a number of the switching voltage vectors $\underline{u}_{\mathrm{f}i}$ within one switching period $T_{\mathrm{sw}}/2$, which is a half of the carrier period T_{sw} (Holmes and Lipo, 2003). If the two active vectors nearest to the reference vector are used, this is (van der Broeck et al., 1988):

$$\int_0^{T_{\mathrm{sw}}/2}\underline{u}_{\mathrm{f}}^{*}\,dt=\int_0^{T_{\mathrm{f}i}}\underline{u}_{\mathrm{f}i}dt+\int_{T_{\mathrm{f}i}}^{T_{\mathrm{f}i}+T_{\mathrm{f}(i+1)}}\underline{u}_{\mathrm{f}(i+1)}dt+\int_{T_{\mathrm{f}i}+T_{\mathrm{f}(i+1)}}^{T_{\mathrm{sw}}/2}\underline{u}_{\mathrm{f}0}dt\,, \tag{2.25}$$

where $T_{\mathrm{f}i}$ and $T_{\mathrm{f}(i+1)}$ are, respectively, the switching durations of the active vectors $\underline{u}_{\mathrm{f}i}$ and $\underline{u}_{\mathrm{f}(i+1)}$, while $\underline{u}_{\mathrm{f}0}$ corresponds to the zero vector. Equations for the switching periods $T_{\mathrm{f}i}$ and $T_{\mathrm{f}(i+1)}$ can be derived from (2.25):

$$T_{\mathrm{f}i} = \frac{\sqrt{3}T_{\mathrm{sw}}}{2}\frac{\left|\underline{u}_{\mathrm{f}}^{\,*}\right|}{u_{\mathrm{dc}}}\sin(\theta_{\mathrm{f}(i+1)} - \varphi^*) \tag{2.26}$$

$$T_{\mathrm{f}(i+1)} = \frac{\sqrt{3}T_{\mathrm{sw}}}{2}\frac{\left|\underline{u}_{\mathrm{f}}^{\,*}\right|}{u_{\mathrm{dc}}}\sin(\varphi^* - \theta_{\mathrm{f}i})\,, \tag{2.27}$$

where $|\underline{u}_{\mathrm{f}}^{\,*}|$ and φ^* refer to the magnitude and angle of the reference voltage vector, respectively. The switching period is completed with the zero vectors. A conventional approach is to split the remaining time equally between both zero vectors $\underline{u}_{\mathrm{f}7}$ and $\underline{u}_{\mathrm{f}8}$:

$$T_{\mathrm{f}7} = T_{\mathrm{f}8} = \left[T_{\mathrm{sw}}/2 - \left(T_{\mathrm{f}i} + T_{\mathrm{f}(i+1)}\right)\right]/2\,, \tag{2.28}$$

but also other alternatives are possible (Holmes and Lipo, 2003). Equations (2.25) – (2.28) hold true if the reference vector $\underline{u}_{\mathrm{f}}^{\,*}$ lies within the hexagon defined by the switching voltage vectors $\underline{u}_{\mathrm{f}i}$ seen in Fig. 2.4. In this thesis, the magnitude of the reference vector is restricted to so-called linear modulation region (Kazmierkowski et al., 2002; Holmes and Lipo, 2003), i.e.

$$\left|\underline{u}_{\mathrm{f}}^{\,*}\right| \le \frac{2}{\sqrt{3}}\frac{u_{\mathrm{dc}}}{2}\,. \tag{2.29}$$

This is illustrated in Fig. 2.4 with a dotted circle.

The switching sequence applied in this study is described in the following. Every carrier period T_{sw} consists of two switching periods. The first of them begins with the zero vector $\underline{u}_{\mathrm{f}8}$ and this is followed by the active vector that is adjacent to the reference vector in the sector. The active vector is chosen so that the state of switches in only one phase needs to be changed at any time. After that, the other active vector in the sector is applied and finally the zero vector $\underline{u}_{\mathrm{f}7}$. Then the new switching times are calculated for the latter switching period using (2.26) – (2.28) and the vectors are applied in inverse sequence. Figure 2.5 illustrates the switching sequence if the reference vector $\underline{u}_{\mathrm{f}}^{\,*}$ lies in sector I, as shown in Fig. 2.4.

	sector I							
$\underline{u}_{\mathrm{f}i}$	8	1	2	7	7	2	1	8
phase a	-	+	+	+	+	+	+	-
phase b	-	-	+	+	+	+	-	-
phase c	-	-	-	+	+	-	-	-

0 $T_{\mathrm{sw}}/2$ T_{sw}

Fig. 2.5. Switching sequence when the reference vector lies in sector I.

To ensure precise operation, the switching durations are calculated and updated twice in the PWM carrier period T_{sw}. In this way the average delay caused by the modulator can be reduced from $T_{\mathrm{sw}}/2$ to $T_{\mathrm{sw}}/4$ (Van de Sype et al., 2004). Holmes and Lipo (2003) call the modulation strategy applied ‘asymmetric regular sampled space-vector modulation’ (Holmes

and Lipo, 2003), while Kazmierkowski et al. (2002) refer to this as ‘space vector modulation with symmetrical placement of zero vectors’.

To avoid the short-circuiting of the dc-link capacitor, both the upper and the lower switch of the phase are not allowed to be simultaneously in the on-state. In practical implementations, there is a short time period called dead time between the turn-off of one of the two switching devices in a phase and the turn-on of the other device in the phase. The dead time consists of a turn-off delay of the switching device plus a safety time interval (Holtz, 1992). However, the effect of the delay time is not taken into account in the previous equations.

2.2.2. Supply Filter

An ideal shunt active filter operates as a controlled current source. Thus, the purpose of the supply filter of the active filter is to allow the bridge, which is a voltage source by nature, to act as a current source. Another objective is to limit the switching ripple current components originating in the PWM voltage from entering the supply network. Supply filters used with the voltage-source active filter are typically either L- or LCL-type. It is also possible to use a CL filter, but often a line side inductor is installed to prevent current harmonics injected by parallel loads from overloading the capacitors of the filter (Lindgren and Svensson, 1998). In the following a space-vector model for an L-type filter is presented.

Frequency-Independent Model for the Inductor

A simple model of the filter choke consists of an inductance L_f and a resistance R_f connected in series. If we assume a symmetrical filter, we can write the following equation for the inductor presented in Fig. 2.3:

$$\underline{u}_\mathrm{s} - \underline{u}_\mathrm{f} = L_\mathrm{f} \frac{d\underline{i}_\mathrm{f}}{dt} + R_\mathrm{f} \underline{i}_\mathrm{f}\,, \tag{2.30}$$

where $\underline{u}_\mathrm{s}$, $\underline{u}_\mathrm{f}$ and $\underline{i}_\mathrm{f}$ are the space vectors of the mains voltage, active filter terminal voltage and active filter current, respectively. In the synchronous reference frame, this is

$$\underline{u}_\mathrm{s}^\mathrm{s} - \underline{u}_\mathrm{f}^\mathrm{s} = L_\mathrm{f} \frac{d\underline{i}_\mathrm{f}^\mathrm{s}}{dt} + \mathrm{j}\omega_\mathrm{s} L_\mathrm{f} \underline{i}_\mathrm{f}^\mathrm{s} + R_\mathrm{f} \underline{i}_\mathrm{f}^\mathrm{s}\,, \tag{2.31}$$

where ω_s is the angular speed of the frame. The corresponding component form is

$$u_\mathrm{sd} - u_\mathrm{fd} = L_\mathrm{f} \frac{di_\mathrm{fd}}{dt} - \omega_\mathrm{s} L_\mathrm{f} i_\mathrm{fq} + R_\mathrm{f} i_\mathrm{fd} \tag{2.32a}$$

$$u_\mathrm{sq} - u_\mathrm{fq} = L_\mathrm{f} \frac{di_\mathrm{fq}}{dt} + \omega_\mathrm{s} L_\mathrm{f} i_\mathrm{fd} + R_\mathrm{f} i_\mathrm{fq}\,. \tag{2.32b}$$

This model does not take into account the frequency dependence of the inductance and the resistance. Because damping in the system, for example, may be incorrect, the simple choke model is not useful in frequency response analysis. In this thesis, the frequency-independent model is used in operational analysis.

Frequency-Dependent Model for the Inductor

In practice, the inductance and resistance of an inductor are not constants. Instead, they change with frequency and temperature. In order to model the frequency characteristics where the inductance decreases and the resistance increases when the frequency increases, a series Foster model of an inductor can be used (de Leon and Semlyen, 1993). The model is constructed with a dc resistance and a series of parallel-connected RL blocks, as illustrated in Fig. 2.6.

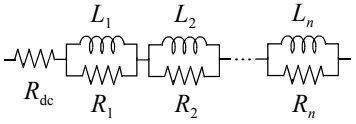

Fig. 2.6. Series Foster model modeling frequency-dependent inductor.

In this thesis, the series Foster model is used in the frequency-domain analysis of the active filters. Thus, instead of the time-domain model, a Laplace-domain transfer function for the inductor is given. The impedance of the inductor is

$$Z_{\mathrm{L}}(s) = R_{\mathrm{dc}} + \sum_{i=1}^{n} \frac{sL_i R_i}{sL_i + R_i}. \tag{2.33}$$

The accuracy of the Foster model increases with the number of RL blocks. In this thesis, a third-order Foster model consisting of three RL blocks is used. The frequency-dependent model of the choke is used in the frequency response analysis.

2.2.3. Dc link

The instantaneous power flowing through the PWM bridge can be written according to (2.14) as

$$p_{\mathrm{ac}} = \frac{3}{2}\mathrm{Re}\left\{\underline{u}_{\mathrm{f}}\,\underline{i}_{\mathrm{f}}^{\,*}\right\}. \tag{2.34}$$

With (2.24), this yields

$$p_{\mathrm{ac}} = \frac{3}{2}\mathrm{Re}\left\{\underline{sw}\,u_{\mathrm{dc}}\,\underline{i}_{\mathrm{f}}^{\,*}\right\} = \frac{3}{2}u_{\mathrm{dc}}\,\mathrm{Re}\left\{\underline{sw}\,\underline{i}_{\mathrm{f}}^{\,*}\right\}. \tag{2.35}$$

At the same time, the instantaneous dc power is

$$p_{\mathrm{dc}} = u_{\mathrm{dc}} i_{\mathrm{dc}}. \tag{2.36}$$

If we assume a lossless PWM bridge, the power on the ac side equals the dc power. Hence, the dc-link current i_{dc} can be calculated as

$$i_{\mathrm{dc}} = \frac{3}{2}\mathrm{Re}\left\{\underline{sw}\,\underline{i}_{\mathrm{f}}^{\,*}\right\}, \tag{2.37}$$

which in the component form is

$$i_{\mathrm{dc}} = \frac{3}{2}\left(sw_{\alpha}\,i_{\mathrm{f}\alpha} + sw_{\beta}\,i_{\mathrm{f}\beta}\right) = \frac{3}{2}\left(sw_{\mathrm{d}}\,i_{\mathrm{fd}} + sw_{\mathrm{q}}\,i_{\mathrm{fq}}\right). \tag{2.38}$$

In the pure active power filter, there is no load connected on the dc link. Thus, the dc link consists of the capacitor operating as an energy storage element. Effect of the dc-link losses and the losses in the PWM bridge, e.g. switching and conducting losses, on the instantaneous

power can be modeled by connecting a resistor parallel to the capacitor. The dc-link voltage can now be expressed as

$$u_{\mathrm{dc}} = \frac{1}{C_{\mathrm{dc}}} \int \left(i_{\mathrm{dc}} - \frac{u_{\mathrm{dc}}}{R_{\mathrm{dc}}} \right) dt \,. \tag{2.39}$$

2.3. Active Filtering

2.3.1. Control

Control of the voltage-source shunt active power filter is basically similar to the control of the pulse-width-modulated voltage-source converter. Figure 2.7 shows the principle of the vector control implemented in the synchronous reference frame (Kazmierkowski et al., 2002). In Fig. 2.7, PLL refers to phase-locked loop and "abc/dq" blocks are the reference frame transformations presented in (2.11).

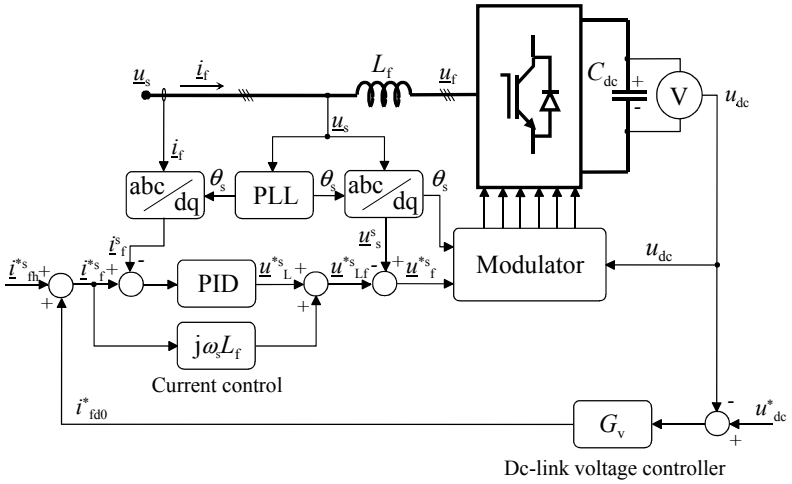

Fig. 2.7. Principle of the active filter control.

The figure above presents a cascaded control system in which the outer control loop regulates the dc-link voltage, while the inner loop controls the ac currents. The generation of the filtering current reference vector $\underline{i}^{*s}_{f}$ is ignored. The output of the dc-link voltage controller is the d-axis reference i^{*}_{fd0} for the fundamental frequency current. The active filter current vector $\underline{i}_f$ is controlled with a PID controller in a closed loop by affecting the voltage vector $\underline{u}_{Lf}$ applied over the filter inductor L_f. In the control system, the reference vector $\underline{u}^{*s}_{f}$ for the bridge voltage is calculated by subtracting the reference $\underline{u}^{*s}_{Lf}$ from the supply voltage vector $\underline{u}^{s}_{s}$. Finally, the voltage vector reference $\underline{u}^{*s}_{f}$ is given to the space-vector modulator.

Because of the cross-coupling terms in the rotating reference frame in (2.32a), the d-axis filter current i_{fd} cannot be independently controlled with the d-axis filter voltage u_{fd}, but the change in u_{fd} affects also the q-axis filter current i_{fq}. Correspondingly, according to (2.32b), the change in u_{fq} leads to a change not only in i_{fq} but also in i_{fd}. This is why a cross-coupling compensation term $j\omega_s L_f$ is introduced in the control system presented in Fig. 2.7. Thus, the reference for the voltage vector over the filter inductor is

$$\underline{u}_{\mathrm{Lf}}^{*\mathrm{s}} = \underline{u}_{\mathrm{L}}^{*\mathrm{s}} + \mathrm{j}\omega L_{\mathrm{f}} \underline{i}_{\mathrm{f}}^{*\mathrm{s}}, \tag{2.40}$$

where $\underline{u}^{*\mathrm{s}}_{\mathrm{L}}$ is the output of the current controller. Equation (2.40) can be written in the component form as

$$u_{\mathrm{Lfd}}^{*} = u_{\mathrm{Ld}}^{*} - \mathrm{j}\omega L_{\mathrm{f}} i_{\mathrm{fq}}^{*} \tag{2.41a}$$

$$u_{\mathrm{Lfq}}^{*} = u_{\mathrm{Lq}}^{*} + \mathrm{j}\omega L_{\mathrm{f}} i_{\mathrm{fd}}^{*}. \tag{2.41b}$$

These compensation terms decouple the control of the d- and q-axis currents. Although the cross-coupling compensation of the current control has not been shown in the block diagrams, in this thesis this is included in the PID controllers presented, unless otherwise specified.

Controllers

The algorithm for the PID controller can be written as (Åström and Hägglund, 2006)

$$u(t) = P\left(e(t) + \frac{1}{T_{\mathrm{I}}} \int_0^t e(\tau) d\tau + T_{\mathrm{D}} \frac{de(t)}{dt} \right), \tag{2.42}$$

where u is the controller output and e the error between the reference and the measured signal. P, T_{I}, and T_{D} refer to the proportional gain, integration time, and derivative time, respectively. For the means of digital control, the discrete-time form approximated using the backward difference method with the sampling period T_{cc} can be written as

$$u(k) = u_{\mathrm{P}}(k) + u_{\mathrm{I}}(k) + u_{\mathrm{D}}(k), \tag{2.43a}$$

where

$$u_{\mathrm{P}}(k) = Pe(k) \tag{2.43b}$$

$$u_{\mathrm{I}}(k) = P\frac{T_{\mathrm{cc}}}{T_{\mathrm{I}}} e(k) + u_{\mathrm{I}}(k-1) \tag{2.43c}$$

$$u_{\mathrm{D}}(k) = P\frac{T_{\mathrm{D}}}{T_{\mathrm{cc}}} \big(e(k) - e(k-1) \big). \tag{2.43d}$$

Figure 2.8 presents the block diagram for the PID controller based on (2.43). In the figure, the saturation block ('Satur.') in the output of the integrator part limits the output within the operation region, thus preventing integrator windup. The latter saturation block restricts the controller output to the actuator operation region.

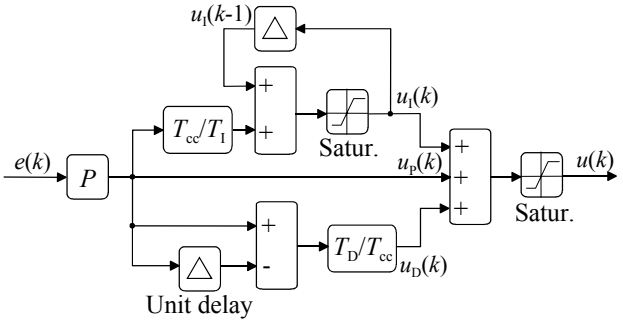

Fig. 2.8. PID controller with anti-windup ('Satur.').

The dc-link voltage is not the primary control quantity in the voltage-source active filters. This is maintained at a desired level to make control of the filter currents possible. Thus, the

dc-voltage regulation does not have to be precise. In this thesis nonlinear controllers are used. They allow a slight deviation between the reference and the actual control quantity without affecting the controller output $u(k)$. The block diagrams are shown in Figs. 2.9 and 2.10. The output of the P(e^2) controller presented in Fig. 2.9 is proportional to the square of the input. In contrast, PI(e^2) shown in Fig. 2.10 operates as a conventional PI controller, but its proportional gain changes depending on the error signal. The PI(e^2) controller is discussed in detail in Publication [P3]. In Fig. 2.10, T_{vc} refers to the sampling period of the discrete-time voltage control.

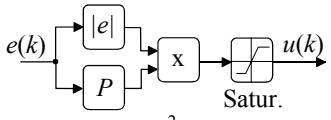

Fig. 2.9. P(e^2)-controller

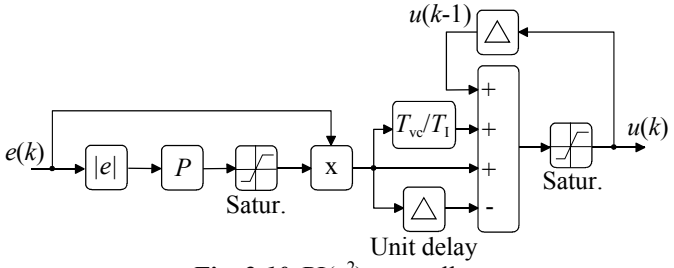

Fig. 2.10. PI(e^2)-controller.

Synchronization and Phase-Locked Loop

The synchronization of the control system presented in Fig. 2.7 is based on the phase-locked loop. Various techniques for implementing this have been reviewed e.g. by Hsieh and Hung (1996), Timbus et al. (2005), and Limongi et al. (2007). In this thesis, the synchronization is implemented exploiting the PLL together with zero-crossing detection of the phase-a supply voltage. The synchronization signal can be generated with the circuit shown in Fig. 2.11. The measurement signal is led through the low-pass filter, which has a corner frequency of 169 Hz. Then, the Schmitt trigger generates a rectangular wave, which is finally monitored by the phase-locked loop implemented by software.

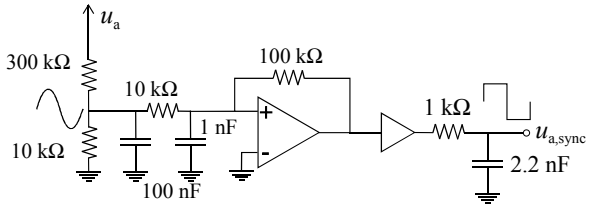

Fig. 2.11. Circuit for synchronization signal generation.

Figure 2.12 illustrates the block diagram of the discrete time PLL implemented by the software. The difference between the zero-crossing time of the phase angle of $u_{a,sync}$ signal and that of the estimated phase angle θ_{ua} is led to the PI controller, the output of which is the angle increment $\Delta\theta_{ua}$. At every sampling instant, the increment $\Delta\theta_{ua}$ is added to the previous value of the estimated phase angle θ_{ua}. The execution of the PI control is triggered by the zero-crossing of the voltage $u_{a,sync}$, but the estimated phase angle θ_{ua} is updated every sampling period.

Because of the circuit shown in Fig. 2.11, there exists phase displacement between the actual phase angle of the supply voltage u_a fundamental component and the estimated phase angle θ_{ua}. This is compensated with a constant value added to the phase angle, as shown in Fig. 2.12. Finally, the alignment angle θ_s of the supply voltage space vector is obtained by subtracting constant $\pi/2$.

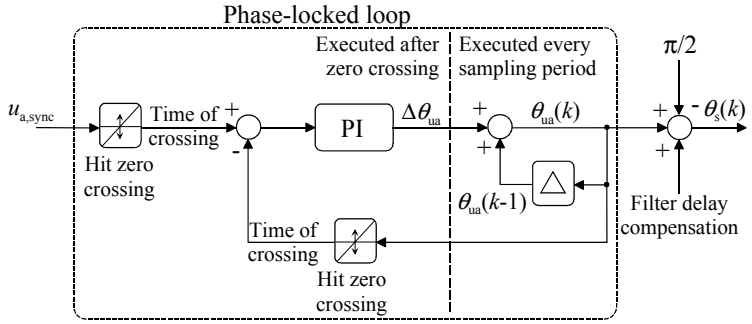

Fig. 2.12. Calculation of the alignment angle of the rotating reference frame exploiting phase-locked loop.

Because the PLL implemented in this thesis measures only the phase-a supply voltage, this does not detect the phase order of the supplying network. Another drawback of the solution is that because the PLL is based on detecting the zero-crossings of the voltage, the crossing instants can only be detected once during every half cycle of the utility voltage. Thus, the solution has quite slow dynamic to the voltage waveform distortion. This issue could be solved by using more sophisticated PLL methods such as synchronous reference frame based or adaptive solutions which offer better performance, as shown e.g. by Timbus et al. (2005) and Limongi et al. (2007).

2.3.2. Reference for the Compensating Current

The control goal of the active filters examined in this thesis is to mitigate current distortion and fundamental frequency reactive power produced by a nonlinear load. In the literature, various methods for achieving this goal have been presented. In general, these methods can be divided into load current detection and supply current detection methods on the basis of the current reference generation configuration applied. The methods are also termed load current feedforward and supply current feedback -based methods, respectively.

The idea of the load current detection -based control system is that the active filter generates current components which have equal amplitude but are in opposite phase with the distortion components detected in the load current. Consequently, only the fundamental frequency current component would be drawn from the mains. The method compensates the distortion entering the supply network in open-loop manner: the compensating current reference is obtained by extracting the fundamental component $i_{l(1)}$ from the load current and constructing the reference current for the active power filter as

$$i_f^* = -(i_l - i_{l(1)}). \tag{2.44}$$

The load current detection -based control is typically implemented using the pq-theory (Akagi et al., 1984), the synchronous reference frame method (Takeda et al., 1987), or a notch filter (Newman et al., 2002). A similar compensation principle was already used in the magnetic flux compensation proposed by Sasaki and Machida (1971).

Figure 2.13 illustrates the principle of the reference generation method in the synchronous reference frame. Since the fundamental frequency components are seen as dc quantities, harmonics and interharmonics of the d-axis current (i_{ldh}) can be extracted using a low-pass filter and by subtracting the result from the current i_{ld}. To compensate both fundamental frequency reactive power and distortion, the q-axis current component is not filtered. Finally, the compensating current reference $\underline{i}^{*s}_{f}$ is formed by combining negations of components i_{ldh} and i_{lq}.

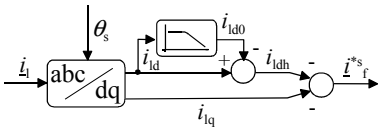

Fig. 2.13. Principle of load current detection -based current reference generation method in synchronous frame.

Supply current detection methods are sometimes also referred to as methods without harmonic detection. The control goal is to keep the supply current sinusoidal by closed-loop control. The control problem can be considered a disturbance rejection problem (Griño et al., 2007), where the load causes disturbances that should be rejected. The control system shown in Fig. 2.7 can be applied also to supply current detection: the output of the dc-link controller would be the reference for the fundamental supply current i^{*}_{sd0} and the feedback current $\underline{i}_{f}$ would be replaced with the measured supply current $\underline{i}_{s}$. In this case, the reference $\underline{i}^{*s}_{fh}$ shown in Fig. 2.7 could be omitted.

Both of the reference generation methods discussed above are suitable for overall current harmonic filtering. In addition to them, selective harmonic compensation methods have been proposed, e.g. by Mattavelli (2001), Fukuda and Imamura (2005), Etxeberria-Otadui et al., (2006), Dumitrescu et al. (2007), and Lascu et al. (2007). The methods are designed to compensate only the desired harmonic components. A benefit is that in this way only the most harmful harmonics can be filtered and thus the active filter ratings can be limited. The selective methods can be thought to be special cases of the load and supply current detection -based systems discussed above.

2.4. Test Setups

The active filter prototypes used in Publications [P1] – [P7] operate at the switching frequency of 10 kHz and they have been designed according to a rated power of 5 kVA. The prototype implementations have been briefly presented in Appendix A. More detailed descriptions can be found in (Routimo, 2002; Routimo, 2005; Salo, 2002). In the experiments

presented in Publication [P8], three parallel-connected MaxSine 100A-3L v5.0 active filters have been used. The filters were made by Nokian Capacitors Ltd.

In Publications [P1] – [P7], two different harmonics-producing loads have been used in the experiments presented. Both of them have been constructed using a diode rectifier with 2.3-mH three-phase commutation (or smoothing) chokes installed on the ac side of the rectifier. The load on the dc side of the rectifier is either a series-connected 10-mH dc choke and a resistor, or a parallel-connected 1-mF electrolytic capacitor and a resistor.

2.4.1. Measurement Equipment

In the experiments, LeCroy Waverunner LT354M and LT463L digital oscilloscopes were used. In Publications [P1] – [P7], the currents were measured using Tektronix TCPA300 amplifiers and TCP312 current probes. The dc-link voltages were obtained via differential mode measurements using LeCroy PPE 2kV voltage probes. The attenuation ratio of the probes was 1:100. The oscilloscope sampling rate was 500 kHz. In addition, a PEM CWT03 ultra mini Rogowski current waveform transducer with an oscilloscope sampling rate of 200 MHz was also used in Publication [P6].

In the experiments presented in Publication [P8], currents were measured with Fluke i1000s and Fluke i3000s current probes and with LEM~flex RR3030 current probes that utilize the Rogowski principle. The phase-to-ground voltages were measured with Tektronix P5200 differential voltage probes with an attenuation of 1:500. The sampling rate was 500 kHz.

The current and voltage data measured with the oscilloscopes were transferred to the laptop computer, on which the data were low-pass filtered with a digital filter in Matlab program. The corner frequencies of the digital filter had been selected so that the frequencies of interest remained unchanged but the measurement noise was filtered. The measurement filter used was a Butterworth filter with an attenuation of 1 dB at 23 kHz and 10 dB at 30 kHz. Figures of the measurement results were drawn using Matlab.

2.4.2. Power Loss Measurements

In the following, power loss measurement setups used in Publications [P3], [P5] – [P7] are introduced. In the measurements, the averages of the total three-phase power drawn from the mains (P_s) and the three-phase power drawn by the diode rectifier load (P_l) were measured using a LEM Norma D6000 wideband power analyzer and a Yokogawa WT1030 digital power meter, respectively. The active filter efficiency is defined as

$$\eta = P_l / P_s \tag{2.45}$$

and estimates for the total power losses in the active filters were calculated as the differences of these two powers. The measurement setups are illustrated in Fig. 2.14(a) and (b).

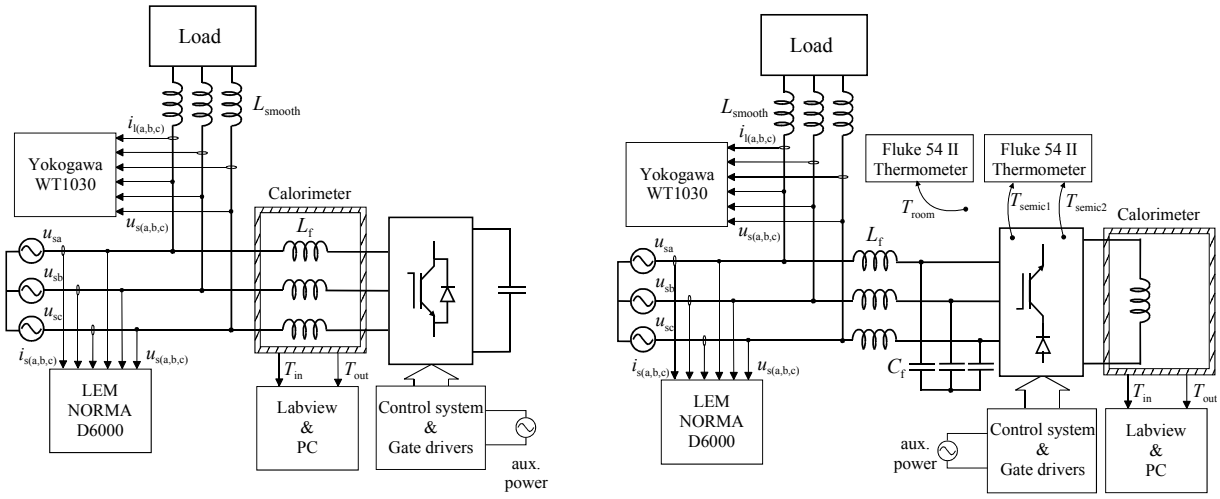

Fig. 2.14. Power loss measurement setup for (a) voltage-source active power filter and (b) current-source active power filter.

The power loss distributions between the main circuit components in Publications [P6] and [P7] were determined using calorimetric methods. They are used to determine the total power which is dissipated by the examined device as heat in a measurement chamber. Because this heat results in a temperature rise of the air surrounding the device, the temperature rise indicates total power losses of the device if the heat is completely absorbed by the coolant (Xiao et al., 2007). In this study, two different calorimetric measurement setups were used.

Voltage-Source Active Filter

The power loss measurement setup for the voltage-source active power filter is shown in Fig. 2.14(a). In the measurements, the active filter was used to compensate harmonics of the diode bridge with a constant load and the supply filter chokes (L_f) were located in an open-type calorimeter chamber described in (Parkatti et al., 2007). During the measurements, the filter chokes L_f were cooled with a constant air flow with the temperature T_{in}, but due to the power losses in the chokes the temperature of the outflow was T_{out}. The temperatures were monitored with a laptop computer using LabVIEW software. The active filter was kept compensating the harmonics until the temperature difference $T_{out} - T_{in}$ stabilized. In the tests carried out in Publication [P6] this took 120 – 150 min and in Publication [P7] 90 – 120 min. The differences in times are due to the different semiconductors and heat sinks. Since the calorimeter had been calibrated so that the dependence between the temperature rise and the heating power was known, the power loss P_{Lf} of the filter chokes could be determined. Finally, the power losses of the active filter semiconductor bridge were estimated as

$$P_{semicond} = P_s - P_l - P_{Lf} . \tag{2.46}$$

The measurements were repeated for four load power levels and two different load types.

It should be noted that $P_{semicond}$ defined as in (2.46) contains the losses both in the IGBT bridge and the dc-link capacitors. However, since the equivalent series resistance (ESR) of the

capacitors is low, the losses in the capacitors are minimal compared with the semiconductor losses.

Current-Source Active Filter

The power loss measurement setup for the current-source active power filter was shown in Fig. 2.14(b). The arrangement described in the following was used to determine the individual power losses of the supply filter chokes, the semiconductor bridge, and the dc-link choke. In the measurement setup, the dc-link choke was located inside the calorimeter discussed previously. Furthermore, the supply filter chokes were moved outside the prototype box. Therefore the temperature variation inside the box is mainly due to the power dissipation of the semiconductors. Next, the semiconductors were heated with the known dc power, similarly as in (Viitanen, 2005), and the corresponding temperature rises in the heat sink were measured as

$$\Delta T_{\text{semic}} = \frac{T_{\text{semic1}} + T_{\text{semic2}}}{2} - T_{\text{room}} . \tag{2.47}$$

Then, the active filter was used to compensate a static diode rectifier load and the temperature rises in the active filter components were measured. The active filter was kept compensating as long as the temperature rises were stabilized. This took about 120 – 150 min. Finally, the power losses were estimated by comparing the temperature rises. The measurements were repeated with different load powers and types.

During the measurements, the total power loss of the active filter was also measured using the power meters illustrated in Fig. 2.14(b). Furthermore, the calorimeter was used to obtain the power losses in the dc-link choke. Finally, the power losses in the filter inductors were estimated as

$$P_{\text{Lf}} = P_{\text{s}} - P_{\text{l}} - P_{\text{Ldc}} - P_{\text{semic}}. \tag{2.48}$$

To prevent overvoltages in the measurement setup, the supply filter capacitors (C_{f}) of the current-source active filter were mounted directly on the semiconductor bridge terminals. Thus, the semiconductor power losses obtained include the losses in the diodes, IGBTs, and capacitors. However, the losses in the capacitors are minimal compared with the semiconductor losses, as discussed previously.

3. Improving the Compensation Characteristics of the Voltage-Source Active Power Filter

In general, compensation characteristics of the active power filter depend on the compensating reference signal, control method, pulse width modulation method, and power converter characteristics (Dixon et al., 1994; le Roux and van Wyk, 2001; Tong et al., 2007). That is, every part of the active filter affects the filtering characteristics. The generation of the compensating current reference and the current control method applied are among the key elements which determine the performance of the load current detection -based active power filters. This is because in theory they may determine the order of harmonics that can be compensated, i.e. the compensation capacity of the active power filter (Newman et al., 2002; Han et al., 2005; Corradini et al., 2007; González et al., 2007). In other words, if the reference is poor or lags, or the control bandwidth is narrow, effective compensation is impossible to obtain.

In theory, the reference generation for the shunt active filter is simple, as discussed in the previous chapter. However, in practice, it is difficult to identify and to remove the fundamental component from the distorted load current in real-time. Compared with analog techniques, the use of microcontrollers and digital signal processors offers advantages in reference generation algorithm and control system implementations in terms of ease of development and modifications. The drawback of digital systems is the non-negligible time required to perform e.g. digital control algorithm, pulse width modulation, and analog-to-digital conversions of the measurement signals. Due to this delay, the control is always late and compensation of the harmonics deteriorates. (le Roux and van Wyk, 2001)

The effect of the sampling and processing delays can be studied by examining the resulting sampled sinusoidal waveforms. If the actual load current is

$$i_\mathrm{l} = \hat{i}\sin(2\pi f t), \tag{3.1}$$

due to the delay t_Δ this current is seen by the control system as

$$i_\mathrm{l,meas} = \hat{i}\sin(2\pi f t + \varphi_\Delta), \tag{3.2}$$

where $\varphi_\Delta = -2\pi f t_\Delta$ is the phase error (le Roux and van Wyk, 2000). Figure 3.1(a) demonstrates the effect of different time delays t_Δ by illustrating the resulting current $i_\mathrm{l,meas}$ seen by the control system as a function of frequency f. In the figure, the sampling frequency is assumed to be higher than or equal to 20 kHz. The phase error increases with the frequency. Consequently, for the active filter it is difficult to compensate the higher order harmonics, but the compensation of lower order harmonics is also affected. This can be clearly seen by examining the equation

$$i_\mathrm{s} = i_\mathrm{l} + i_\mathrm{f} = i_\mathrm{l} - i_\mathrm{l,meas}, \tag{3.3}$$

where i_s and i_f refer to the supply current and the current produced with the active filter, respectively. Figure 3.1(b) shows the magnitude and phase of the supply current as a function of frequency, i.e. the theoretical filtering characteristics for the active filter affected only by the sampling delay. The results show that the bandwidth of the harmonic filtering decreases drastically as a function of increased sampling delay. As can be deduced form Fig. 3.1(a) and (b), the active filtering characteristics can be improved if the delay is compensated.

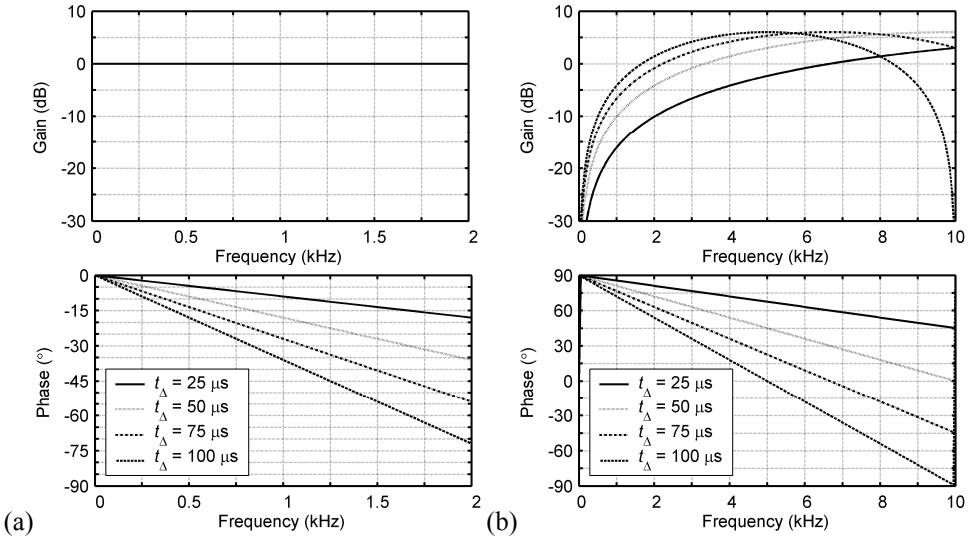

Fig. 3.1. Effect of time delay. (a) Current seen by the control system and (b) theoretically obtainable filtering characteristics of the active filter for different time delays as a function of the frequency.

This chapter concentrates on the methods for improving the current compensation characteristics of the voltage-source active power filter by compensating the delays or by reducing their effect on the control system. First, literature overview covering current reference generation methods and solutions for overcoming the problems caused by the delays is presented. Second, the methods proposed in Publications [P1] and [P2] for compensating control delays are presented. Third, two methods in which the effect of the processing delay is eliminated using current-sensorless control are proposed for a modified main circuit structure. These are based on Publications [P3] and [P4]. Finally, experimental results obtained with the methods presented in Publications [P1] – [P4] are presented and compared.

3.1. Overview of Reference Generation Methods

In the literature, several compensating current reference generation methods for the active power filter are proposed. However, they are influenced by various sources of errors studied e.g. by le Roux and van Wyk (2000) and (2001), and Maza Ortega et al. (2005). First in this section, typical reference generation methods are presented. This is followed by an overview of the methods proposed for compensating effects caused by the delay.

Figure 3.2 shows principles and simplified block diagrams of the current reference generation methods presented in the literature e.g. in (Mendalek and Al-Haddad, 2000; Newman et al., 2002; Han et al., 2005; Sozanski and Jarnut, 2005; Borisov et al., 2007; González et al., 2007;

Tong et al., 2007). All of these methods have been proposed for the shunt active power filter controlled with the load current detection -method. Newman et al. (2002) present a stationary frame reference generation method utilizing a notch filter (Fig. 3.2(a)) which blocks the fundamental frequency component. As a result, the compensating current reference $\underline{i}^*_{\mathrm{fh}}$ consists solely of distortion, such as the harmonics etc. In contrast, methods which are based on the determination of the fundamental frequency component have been considered e.g. in (Mendalek and Al-Haddad, 2000; Sozanski and Jarnut, 2005; Borisov et al., 2007; González et al., 2007; Väliviita and Ovaska, 1998; Han et al., 2005; Tong et al., 2007). Mendalek and Al-Haddad (2000) present a current reference generation method (Fig. 3.2(b)), implemented in the synchronous reference frame, in which the fundamental component $\underline{i}^{\mathrm{s}}_{\mathrm{l0}}$ is first extracted from the load current $\underline{i}^{\mathrm{s}}_{\mathrm{l}}$ by utilizing a fourth-order Butterworth low-pass filter. Then the compensating reference $\underline{i}^{*\mathrm{s}}_{\mathrm{fh}}$ is generated by subtracting the load current $\underline{i}^{\mathrm{s}}_{\mathrm{l}}$ from the fundamental component $\underline{i}^{\mathrm{s}}_{\mathrm{l0}}$. Sozanski and Jarnut (2005), Borisov et al. (2007), and Conzález et al. (2007) propose solutions in which the fundamental component $\underline{i}^{\mathrm{s}}_{\mathrm{l0}}$ is determined based on the frequency domain analysis (Fig. 3.2(c)). Väliviita and Ovaska (1998) and Han et al. (2005) proposed a current reference generation method (Fig. 3.2(d)) where an adaptive predictive filter determines the fundamental frequency component $\underline{i}_{\mathrm{l0}}$. Furthermore, Tong et al. (2007) proposed a time domain method that was based on the reference frame transformations (Fig. 3.2(e)).

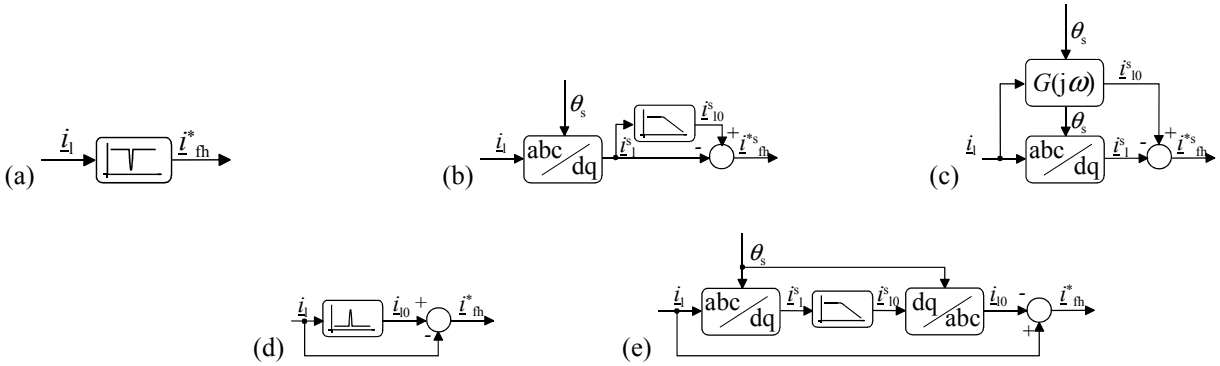

Fig. 3.2. Principle of the current reference generation: (a) a notch filter (Newman et al., 2002), (b) synchronous reference frame (Mendalek and Al-Haddad, 2000), (c) frequency domain approach (Borisov et al., 2007), (d) an adaptive predictive filter (Han et al., 2005), and (e) time-domain and rotating reference frame approach (Tong et al., 2007).

As can be seen in Fig. 3.2(a) – (e), the principles of the reference generation methods are quite similar: the final objective is to separate the fundamental frequency component and the distorted load current. However, alternative implementation of the same basic principle may introduce various benefits, but also give rise to drawbacks. For example, Newman et al. (2002) point out that by using the stationary frame method Fig. 3.2(a) instead of the synchronous frame Fig. 3.2(b), the whole control system can be implemented without reference frame transformations and hence classical control techniques can be used to analyze the system performance. In addition, by avoiding the reference frame transformations, the implementation of the controller software can be simplified since the sine/cosine lookup tables are no longer required and thus the controller execution time can be reduced. However, if drift of the supply frequency is possible, this has to be taken into account in the design of

the reference filter. Benefits of the recursive discrete Fourier transform -based solution Fig. 3.2(c) proposed by Borisov et al. (2007) are computationally efficient implementation and fast convergence in the case of change in the load power. The results presented in the paper show that the algorithm settles down to the new operating point faster than the method based on the second-order Butterworth low-pass filter implemented in the synchronous frame.

3.1.1. Solutions to Control-Delay-Related Problems

Various methods for overcoming the issues related to the delays in the active filter have been proposed in the literature. This section presents a short overview of the methods.

Hysteresis control has been used in active filters since they were invented (Gyugyi and Strycula, 1976; Akagi et al., 1984). Benefits of the method are simple and robust implementation that is moreover computationally light since this does not require separate current controllers and a modulator. However, hysteresis control typically introduces varying switching frequency and heavy interference among phases (Chaoui et al., 2007; Etxeberria-Otadui et al., 2006). These can be considered as drawbacks because they may cause problems e.g. in supply filter design. A solution for overcoming the disadvantages has been proposed e.g. by Malesani et al. (1996).

A method for compensating sampling delay by calculating correction terms for the most important harmonics is proposed by Jeong and Woo (1997). The principle is shown in Fig. 3.3. The objective is to correct the phase angles of the selected harmonics $\underline{i}_{f(n)}$ in the compensating current reference $\underline{i}^*_f$. A drawback of the solution is the time-consuming calculation. This is due to the fact that the correction of the error is performed separately for several harmonics. The measurement results presented in (Jeong and Woo, 1997) indicate effective reduction of the delay effects.

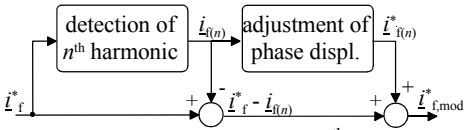

Fig. 3.3. Principle of the delay compensation for the n^{th} harmonic (Jeong and Woo, 1997).

In (Hayashi et al., 1991) and (Lindgren and Svensson, 1998) control delay is compensated by predicting periodically repeating load current based on the measurement made in the previous fundamental period. The principle is shown in Fig. 3.4. The time delay is approximated to be two sample periods and thus the harmonic filtering reference $\underline{i}^*_{fh}(k)$ is comprised with the load current harmonics delayed for $(m - 2)$ sampling periods, where m refers to the samples per fundamental period (Hayashi et al., 1991) or to the samples per half of a fundamental period (Lindgren and Svensson, 1998). A similar approach is presented also in (Sozanski, 2004), where unlike in (Hayashi et al., 1991) and (Lindgren and Svensson, 1998) the load change situation is also considered. Sozanski (2004) proposes that if the measured value $i_{lh}(k)$ differs from the value $i_{lh}(k - m)$, the prediction is turned off. In this case the currently measured value

$i_{lh}(k)$ should be used instead of the prediction. The measurement results presented in (Sozanski, 2004) show that in the case of load transient the prediction can be turned on again after a couple of fundamental periods of steady-state operation. Detection of the load current harmonics is performed at sampling frequency 12.8 kHz, while the compensating current sampling and control frequency is 102.4 kHz. Thus, the compensating current reference is interpolated from the measured load current. The implementation is realized using both DSP and FPGA circuits. The prediction method is also used in (Sozanski and Jarnut, 2005), where this is applied to a recursive discrete Fourier transform -based reference generation.

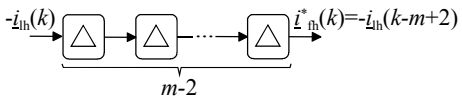

Fig. 3.4. Principle of prediction-based current reference generation.

One-cycle control, which is a nonlinear method to control the pulse width, has been proposed for switching converters e.g. by Smedley and Ćuk (1995). A one-cycle controlled active power filter has been shown to be effective in compensating harmonics e.g. in (Smedley et al., 2001; Qia et al., 2001; Qia and Smedley, 2002; Jin and Smedley, 2006). The control of the active filter is based on the supply current detection method, and thus extraction of the compensation reference is not needed. The control system is simple: it comprises comparators, flip-flops, and a clock, but not any multipliers. It can be easily implemented without microcontroller or DSP. Consequently, the computing time executed by the processor unit does not limit the switching frequency, thus enabling the use of a switching frequency of dozens of kilohertz. Figure 3.5 illustrates the control scheme of the one-cycle controlled single-phase active power filter. In the figure, R_s refers to resistance of the current sensing resistor. As can be deduced from the figure, one-cycle control is based on a current control loop similar to that in the conventional supply current detection method without harmonic extraction examined e.g. in (Buso et al., 1998). However, due to the PWM signal generated with the nonlinear modulation method incorporating one-cycle control, a better dynamic response is obtained (Liu et al., 2007).

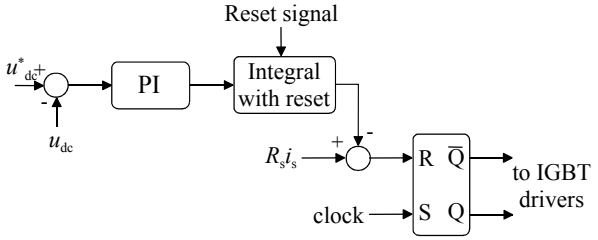

Fig. 3.5. Control scheme of one-cycle controlled single-phase active power filter (Liu et al., 2007).

Corradini et al. (2007) point out that one of the main factors limiting the maximum achievable current control bandwidth in digital control systems is the computational delay between the sampling instant and the corresponding change in the PWM bridge output. The proposed solution is to reduce the delay by applying multi-rate sampling technique, where the system variables are sampled and current control performed several times during the switching period

of the PWM bridge. Because of the limited execution time of microcontrollers and DSPs, the implementation requires fast AD converters and the use of FPGAs, for example. In addition, because of the multiple samples during the switching period, the control algorithm has to take care also of the filtering of the switching ripple. The results presented in the paper show that the filtering characteristic is improved and the effect of the modulation delay is reduced.

Marks and Green (2002) propose a solution which exploits a neural network. The principle of the solution is shown in Fig. 3.6. The neural network is used to predict the fundamental frequency component of the load current based on the measurements of the dc-link voltage $u_{l,dc}$ and current $i_{l,dc}$ of the disturbing load. The objective of the solution is used to improve the transient performance of the active filter. The results obtained show excellent performance. However, the proposed system is not applicable as a solution for harmonics-related problems caused by an unknown load.

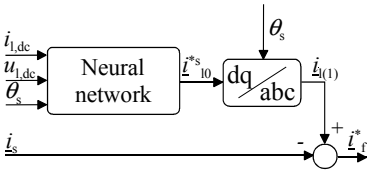

Fig. 3.6. Principle of the predictive reference generation method adopting neural network (Marks and Green, 2002)

An adaptive neural network is used in (Nishida et al., 2005). In the method, the neural network minimizes the error between the measured samples of the actual load current and the reconstructed load current obtained with the network in the control system. This is achieved by adaptive determination of the Fourier series coefficients. The active filter current reference is finally obtained by subtracting the measured load current from the fundamental component which is determined using the adaptive neural network, as shown in Fig. 3.7. A benefit of the proposed method is that it can be applied to both single-phase and three-phase systems. Furthermore, the training data for the network is not needed, because the network determines the coefficients for the Fourier series adaptively on-line. A drawback is the complicated calculations required. Results presented by Nishida et al. (2005) indicate effective filtering characteristics.

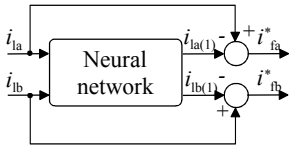

Fig. 3.7. Current reference extraction method proposed by Nishida et al. (2005).

Selective harmonic compensation has been examined in various papers and both load current and supply current detection -based solutions have been proposed, see (Bojrup et al., 1999; Mattavelli and Marafão, 2004; Etxeberria-Otadui et al., 2006; Dumitrescu et al., 2007; Lascu et al., 2007; Nascimento et al., 2007). In selective methods, the compensated harmonics are selected either by means of Fourier transform, see e.g. (Mattavelli and Marafão, 2004), by means of time domain methods such as a resonant, internal model, or repetitive current

control, see e.g. (Bojrup et al., 1999; Etxeberria-Otadui et al., 2006; Dumitrescu et al., 2007; Lascu et al., 2007), or by means of an artificial neural network (Nascimento et al., 2007). A drawback of the selective control methods is that the required computing power is proportional to the number of the harmonics to be compensated. Furthermore, in FFT-based methods a delay of at least an half of a mains cycle is induced and thus FFT is not very suitable for detecting harmonics produced by varying load. Time domain methods typically require multiple controllers, several reference frame transforms, or notch filters. In contrast, appropriate data are often required to train neural networks. This is because in the case of an operating point or load that is not trained for the neural network, the harmonic filtering may be severely impaired. Furthermore, complicated algorithm can also be considered a drawback. However, the selective compensation also offers several advantages compared with total harmonic compensation: the effect of the delays as well as the supply filter parameters change with frequency, but these changes can be taken into account in the selective control system. Thus, the overall stability of the compensator can be improved (Lascu et al., 2007). Furthermore, the active filter ratings can be minimized by compensating only the most harmful harmonics.

Table 3.1 summarizes the overview of the methods for overcoming the control-delay-related problems presenting benefits and drawbacks.

Table 3.1.
Summary of the Literature Overview

METHOD	BENEFITS	DRAWBACKS
Hysteresis control	- simple and robust implementation - computationally light	- varying switching frequency → problems in supply filter design - interference among phases
Phase-angle correction	- delay effects for selected harmonics can be corrected accurately	- time-consuming calculations
Reference Prediction	- effective with static loads	- filtering impairs if load changes
One-cycle control	- simple implementation using comparators, flip-flops and a clock	- the control is implemented with hardware → modification of the control system is difficult
Multi-rate sampling	- fast response to changes in filtering reference	- requires fast AD converters and FPGAs
Neural-network predicting reference	- effective compensation of a selected load	- requires dc link variables of the load to be measured - not applicable for an unknown load
Adaptive neural network	- training of the neural network is not needed	- time-consuming and complicated calculations
Selective harmonic compensation methods	- frequency dependent parameters can be taken into account in the control	- computing power required increases with the count of harmonics to be compensated

3.2. Computational Control Delay Compensation

This section presents a summary of the computational control delay compensation method examined in Publication [P1]. Originally, the method was proposed by co-author Mika Salo in (Salo, 2002; Salo and Tuusa, 2003), where it was used for the current-source shunt active power filter. Publication [P1] applies the method to the voltage-source shunt active power filter and presents the frequency domain analysis of the filtering characteristics.

3.2.1. Theory

Figure 3.8 illustrates the theoretical current curves presented in the synchronous reference frame for the load current detection -based compensation method. The upper curve ($i_{\mathrm{lh(d,q)}}$) represents the step change of the load current $\underline{i}^{\mathrm{s}}_{\mathrm{l}}$ to be compensated. In the digital control system, the currents are measured and the current control algorithm is executed at discrete time instants $t_{\mathrm{k-1}}$, t_{k}, $t_{\mathrm{k+1}}$ etc. As a result of the delay due to sampling and calculation, the output of the control system lags on average 1.5 discrete time periods. That is, the control system detects at time instant t_{k} the step change in the load current that has occurred between time instants $t_{\mathrm{k-1}}$ and t_{k}. The detected step change results in a change in the active filter compensating current reference $\underline{i}^{*\mathrm{s}}_{\mathrm{fh}}$ at time instant $t_{\mathrm{k+1}}$. This is illustrated in Fig. 3.8 with the curve $i^{*}_{\mathrm{fh(d,q)}}$. After the change in the reference $\underline{i}^{*\mathrm{s}}_{\mathrm{fh}}$, the rate of change of the realized active filter compensating current $\underline{i}^{\mathrm{s}}_{\mathrm{fh}}$ depends on the current controller parameters, the supply filter, and the active filter dc-link voltage. In Fig. 3.8, this current is approximated with the lowest solid line curve $i_{\mathrm{fh(d,q)}}$.

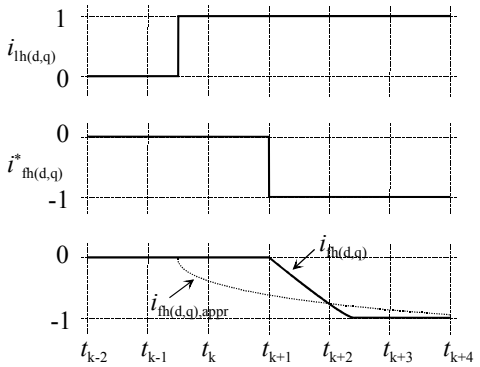

Fig. 3.8. Theoretical current curves for the load current detection -based current compensation method.

The computational control delay compensation proposed by Salo (2002) and applied in Publication [P1] is based on the idea that since the delay time and the characteristic of the compensating current $\underline{i}^{\mathrm{s}}_{\mathrm{fh}}$ resulting in the change in the current reference $\underline{i}^{*\mathrm{s}}_{\mathrm{fh}}$ are known, the active filter current reference $\underline{i}^{*\mathrm{s}}_{\mathrm{fh}}$ should be modified so that the delay is compensated. A rough approximation to model the transition from $\underline{i}^{\mathrm{s}}_{\mathrm{lh}}$ to $\underline{i}^{\mathrm{s}}_{\mathrm{fh}}$ can be made using a first-order low-pass filter

$$\underline{I}^{\mathrm{s}}_{\mathrm{fh}}(s) \approx \underline{I}^{\mathrm{s}}_{\mathrm{fh,\,appr}}(s) = \frac{-1}{\tau_{\mathrm{c}} s + 1} \underline{I}^{\mathrm{s}}_{\mathrm{lh}}(s) \ , \tag{3.4}$$

where τ_{c} refers to a time constant that depends on the active filter parameters and the capital letters refer to Laplace transforms of the currents. This is illustrated in Fig. 3.8 with a dotted

line. In order to compensate the time lag, the active filter current reference vector calculation is based on

$$\underline{I}^{*s}_{fh}(s) = -(\tau_c s + 1)\underline{I}^{s}_{lh}(s) \tag{3.5}$$

instead of

$$\underline{I}^{*s}_{fh}(s) = -\underline{I}^{s}_{lh}(s)\,. \tag{3.6}$$

Equation (3.5) can be written in the discrete form obtained using the backward difference approximation (Åström and Wittenmark, 1997) as

$$\underline{i}^{*s}_{fh}(k) = -\frac{\tau_c}{T_s}\left[\underline{i}^{s}_{lh}(k) - \underline{i}^{s}_{lh}(k-1)\right] - \underline{i}^{s}_{lh}(k)\,, \tag{3.7}$$

where T_s refers to the sampling period. In the following, (3.7) is referred to as the computational control delay compensation.

Figure 3.9 illustrates the theoretical curves obtained using the computational control delay compensation. The solid line at the bottom of the figure represents the active filter current reference vector $\underline{i}^{*s}_{fh}(k)$ and the dotted line the resulting active filter current vector $\underline{i}_{fh}$.

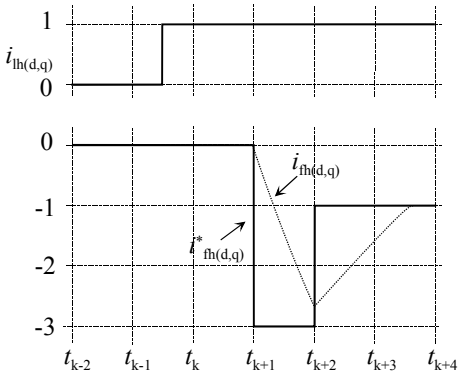

Fig. 3.9. Theoretical current curves produced by computational control delay compensation.

A control system for the active power filter is shown in Fig. 3.10. The active filter control is similar to that presented in Fig. 2.7, but Fig. 3.10 shows also the generation of the current reference. The current reference generation contains the high-pass filter (the block labeled "HP") and the control delay compensation (the block labeled "CDC"). The high-pass filter is implemented as presented in Fig. 2.13 and the implementation exploits a first-order low-pass filter approximated using the forward Euler method (Åström and Wittenmark, 1997). The corner frequency of the filter is 20 Hz ($\tau \approx 7.96$ ms). The block "CDC" is based on (3.7) and its content is presented in Fig. 3.11.

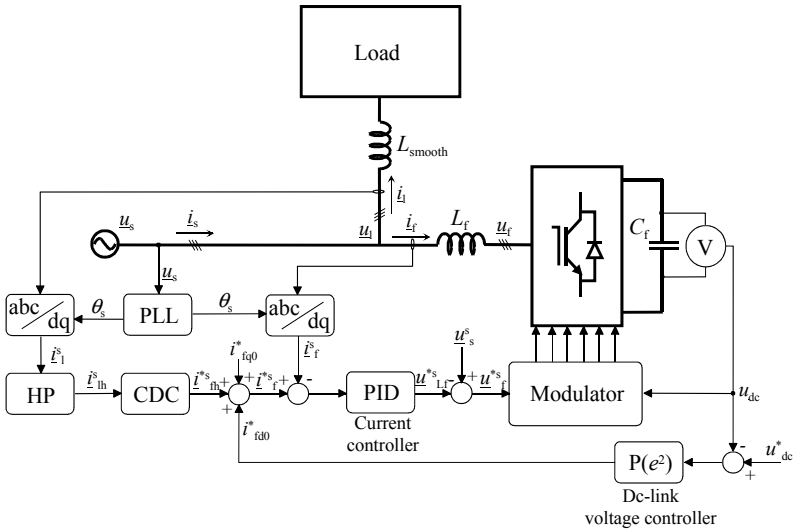

Fig. 3.10. Control system using computational control delay compensation method.

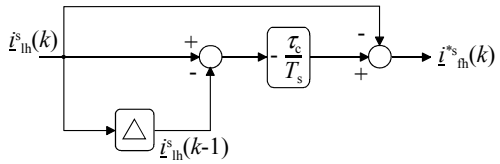

Fig. 3.11. Control delay compensation (CDC).

3.2.2. Filtering Characteristics

In the following, the characteristics of the control system presented in Fig. 3.10 are examined with a simplified model of the active filter. A similar analysis was done in Publication [P1]. However, in the publication a simple frequency-independent model of the filter choke was used. Furthermore, the cross-couplings between the d- and q-axis components were ignored and the compensating characteristics only on the d-axis were presented. In the following, the cross-coupling terms are taken into account and the frequency-dependent choke model discussed in section 2.2.2 is used.

Figure 3.12 presents the block diagram used in the frequency domain study. The input of the system is the load current vector $\underline{i}^s_l$ and the output the supply current vector $\underline{i}^s_s$. According to Ollila (1993), the space-vector modulator and the PWM bridge can be assumed to be linear up to about half of the carrier frequency in the linear modulation range. In the following examination, the active filter PWM bridge is assumed to be a linear voltage source which produces the voltage reference delayed by the calculation period. Furthermore, the dc-link voltage control is ignored and the load is assumed to be a current source. The mains voltages are omitted. Thus, the effect of the distorted mains voltages on the current compensation is ignored. To avoid the non-linear coordinate transformations, the control and the process are represented in the synchronously rotating reference frame. In addition, to model the measurement signal filters, first order low pass filters with 10 µs time constants have been used. In Fig. 3.12, the block "Ref. gen." includes the blocks labeled as "HP" and "CDC" in Fig. 3.10. Furthermore, "zoh" refers to the zero-order-hold sampling (Åström and Wittenmark, 1997) and "AD" to the analog-to-digital conversion. The parameters for the

control system can be found in Appendix B and those for the filter choke model in Appendix C.

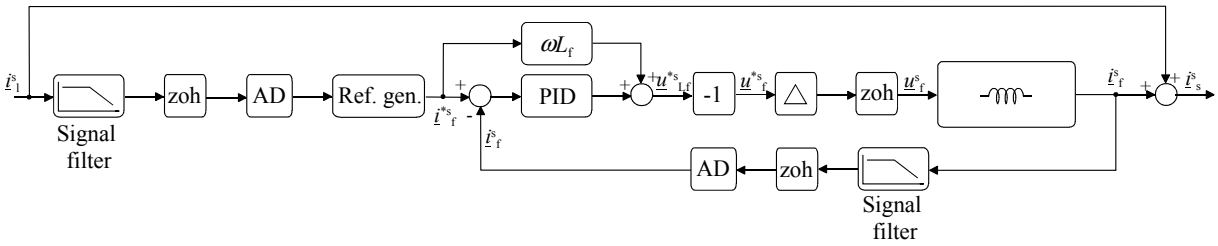

Fig. 3.12. Simplified active filter model in synchronous reference frame.

Figure 3.13(a) – (d) shows the Bode magnitude plots for the system presented in Fig. 3.12. The calculation period of the control system is 50 µs. Since in this thesis the modulator carrier frequency is chosen to be 10 kHz, the Bode plots have been drawn up to 5 kHz. The phase plots have been omitted since the phase angles of the remaining supply current harmonics are not important from the point of view of harmonic compensation. It can be seen in Fig. 3.13(a) – (d) that by selecting the time constant τ_c properly, the filtering characteristics of the active power filter can be improved. In Fig. 3.13(a), the minimum of the Bode magnitude plot lies at 300 Hz if time constant $\tau_c = 2T_s$. This is the optimal case since the fifth and the seventh harmonics produced by diode and thyristor rectifier loads are seen as 300 Hz components in the synchronous reference frame. In contrast, Fig. 3.13 shows that the filtering at frequencies above 2 kHz is impaired.

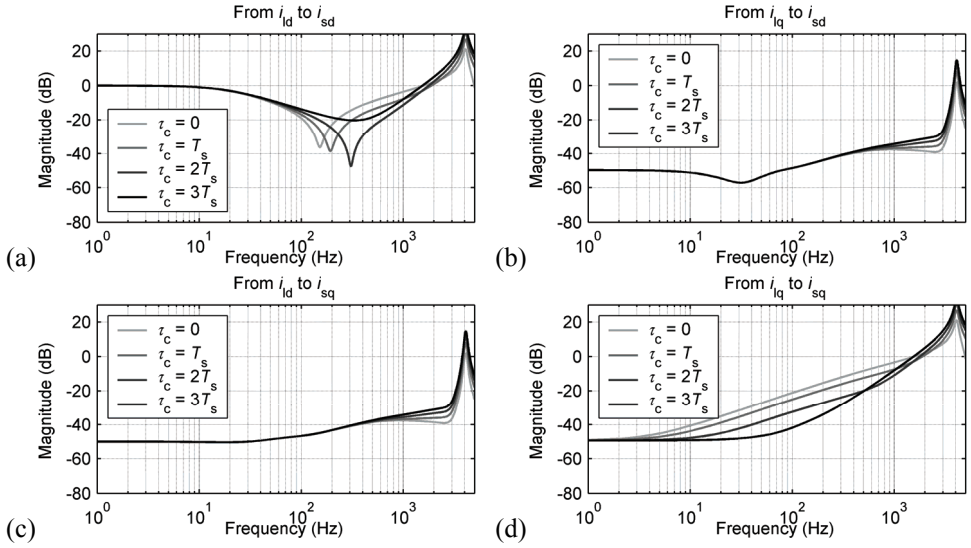

Fig. 3.13. Bode magnitude plots for CDC method applied to voltage-source active power filter.

3.3. Prediction-Based Current Reference Generation

In the following, a summary of the method proposed in Publication [P2] and the frequency responses for the active filter using this are presented.

Disturbing loads can be divided into predictable and non-predictable, noise-like loads. Just as the name implies, in steady state the current characteristic of loads of the first category can be

predicted in subsequent periods after a few periods of observation (Sozanski, 2004). This category consists, for example, of diode and thyristor rectifier loads. In the following, the reference generation method designed for predictable harmonic loads is presented.

In the literature, prediction-based reference generation methods have been proposed e.g. by Hayashi et al. (1991), Lindgren and Svensson (1998), and Sozanski (2004), as discussed in section 3.1.1. Sozanski (2004) generates the compensating current references separately for each of the three phases. In contrast, in the methods proposed by Lindgren and Svensson (1998) the reference generation is based on the space vectors in the synchronous reference frame. The prediction is not valid in the case of load change, for example. Such a situation has not been considered in (Hayashi et al., 1991; Lindgren and Svensson, 1998). Instead, Sozanski (2004) proposes simply to turn-off the prediction until the prediction is valid again. This lasts a couple of fundamental periods.

The prediction-based current reference generation method proposed in Publication [P2] is a combination of the reference generation methods presented in (Lindgren and Svensson, 1998) and in Publication [P1]. The method proposed in Publication [P2] exploits the space-vector approach similarly to (Lindgren and Svensson, 1998). In the case of the non-predictable situation, the prediction is not used, as proposed also by Sozanski (2004). However, instead of simply turning off the prediction as in (Sozanski, 2004), the method proposed in [P2] improves the operation by applying the computational control delay compensation method presented in Publication [P1]. Thus, the effects of the delays are reduced also in this case.

3.3.1. Theory

Symmetrical three-phase diode and thyristor rectifier loads connected to balanced sinusoidal mains produce harmonic currents of the order

$$n = 6p \pm 1, p \in [1, 2, 3, \ldots]. \tag{3.8}$$

However, the fifth harmonic has only so-called negative-sequence components and the seventh harmonic only so-called positive-sequence components (Arrillaga and Watson, 2003). Thus, in the synchronous reference frame both harmonics are seen as a sixth harmonic. The same holds true also of the higher-order harmonics. Consequently, the harmonics of orders presented in (3.8) are seen in the synchronous reference frame as the supply frequency multiples of the order

$$n^{\mathrm{s}} = 6p. \tag{3.9}$$

That is, in the synchronous frame tied to the 50 Hz mains, the harmonics are seen as multiples of 300 Hz and the period of the load current is 3.33 ms. Thus, the value of the next current sample can be predicted on the basis of the load current sampled in the previous period.

Unbalanced sinusoidal three-phase quantities can be considered as two vectors rotating counterclockwise and clockwise with the same fundamental angular frequency. These vectors correspond to so-called positive- and negative-sequence components, respectively. In the synchronous reference frame the positive-sequence quantities are seen as a dc component,

while the negative-sequence component corresponds to a harmonic with a frequency of $2f_s$. Thus, from the active filtering viewpoint the unbalance is seen as a harmonic. To be able to compensate the unbalance of the phase currents, the prediction should be done on the basis of the load current measured 10 ms ago. Since this is a multiple of 3.33 ms, both the harmonics and the unbalance can be predicted using the data collected during the previous 10 ms.

In the previous section it was explained that the control delay is approximately $1.5T_s$, where T_s is the sampling period. In the discrete time system, only sampling interval multiples can be handled. Thus, the delay is rounded to $2T_s$. Let us assume that we have stored m samples of the load current in a table during the last 10 ms period. The load current performance at the next sampling instant $t(k+1)$ can be predicted and the control delay compensated using the data measured at time instant $t(k–m+2)$. This yields the active filter current reference equations:

$$i_{\mathrm{fdh}}^{*}(k+1)=i_{\mathrm{ld0}}(k)-i_{\mathrm{ld}}(k-m+2) \tag{3.10}$$

$$i_{\mathrm{fqh}}^{*}(k+1)=-i_{\mathrm{lq}}(k-m+2)\,, \tag{3.11}$$

where k is a discrete time instant, m the number of samples, and i_{ld0} the dc component of the load current represented in the synchronous reference frame.

The method presented previously can be used if the load currents are predictable. However, in the case of the load change the prediction is no longer valid. A solution for this is to use the computational control delay compensation method presented in (3.7) instead of the prediction.

The algorithm change is done by comparing the measured current with the value measured one period ago. In the predictable situation these should be equal. However, because of the inaccuracies in the system (e.g. noise), the new and the old current do not necessarily have exactly the same values. Thus, the condition for the unpredictable load is defined by

$$\left|\underline{i}_1^{s}(k)-\underline{i}_1^{s}(k-m)\right|>\underline{e}_{\max}\,, \tag{3.12}$$

where $\underline{e}_{\max}$ defines the accepted maximum error between the new and the old values.

The reference prediction requires the measured load currents to be stored in the memory. This makes it possible also to determine the d-axis component of the load current as the average of the samples, as proposed also in (Xie et al., 2006). The algorithm for the moving average is

$$\begin{aligned} i_{\mathrm{ld0}}(k)&=\frac{1}{m}\sum_{k-(m-1)}^{k} i_{\mathrm{ld}}(k) \\ &=\frac{1}{m}i_{\mathrm{ld,\,sum}}(k) \\ &=\frac{1}{m}\left[i_{\mathrm{ld,\,sum}}(k-1)+i_{\mathrm{ld}}(k)-i_{\mathrm{ld}}(k-m)\right] \end{aligned}\,. \tag{3.13}$$

In the case of step change in the fundamental load current component, the new dc value will be found after m samples.

The average can be determined using a 10 ms period only if a half-wave symmetrical load current can be assumed. If this assumption cannot be made, the measurement data collected during the whole fundamental period has to be used. In the case of a 10 ms averaging period, the system can be considered as a low-pass filter that filters completely only the multiples of 100 Hz, while the other frequencies impair the performance. However, the prediction-based reference generation method was suitable for use with predictable loads where the distortion is within the allowed harmonic frequencies.

The block diagram of the proposed reference generation algorithm constructed with the computational control delay compensation (CDC) and the prediction-based reference generation is illustrated in Fig. 3.14. The content of the block "CDC" was shown in Fig. 3.11. In Fig. 3.14, $\underline{i}^{*s}_{fh,CDC}$ and $\underline{i}^{*s}_{fh,pred}$ correspond to the current reference candidate calculated using the CDC method and the prediction method, respectively.

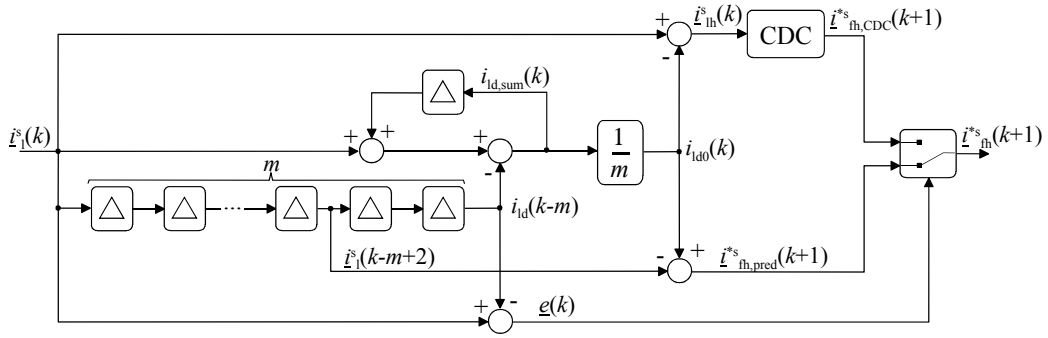

Fig. 3.14. Block diagram of proposed prediction-based reference generation and calculation of moving average.

3.3.2. Filtering Characteristics

The performance of prediction-based reference generation applied to the voltage-source shunt active filter can be examined with the simplified model shown in Fig. 3.12. In this case the block "Ref. gen." contains the block diagram shown in Fig. 3.14. The parameters can be found in Appendices A, B, and C.

The resulting Bode magnitude diagrams presenting the transfer function from the load current to the supply current in the synchronous reference frame are presented in Fig. 3.15(a) – (d). The results show that harmonics at the frequencies that are multiples of 100 Hz in the synchronous reference frame are compensated effectively. This is because the prediction period is 10 ms. The frequency response for the unpredictable load situation was shown in Fig. 3.13(a) – (d).

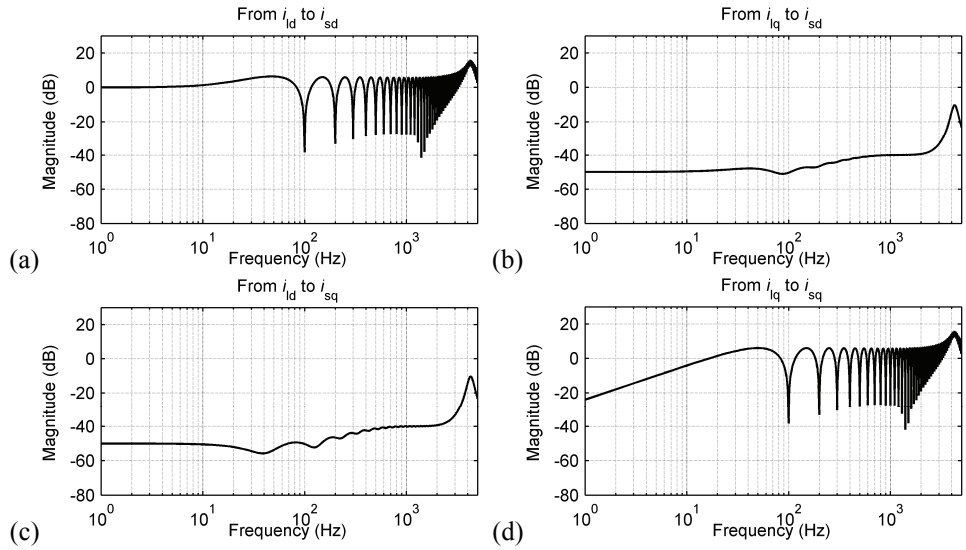

Fig. 3.15. Bode magnitude plots for prediction-based method applied to voltage-source active power filter.

3.4. Current-Sensorless Control of Modified Main Circuit Structure

The conventional voltage-source shunt active filter topology examined previously compensates load current harmonics by absorbing the harmonics through the supply filter. In the control methods, current measurements play an important role. In this section, control of a modified main circuit structure is studied and two current-sensorless control methods are proposed. Because of the modified main circuit structure, the control and processing delays does not affect the filtering characteristics. This section is a summary of Publications [P3] and [P4]. Publication [P3] is an extended version of the original work presented in Related Publication [RP5]. In addition to the theory for the current-sensorless control, Publication [P3] studies the effects of the parameter inaccuracies on the characteristics of the proposed open-loop-type control system and examines the power losses of the active filter. Publication [P4] proposes an improved version of the space-vector control method presented in [P3].

The modified main circuit structure of the active filter is presented in Fig. 3.16. The same kind of main circuit configurations are used in line-interactive uninterruptible power supplies (UPSs), VAr compensators, and active filters in (Joos et al., 1991; Wu, 1995; Ho et al., 1997; Ortúraz et al., 2006). Wu (1995) presents a single-phase circuit for line-interactive UPS where a closed-loop current control has been used to charge the battery and to filter current distortion. A three-phase PWM VAr compensator has been presented by Joos et al. (1991). The main circuit is the same as that examined in Publications [P3] and [P4], but the system adopts the power angle control to keep the dc-link voltage constant and the modulator used is based on an optimized PWM pattern and constant modulation index. This leads to certain constraints on the operation of the system. Ortúraz et al. (2006) use the same control principle as Joos et al. (1991), but instead of the two-level PWM bridge, an 81-level voltage-source active power filter with an ultracapacitor dc link has been proposed. A single-phase active filter where the circuit is connected in series with the load is presented in (Pan et al., 2005). The control of the mains currents is based on hysteresis control.

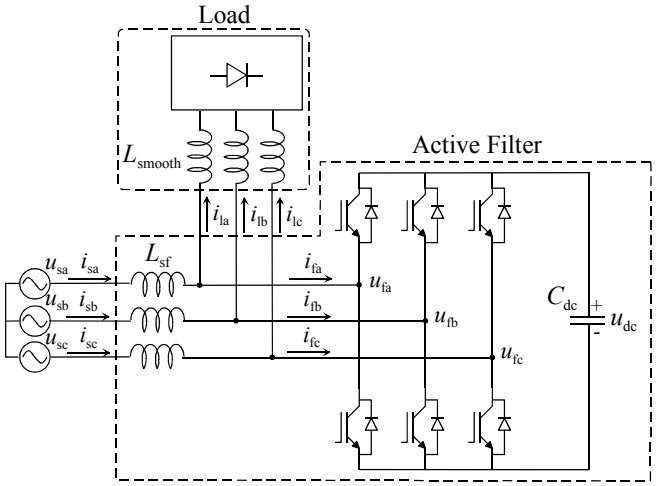

Fig. 3.16. Modified main circuit structure.

In the modified main circuit structure shown in Fig. 3.16, the load is connected directly to the PWM voltage produced with the IGBT bridge. Thus, in the case of a diode or thyristor rectifier load, inductors L_{smooth} are needed to smooth the commutation of the load bridge components. In general, the load to be compensated has to be of a current-source type. The active filter compensates current distortion caused by the load, but the mains reactive power can also be controlled.

3.4.1. Basic Control Method

The basic principle of the proposed current-sensorless active filter is that a sinusoidal current will flow through an inductor if a sinusoidal voltage is applied over this. We can find this in (3.14), which presents the inductor voltage vector $\underline{u}_{\mathrm{L}}$ for the circuit shown in Fig. 3.16:

$$\underline{u}_{\mathrm{L}} = \underline{u}_{\mathrm{s}} - \underline{u}_{\mathrm{f}} = L_{\mathrm{sf}} \frac{d\underline{i}_{\mathrm{s}}}{dt} + R_{\mathrm{sf}} \underline{i}_{\mathrm{s}}, \tag{3.14}$$

where L_{sf} and R_{sf} are, respectively, the inductance and resistance of the inductor. If we write (3.14) in the synchronous reference frame, we have

$$\underline{u}_{\mathrm{L}}^{\mathrm{s}} = \underline{u}_{\mathrm{s}}^{\mathrm{s}} - \underline{u}_{\mathrm{f}}^{\mathrm{s}} = L_{\mathrm{sf}} \left(\frac{d\underline{i}_{\mathrm{s}}^{\mathrm{s}}}{dt} + \mathrm{j}\omega_{\mathrm{s}} \underline{i}_{\mathrm{s}}^{\mathrm{s}} \right) + R_{\mathrm{sf}} \underline{i}_{\mathrm{s}}^{\mathrm{s}}. \tag{3.15}$$

The fundamental frequency quantities are now seen as dc components and usually the angular velocity ω_{s} of the supply voltage vector can also be considered to be constant. Thus, it is obvious in (3.15) that constant current vector $\underline{i}_{\mathrm{s}}^{\mathrm{s}}$ results in the constant voltage vector $\underline{u}_{\mathrm{L}}^{\mathrm{s}}$ since the derivative term in the previous equation becomes zero. Hence, we can write (3.15) as

$$\underline{u}_{\mathrm{L}}^{\mathrm{s}} = \underline{u}_{\mathrm{s}}^{\mathrm{s}} - \underline{u}_{\mathrm{f}}^{\mathrm{s}} = \mathrm{j}\omega_{\mathrm{s}} L_{\mathrm{sf}} \underline{i}_{\mathrm{s}}^{\mathrm{s}} + R_{\mathrm{sf}} \underline{i}_{\mathrm{s}}^{\mathrm{s}}, \tag{3.16}$$

which is in component form

$$u_{\mathrm{Ld}} = u_{\mathrm{sd}} - u_{\mathrm{fd}} = -\omega_{\mathrm{s}} L_{\mathrm{sf}} i_{\mathrm{sq}} + R_{\mathrm{sf}} i_{\mathrm{sd}} \tag{3.17a}$$

$$u_{\mathrm{Lq}} = u_{\mathrm{sq}} - u_{\mathrm{fq}} = \omega_{\mathrm{s}} L_{\mathrm{sf}} i_{\mathrm{sd}} + R_{\mathrm{sf}} i_{\mathrm{sq}}. \tag{3.17b}$$

These equations hold true if the synchronous reference frame voltage $\underline{u}_{\mathrm{L}}^{\mathrm{s}}$ is constant. Consequently, in the stationary reference frame the voltage $\underline{u}_{\mathrm{L}}$ and the current $\underline{i}_{\mathrm{s}}$ are

sinusoidal. The current vector $\underline{i}_s^s$ can be controlled by the voltage $\underline{u}_L^s$ by means of voltage vector $\underline{u}_f^s$ produced with the active filter.

Since the active filter is connected parallel with the load, the load considers the active filter as an ac-voltage source. The supply current $\underline{i}_s^s$ is the sum of the load current $\underline{i}_l^s$ and the active filter current $\underline{i}_f^s$ ($\underline{i}_s^s = \underline{i}_l^s + \underline{i}_f^s$), and we can conclude that if the active filter keeps the voltage over the inductor L_{sf} constant in the synchronous coordinate system (3.15), the mains current $\underline{i}_s^s$ is purely dc and the distortion components of the load current $\underline{i}_l^s$ circulate through the active filter. Thus, the active filter should adjust the voltage vector $\underline{u}_L^s$ so that the average active power drawn from the mains equals the average load power plus the power losses in the active filter. This idea has also been used in (Joos et al., 1991; Wu, 1995; Ortúraz et al., 2006).

The block diagram of the digital current-sensorless space-vector control proposed in Publication [P3] is presented in Fig. 3.17. The system is implemented in the synchronous reference frame. The dc-link voltage can be controlled with the d-axis current i_{fd} (Kwon et al., 1999). The controller used is a PI(e^2) controller presented in section 2.3.1. This is examined in more detail in Publication [P3]. Since the resistance of the choke inductor at the fundamental frequency is negligible compared with the inductance part, the steady-state equation (3.17b) shows that the active filter d-axis current i_{fd} ($i_{fd} = i_{sd} - i_{ld}$) can be controlled by acting on the voltage u_{fq}. Thus, the dc-link voltage controller gives the reference u_{Lq}^* for the q-axis inductor voltage and the active filter voltage reference u_{fq}^* is calculated by subtracting this from the measured supply voltage u_{sq}.

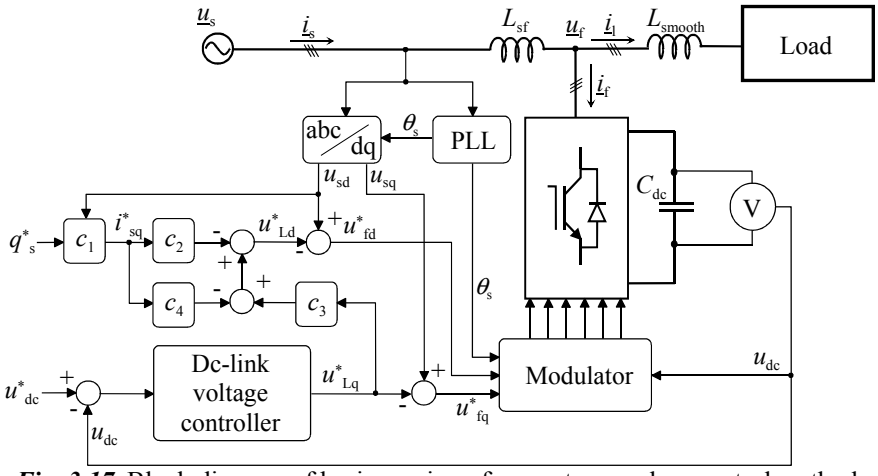

Fig. 3.17. Block diagram of basic version of current-sensorless control method.

The instantaneous imaginary power drawn from the mains can be controlled in open-loop manner. On the basis of (2.17), assuming $u_{sq} = 0$, we can calculate the reference value i_{sq}^* for the supply current quadrature component which carries the given imaginary power reference q_s^*:

$$i_{sq}^* = -\frac{2}{3u_{sd}} q_s^* . \tag{3.18}$$

When the inductance L_{sf} and the resistance R_{sf} of the filter choke used are known, the equation for the active filter voltage reference u_{fd}^* can be derived from (3.17) and (3.18). This can be expressed in the form

$$u_{fd}^* = u_{sd} - \left(-\omega_s L_{sf} i_{sq}^* + \frac{R_{sf}}{\omega_s L_{sf}} u_{Lq}^* - \frac{R_{sf}^{\ 2}}{\omega_s L_{sf}} i_{sq}^* \right). \tag{3.19}$$

According to (3.18) and (3.19), the factors in Fig. 3.17 are: $c_1 = -2/(3u_{sd})$, $c_2 = \omega_s L_{sf}$, $c_3 = R_{sf}/(\omega_s L_{sf})$, and $c_4 = R_{sf}^2/(\omega_s L_{sf})$.

The proposed control system now performs as follows: in the stationary operating point the dc-link voltage controller has adjusted the voltage vector $\underline{u}_L$ so that the active power drawn from the supply equals the average power drawn by the load plus the power losses in the active filter ($P_s = P_l + P_f$). If the load changes, the power balance is disturbed and this is seen as a change in the active filter dc-link voltage. The dc-link voltage controller corrects this change by adjusting the voltage $\underline{u}_L$ to balance the active powers.

Although the control system does not require any information on currents, over-current protection is required to guarantee safe operation and to protect hardware. The functionality could be implemented e.g. by using current transducers or intelligent power semiconductor modules, where the over-current protection is a built-in feature. However, the current measurements used for the protection purposes do not have to be accurate, because the compensation result does not depend on them.

3.4.2. Improved Control Method

If the current-sensorless control of the modified main circuit structure is based on the steady state equations (3.17a) and (3.17b), change in the operating point, e.g. change in the active or reactive powers drawn from the mains, may cause problems. This is examined in Publication [P4], where an improved control method was also proposed. In the following, the problem caused by the control system presented in [P3] and the solution proposed in [P4] are briefly assessed.

In the analysis, the supply is considered to be an ideal three-phase voltage source, i.e. u_{sd} is constant and u_{sq} equals zero. As an initial condition for the examination, the active filter voltage vector $\underline{u}_f(t)$ equals the supply voltage vector $\underline{u}_s$ at $t = 0$:

$$\underline{u}_f(t) = \underline{u}_s(t) = (u_{sd} + j0)e^{j\omega_s t},\ t = 0, \tag{3.20}$$

and current $\underline{i}_s(0) = 0$. If the reference q^* in the control system presented in Fig. 3.17 changes stepwise at time instant $t = 0$, this results in a stepwise change in the d-axis component of the voltage $\underline{u}_f$ and the following equation presented in a stationary reference frame holds true ($u_{sd} \neq u_{fd}$):

$$(u_{sd} - u_{fd})e^{j\omega_s t} = u_{Ld}e^{j\omega_s t} = \left(L_{sf}\frac{d}{dt} + R_{sf} \right)\underline{i}_s(t),\ t > 0. \tag{3.21}$$

If we solve the current $\underline{i}_s(t)$ from (3.21), we have

$$\underline{i}_{\mathrm{s}}(t) = \frac{u_{\mathrm{Ld}}}{\mathrm{j}\omega_{\mathrm{s}} L_{\mathrm{sf}} + R_{\mathrm{sf}}} e^{\mathrm{j}\omega_{\mathrm{s}} t} - \frac{u_{\mathrm{Ld}}}{\mathrm{j}\omega_{\mathrm{s}} L_{\mathrm{sf}} + R_{\mathrm{sf}}} e^{-\frac{R_{\mathrm{sf}}}{L_{\mathrm{sf}}} t}, \; t > 0, \tag{3.22}$$

as shown in Publication [P4]. From the result it can be concluded that the step change in the d-axis component of the active filter voltage results in an attenuating transient

$$\underline{i}_{\mathrm{s,dc}} = \frac{u_{\mathrm{Ld}}}{\mathrm{j}\omega_{\mathrm{s}} L_{\mathrm{sf}} + R_{\mathrm{sf}}}, \tag{3.23}$$

the time constant of which is $L_{\mathrm{sf}}/R_{\mathrm{sf}}$. Thus, if the resistance R_{sf} in the filter inductor is small compared with the inductance L_{sf}, the change in the voltage u_{fd} leads to a performance that the steady state equations do not predict. The result corresponding to (3.22) is obtained also if the q-axis voltage u_{fq} changes stepwise.

To overcome the problem presented above, the control should be based on the equation that takes into account also the transient performance, i.e. (3.15) and its component forms. If the voltage references $\underline{u}_{\mathrm{f}}^{*\mathrm{s}}$ are calculated on the basis of the current references, we have

$$u_{\mathrm{fd}}^{\;*}(t) = u_{\mathrm{sd}}(t) - R_{\mathrm{sf}} i_{\mathrm{sd}}^{*}(t) - L_{\mathrm{sf}} \frac{di_{\mathrm{sd}}^{*}(t)}{dt} + \omega L_{\mathrm{sf}} i_{\mathrm{sq}}^{*}(t) \tag{3.24a}$$

$$u_{\mathrm{fq}}^{\;*}(t) = u_{\mathrm{sq}}(t) - R_{\mathrm{sf}} i_{\mathrm{sq}}^{*}(t) - L_{\mathrm{sf}} \frac{di_{\mathrm{sq}}^{*}(t)}{dt} - \omega L_{\mathrm{sf}} i_{\mathrm{sd}}^{*}(t). \tag{3.24b}$$

Implementation of pure derivations of (3.24a) and (3.24b) may be a problem in numerical control systems. However, they can be implemented for example by applying low-pass filters to the current references $i_{\mathrm{sd}}^{\;*}$ and $i_{\mathrm{sq}}^{\;*}$, as presented by Ollila (1993). In the Laplace transformed form the resulting voltage references are

$$U_{\mathrm{fd}}^{\;*}(s) = U_{\mathrm{sd}}(s) - \frac{sL_{\mathrm{sf}} + R_{\mathrm{sf}}}{\tau_{\mathrm{c}} s + 1} I_{\mathrm{sd}}^{*}(s) + \frac{\omega L_{\mathrm{sf}}}{\tau_{\mathrm{c}} s + 1} I_{\mathrm{sq}}^{*}(s) \tag{3.25a}$$

$$U_{\mathrm{fq}}^{\;*}(s) = U_{\mathrm{sq}}(s) - \frac{sL_{\mathrm{sf}} + R_{\mathrm{sf}}}{\tau_{\mathrm{c}} s + 1} I_{\mathrm{sq}}^{*}(s) - \frac{\omega L_{\mathrm{sf}}}{\tau_{\mathrm{c}} s + 1} I_{\mathrm{sd}}^{*}(s), \tag{3.25b}$$

where τ_{c} is the time constant of the low-pass filter. The compensator presented was originally proposed for the vector-controlled PWM rectifier by Ollila (1993).

The improved current-sensorless control system for the modified main circuit structure is shown in Fig. 3.18. The dc-link voltage controller gives the reference $i_{\mathrm{sd}}^{\;*}$ for the d-axis component of the supply current. In contrast, the reference $i_{\mathrm{sq}}^{\;*}$ for the q-axis supply current component is calculated in open-loop manner from the reactive power reference $q_{\mathrm{s}}^{\;*}$, as presented in (3.18). This is done in the block "*c*". The active filter voltage references $u_{\mathrm{fd}}^{\;*}$ and $u_{\mathrm{fq}}^{\;*}$ are calculated on the basis of the discretized forms of (3.25a) and (3.25b), and finally they are given to the space-vector modulator.

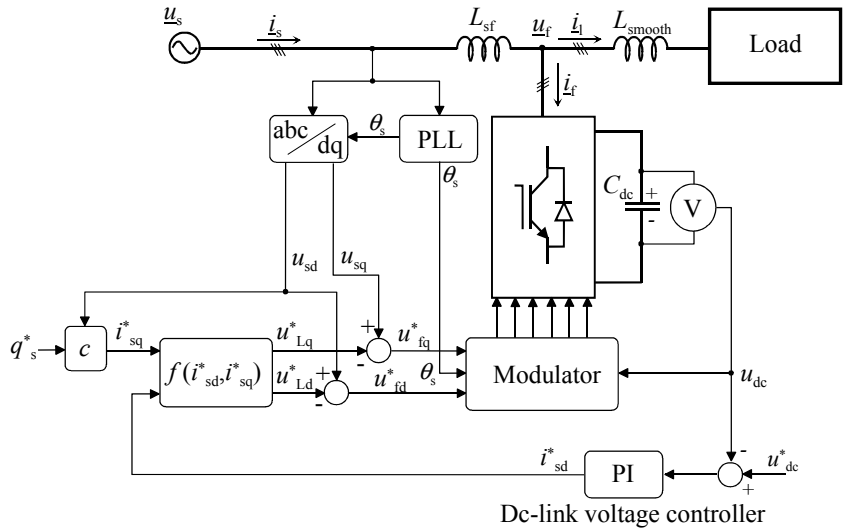

Fig. 3.18. Block diagram of improved version of current-sensorless control.

3.5. Results and Conclusions

In this section, harmonic compensation characteristics of the methods presented in Publications [P1] – [P4] are examined through measurement results. The main circuit and control system parameters can be found in Appendices A and B. In the tests, two different harmonics producing loads have been used. First, a three-phase diode rectifier supplied an RL-type load ($R = 64\ \Omega$, $L = 10$ mH) and, second, the rectifier supplied an RC-type load ($R = 64\ \Omega$, $C = 1$ mF). Figure 3.19 shows the measured load current waveforms and their harmonic contents in the case of the RL-type load. The resulting supply current waveforms obtained using an active filter without control delay compensation [RP1], with the CDC method [P1], with the prediction-based method [P2], and with the current-sensorless solution [P3], are shown, respectively, in Fig. 3.20(a) – (d). Furthermore, harmonic contents of the currents and total harmonic distortions of the currents and the supply voltage are presented, respectively, in Fig. 3.21 and Table 3.2. Similarly, the results corresponding to the RC-type load situation can be found in Figs. 3.22 – 3.24 and Table 3.3. Furthermore, Fig. 3.25(a) – (b) shows the measured supply current harmonic components versus the corresponding load current harmonic components in the case of the RL-type and the RC-type loads. Measurement results of the improved current-sensorless solution proposed in [P4] are not presented here because the results are practically identical with Fig. 3.20 (d).

The total harmonic distortions (THD) presented in Tables 3.2 – 3.3 have been calculated as (Mohan et al., 1995)

$$\mathrm{THD}_{n\cdot 50\,\mathrm{Hz}} = \frac{\sqrt{\sum_{i=2,3,\ldots}^{n} \hat{x}_i^{\,2}}}{\hat{x}_1}, \tag{3.26}$$

where n is either 40 or 400 and the corresponding total harmonic distortion notations are, respectively, $\mathrm{THD}_{2\,\mathrm{kHz}}$ or $\mathrm{THD}_{20\,\mathrm{kHz}}$. The lower limit is chosen, because in the standards

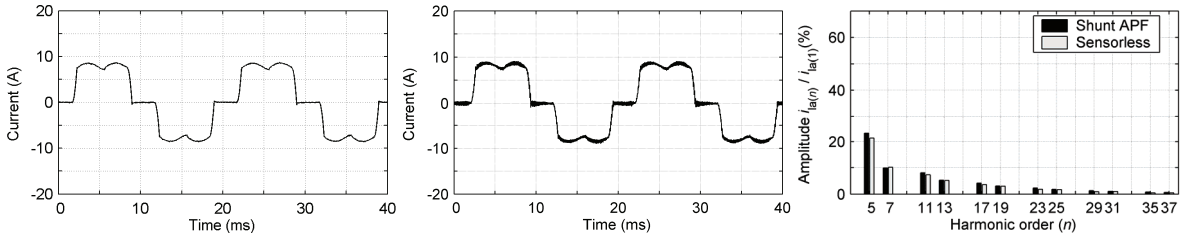

(a) (b) (c)

Fig. 3.19. Measured load current waveform when the diode bridge supplies an RL load and a (a) shunt active filter and (b) modified main circuit structure is used. (c) Harmonic content of currents shown in (a) and (b).

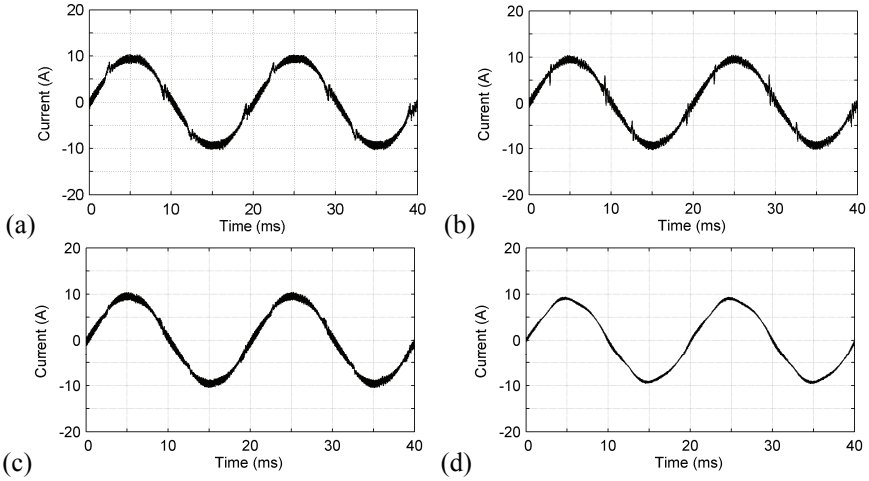

(a) (b) (c) (d)

Fig. 3.20. Measured supply current waveform when an active filter compensates harmonics of a diode bridge with an RL load. A shunt active filter operates (a) without control delay compensation, (b) with computational control delay compensation, and (c) with prediction-based reference generation method. (d) Modified main circuit structure with current-sensorless control.

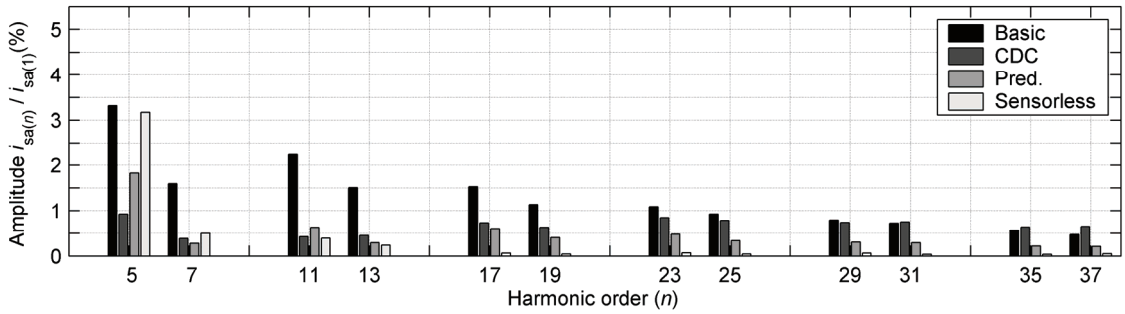

Fig. 3.21. Measurement results. Supply current harmonics versus the fundamental frequency component when the load is a diode rectifier with an RL load.

Table 3.2.
Total harmonic distortions, RL-type load

		Conventional Shunt Active Power Filter				Modified Main Circuit Structure	
		Load	Supply			Load	Supply
			Basic	CDC	Pred		
Current	$THD_{2\ kHz}$	27.8 %	5.3 %	2.4 %	2.3 %	25.9 %	3.3 %
	$THD_{20\ kHz}$	27.9 %	8.5 %	8.7 %	6.6 %	26.2 %	4.2 %
	$i_{s(1)}$		9.5 A	9.4 A	9.5 A		9.0 A
	$i_{l(1)}$		9.0 A	8.9 A	9.0 A		9.0 A
Volt	$u_{s(1)}$		329 V	330 V	331 V		327 V
	$THD_{2\ kHz}$		1.6 %	1.6 %	1.7 %		1.4 %

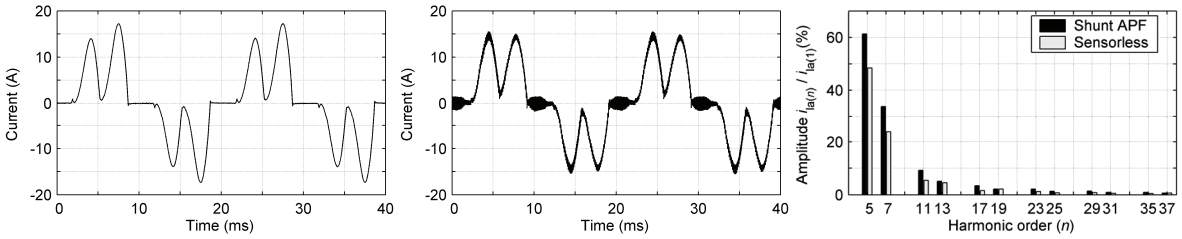

Fig. 3.22. Measured load current waveform when the diode bridge supplies an RC load and a (a) shunt active filter and (b) modified main circuit structure is used. (c) Harmonic content of currents shown in (a) and (b).

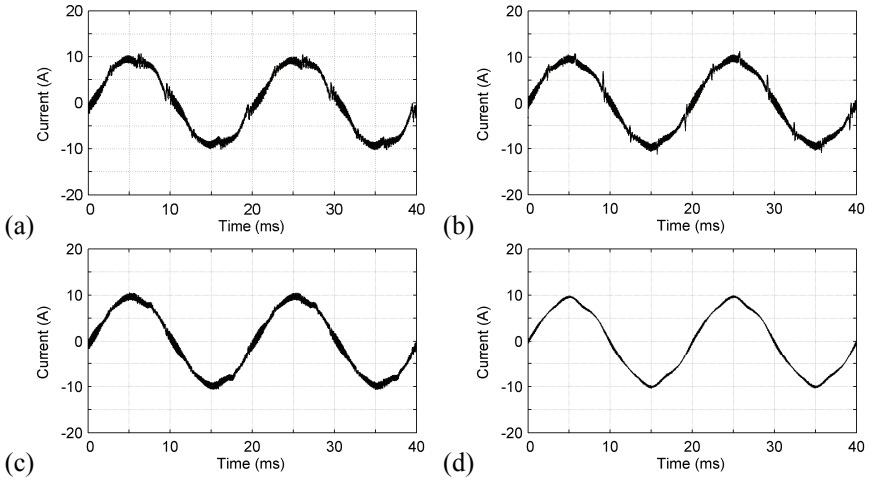

Fig. 3.23. Measured supply current waveform when an active filter compensates harmonics of a diode bridge with an RC load. A shunt active filter operates (a) without control delay compensation, (b) with computational control delay compensation, and (c) with prediction-based reference generation method. (d) Modified main circuit structure with current-sensorless control.

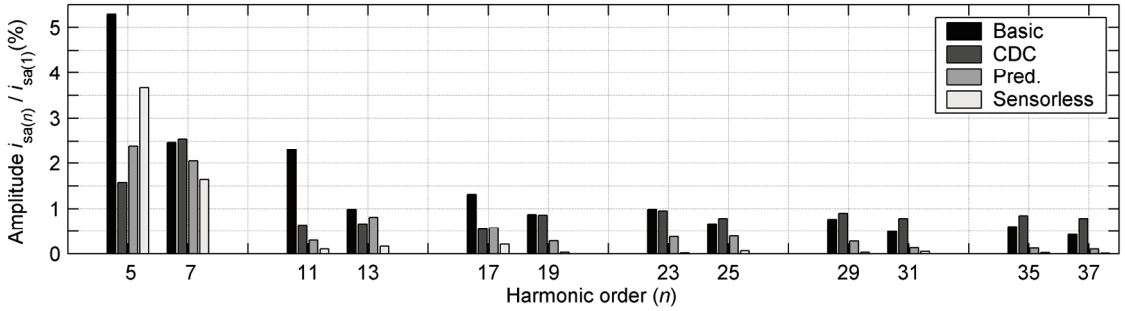

Fig. 3.24. Measurement results. Supply current harmonics versus the fundamental frequency component when the load is a diode rectifier with an RC load.

Table 3.3.
Total harmonic distortions, RC-type load

		Conventional Shunt Active Power Filter				Modified Main Circuit Structure	
		Load	Supply			Load	Supply
			Basic	CDC	Pred		
Current	$THD_{2\,kHz}$	72.0 %	7.0 %	4.6 %	3.6 %	54.7 %	4.1 %
	$THD_{20\,kHz}$	72.1 %	10.4 %	9.6 %	7.6 %	55.1 %	4.7 %
	$i_{s(1)}$		9.4 A	9.5 A	9.6 A		9.4 A
	$i_{l(1)}$		8.9 A	9.3 A	9.1 A		9.8 A
Volt	$u_{s(1)}$		330 V	330 V	330 V		329 V
	$THD_{u,2\,kHz}$		1.7 %	1.7 %	1.8 %		1.1 %

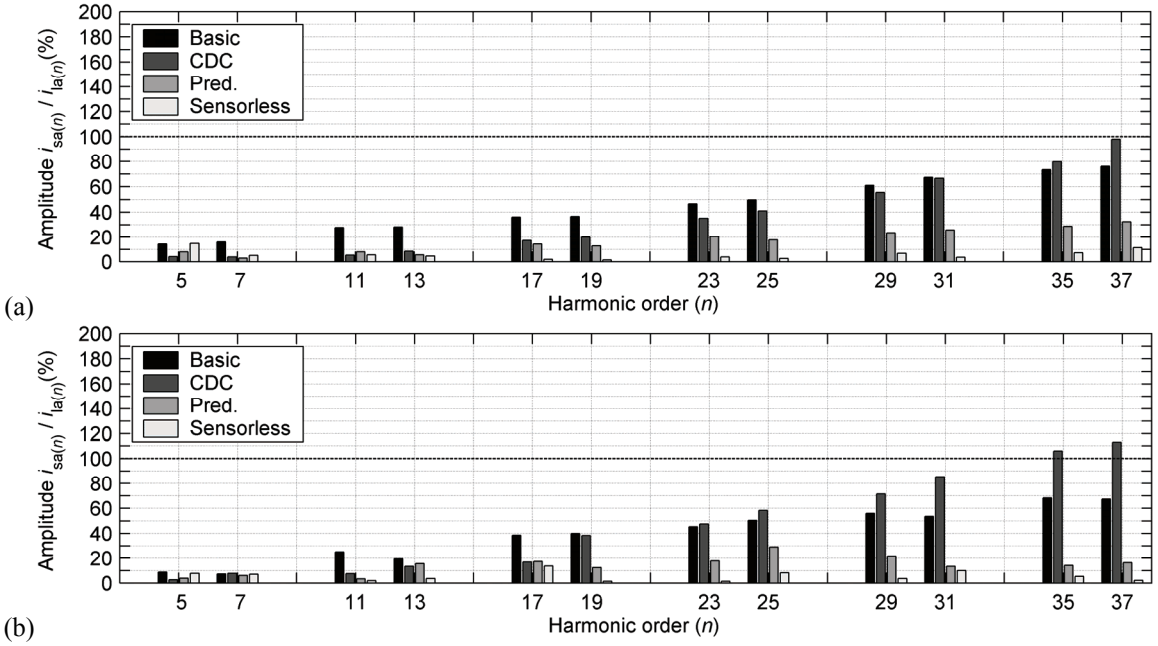

Fig. 3.25. Measurement results. Supply current harmonic components versus the corresponding load-current harmonic components when the load is a diode rectifier with (a) an RL load and (b) an RC load.

CEI/IEC 61000-3-2:2000+A1:2001+A2:2004 (2004) and CEI/IEC 61000-3-12:2004 (2004) the 40th harmonic is the highest-order harmonic taken into account and in the technical report CEI/IEC 61000-3-4:1998 (1998) the THD is defined to be calculated up to the 40th harmonic. However, to figure out the amount of the most important switching ripple component, the $THD_{20\,kHz}$ values calculated up to 20 kHz have also been presented. The harmonic components used in the THD computations have been calculated with discrete Fourier transform algorithm using Matlab. The total harmonic distortions have been calculated throughout this thesis and Publications [P1] – [P8] as defined in (3.26) and as described previously.

Characteristics of each of the methods are clearly seen in the results presented in Figs. 3.20 – 3.25 and Tables 3.2 – 3.3. The control delays cause the current glitches seen in Figs. 3.20(a) and 3.23(a), resulting in the impaired harmonic filtering. The computational control delay compensation method improves the filtering of the low-order harmonics and reduces the glitches. However, the harmonics above 1.5 kHz have been increased compared with the basic method. This behavior was predicted in the frequency responses presented in Fig. 3.13. The filtering characteristic can be further improved using the prediction-based current reference generation, and as a result the lowest $THD_{2\,kHz}$ values are obtained. The results show that also the modified main circuit structure with the current-sensorless control offers effective compensation characteristics. Especially, filtering of high-order harmonics has been improved, but conversely the filtering of the 5th and 7th harmonics has been impaired. This is mainly because of the non-ideal characteristics of the PWM bridge, as discussed in Publication [P3].

In practical implementation of the prediction-based reference generation, problems may arise if the sampling frequency is not a multiple of the fundamental mains voltage frequency. This can be due to slight variations in the supply voltage frequency, for example. Consequently, the prediction is incorrect and the control delay compensation would be used for the reference generation. Furthermore, to ensure robust extraction of the fundamental component regardless of the frequency fluctuations or variations, a low-pass-filter solution different than the averaging-based method presented in Publication [P2] should be preferred. However, the prediction-based reference generation could still be used.

A drawback of the modified main circuit structure is that the load to be compensated is connected directly to the PWM voltage produced with the bridge. Because of this, the active filter cannot be used as a general compensation solution. The system is suitable for the inductive type of loads. To smooth the commutation of a diode or thyristor rectifier bridge components and to filter the PWM frequencies from the load current, the inductors have to be installed in front of the bridge.

It should be noted that the measured waveforms presented in Figs. 3.20 and 3.23 are not exactly the same as those presented in Publications [P1] – [P4]. This is because the measurement results presented here were measured in the fall of 2004, while the results presented in Publications [P1] and [P2] were measured in 2002 and 2003. Because of the non-zero short-circuit impedance of the supplying network, the amplitudes and distortions of the supply voltages vary depending on the loading of the supply network. This affects also the harmonics of the load and the compensation characteristics of the active power filter. In addition, in Publication [P1] and [P2] the dc-link voltage was about 680 V in the case of the RL-type load and 730 V in the case of the RC-type load. In contrast, in the results presented in Figs. 3.20 and 3.23 the dc-link voltage was the same for both RL- and RC-type loads, i.e. 730 V. Furthermore, comparison of Fig. 3.16(b) and Fig. 9(b) in Publication [P1] shows that the compensation characteristic of the CDC method has been improved. This is because an error in the microcontroller implementation of the control system was corrected after publishing Publication [P1].

4. LCL-Type Supply Filter

In pulse-width-modulated voltage-source converter applications, L-type supply filters do not always offer sufficient attenuation of switching ripple currents. In active power filters, this is usually solved by using a separate switching ripple filter, as seen in (Malesani et al., 1999; Asiminoaei et al., 2007a; Dumitrescu et al., 2007; Lascu et al., 2007; Özkaya et al., 2007) and [RP2], [RP3], or by using the CL-type supply filter instead of the L-type filter, see (Qiao et al., 2001; Newman et al., 2002; Han et al., 2005; Sozanski, 2004; Sozanski and Jarnut, 2005; Wu et al., 2007a; Xu et al., 2007). Drawbacks of the CL filter are resonance phenomenon and current distortion injected by parallel loads that may overload the capacitors of the filter. Furthermore, changing network parameters may influence the resonance frequency of the filter. Overloading can be prevented by constructing an LCL filter with an additional inductor installed on the line side of the CL filter (Lindgren and Svensson, 1998). In the literature, LCL filters in voltage-source converter and inverter applications have been widely studied and several methods for damping the resonance have been proposed. However, the active filter control systems presented in the literature have been mainly designed for the first-order L-type supply filter.

In the active filter applications, the use of the LCL filter is challenging because of the resonance phenomenon and, on the other hand, hard dynamic response requirements for the control system. In addition, the control delays and phase errors caused by the supply filter significantly impair the filtering characteristics (Lindgren and Svensson, 1998). Thus, a lot of attention should be paid to the control strategy and proper design of the filter.

The resonance can be attenuated with either passive or active methods. In the passive methods, additional damping resistors are connected to the LCL filter (Liserre et al., 2005), while active methods take resonance into account in the control strategy, see e.g. (Bojrup et al., 1999; Dahono, 2002: Twining and Holmes, 2003; Liserre et al., 2004; Bolsens et al., 2005; Loh and Holmes, 2005; Serpa et al., 2005). In the literature, passive damping methods have been said to have drawbacks such as high power losses (Liserre et al., 2004; Serpa et al., 2005). In contrast, several active methods require additional sensors or complex control strategies to maintain system stability (Twining and Holmes, 2003; Liserre et al., 2004; Bolsens et al., 2005; Loh and Holmes, 2005).

Publication [P5] presents a comparison of an active and a passive method for LCL filter resonance damping, assesses their suitability for the active power filter application, and presents their benefits and drawbacks. The examination in [P5] has been carried out using transfer function models and a laboratory prototype. In the following, a summary of Publication [P5] is presented.

4.1. Control

The active filters are controlled based on the load current detection method. The control strategy used with the passively damped LCL filter is implemented in the synchronous frame and it adopts the prediction-based current reference generation method presented in Publication [P2]. The block diagram of the system is shown in Fig. 4.1(a). The idea of the control strategy is to control the current $\underline{i}_{\mathrm{ff}}$ on the PWM bridge side of the LCL filter in the closed loop. The assumption made is that the current $\underline{i}_{\mathrm{f}}$ on the supply side will behave in the same manner, but the switching ripple current circulates through the capacitor C_{f}.

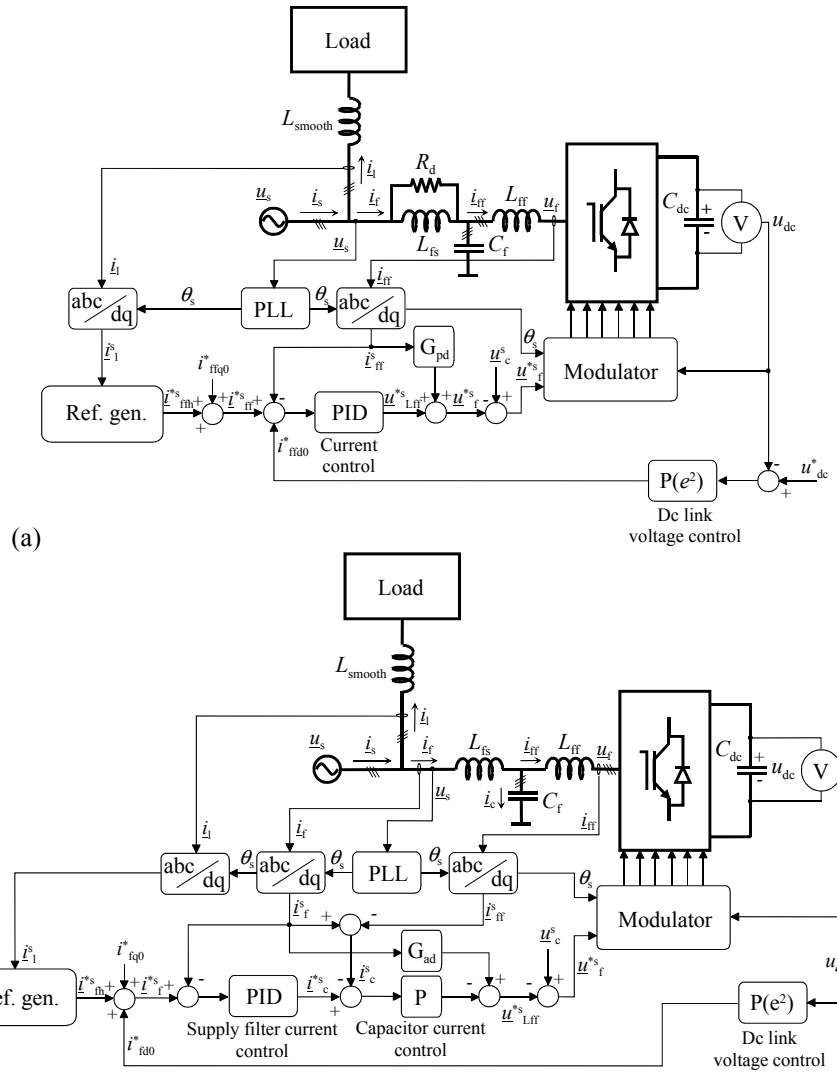

Fig. 4.1. Control system and main circuit configuration for (a) passive damping and (b) active damping.

The control strategy used for the active damping is based on (Twining and Holmes, 2003; Loh and Holmes, 2005), where various active damping methods for the LCL filter in inverter and converter applications have been presented and analyzed. The damping function is based on the cascaded control of the current $\underline{i}_{\mathrm{f}}$ and the capacitor current $\underline{i}_{\mathrm{c}}$. In Publication [P5], the control system presented originally in the stationary reference frame is applied to the active power filter and implemented with rotating coordinate system variables. The block diagram of

the control system is shown Fig. 4.1(b). The harmonic compensation is based on the prediction-based current reference generation method [P2], which generates the reference $\underline{i}_f^{*s}$ for the compensating current vector.

4.1.1. Current Control Characteristics

In Publication [P5], characteristics of the compensating current control are examined using transfer function models. Figures 4.2 and 4.3 show the closed-loop frequency response of the current control. Since the d- and q-axis controls are analogous, only the figures corresponding to the d-axis compensating current are presented. The parameters can be found in Appendices A, B, and C.

Figure 4.2(a) – (b) presenting the control performance of the passively damped LCL filter system shows that the current control bandwidth reaches up to 4 kHz. It can also be seen that at the frequencies close to the LCL circuit resonance frequency (3.1 kHz) there may be a slight oscillation. In addition, the figure shows that the control system prevents the cross couplings between i_{ffq}^* and i_{fd}. Although in Publication [P5] (Section III.B) the active filtering bandwidth is also deduced from Fig. 4.2(a) – (b), this is not the best way to find the bandwidth. Instead of the frequency response between the current reference $\underline{i}_{ff}^*$ and the realized compensating current $\underline{i}_f$, the active filtering bandwidth should be deduced from the frequency response between the load current $\underline{i}_l$ and the supply current $\underline{i}_s$, because this contains the effect of the reference generation.

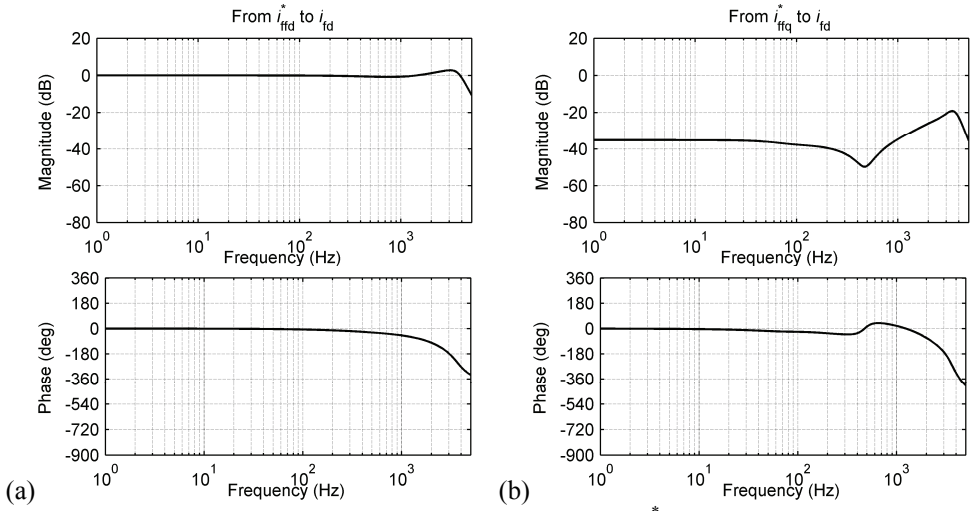

Fig. 4.2. Frequency response (a) from the d-axis current reference i_{ffd}^* to d-axis compensating current i_{fd}, and (b) from the current reference i_{ffq}^* to d-axis compensating current i_{fd} with the closed loop current-controlled passively damped LCL filter.

Figure 4.3(a) and (b) present the behavior of the actively damped LCL filter control. In the figures, different capacitor current control gains (P_{ic}) have been used to show its effect on the closed-loop filter current $\underline{i}_f^s$ control. The figures show that the control causes oscillation near the LCL filter resonance frequency. In addition, the control of the current component i_{fq} causes resonance frequency oscillations in the current component i_{fd}. The oscillation effects

can be reduced by lowering the capacitor current control gain P_{ic}, as can be seen in the figures. However, this also decreases the control bandwidth.

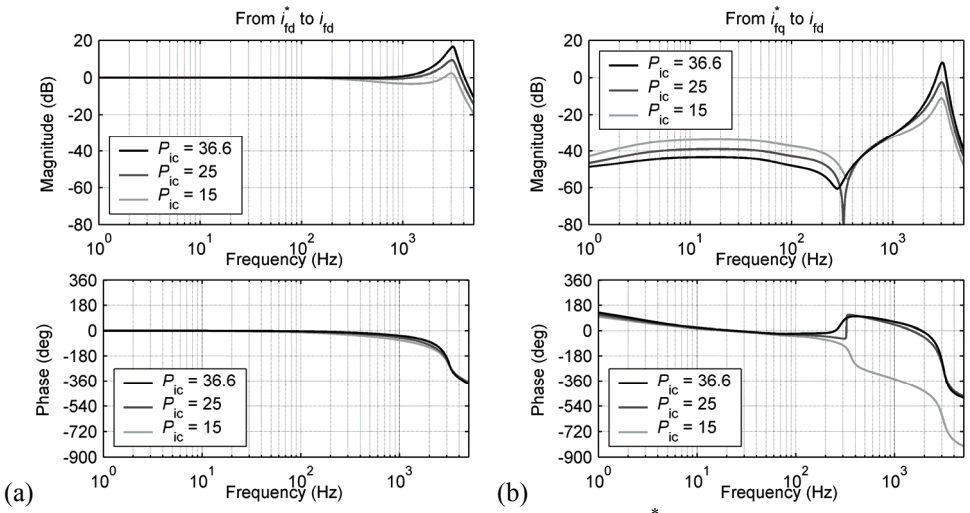

Fig. 4.3. Frequency response (a) from the d-axis current reference i_{fd}^* to the d-axis compensating current i_{fd}, and (b) from the q-axis current reference i_{fq}^* to the d-axis compensating current i_{fd} with the closed-loop current-controlled actively damped LCL filter using different gains (P_{ic}) in capacitor current control.

4.2. Experimental Results

The operational performances of the systems were examined in the laboratory with prototypes designed to compensate harmonics produced by a nonlinear load of 5 kVA nominal power. The parameters of the prototypes can be found in Appendix A. The load current waveform obtained and its harmonic content have been shown in Fig. 4.4(a) – (b).

Figure 4.5 presents the resulting supply currents and their harmonic content. The figures and the $THD_{2\,kHz}$ values show that there is no notable difference in the filtering of harmonics below 2 kHz. In addition, the $THD_{20\,kHz}$ values indicate that both of the systems attenuate the switching ripple effectively. The operation of the systems in the case of the stepwise load changes are presented in Fig. 4.6(a) – (d). As can be seen, the results are similar.

In the tests, the gain of the capacitor current control was selected experimentally. If the gain P_{ic} was 15 or 25, the active filtering did not behave effectively and the resulting supply current contained low-order harmonics. This is in agreement with the frequency responses presented in Fig. 4.3, where it can be seen that the closed-loop performance in active filtering application decreases with low gain values. The supply current $THD_{2\,kHz}$ was minimized using the gain 36.6, and this was chosen to be used in the tests. On the basis of the frequency responses presented in Fig. 4.3, the chosen gain was expected to cause oscillation. However, as can be seen in Fig. 4.5(b), the supply current obtained with the actively damped method behaves smoothly without notable oscillations. This indicates that there is no important excitation at the resonance frequency in stationary operation. In addition, since the system built contains more damping at the resonance frequency than the modeled system, the oscillations do not have as harmful effects as could be predicted with the simulated frequency

responses. However, the results in Fig. 4.6(d) presenting the changing load situation show that the control system causes slight resonances if the compensating current reference changes rapidly, but these decay when a new operating point is achieved.

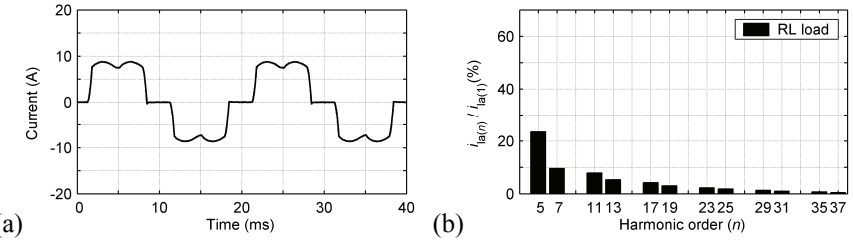

Fig. 4.4. (a) Measured load current waveform under stationary state when the diode bridge supplies an RL load. (b) The load current harmonic components.

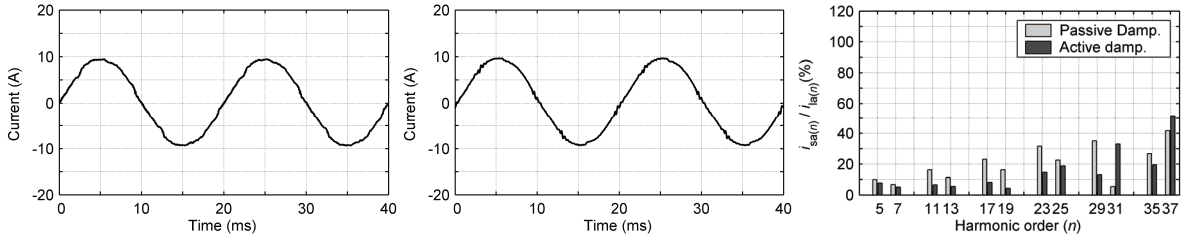

Fig. 4.5. Measured supply current waveforms in stationary state operation with an RL-type diode rectifier load using (a) a passive damping method (THD_{2kHz} 3.2 %, THD_{20kHz} 3.4 %) and (b) an active damping method (THD_{2kHz} 2.1 %, THD_{20kHz} 3.0 %). (c) Harmonics in the supply currents versus the corresponding harmonics in the load current.

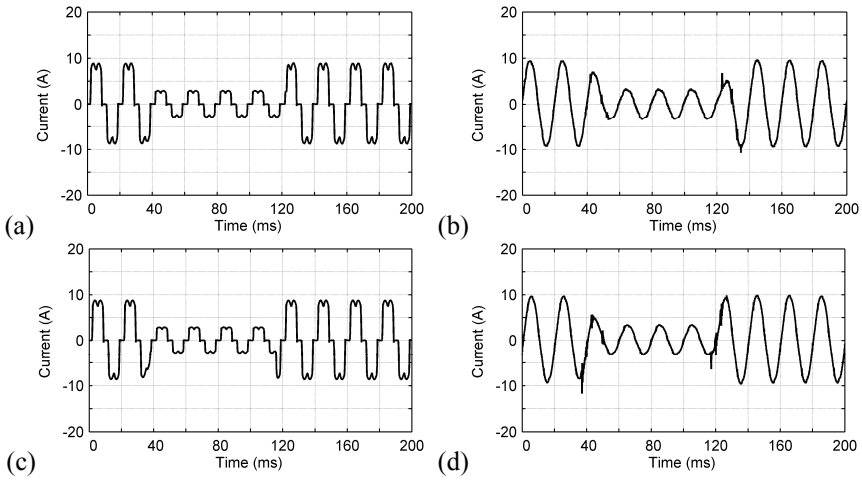

Fig. 4.6. Measurement results when the RL-type diode rectifier load changes stepwise. (a) Load current and (b) supply current using the passive damping method. (c) Load current and (d) supply current using the active damping method.

4.3. Conclusions

The results presented show that in addition to the fast dynamic responses needed in active power filter use, both of the resonance damping methods provide efficient current ripple attenuation. The results can be compared with those in Chapter 3 regarding use of the first-order L-type supply filter. The control system used is the same as that used to control the passively damped LCL filter. The total harmonic distortions of the load and the supply currents presented in Publications [P5] and section 3.5 have been collected in Table 4.1. The

table contains also the total harmonic distortions of the supply voltages. As can be seen, the use of LCL-type supply filters slightly increases $THD_{2\,kHz}$ values compared with the active filter with the L-type filter. However, when an LCL filter has been used, the switching ripple can be greatly reduced. This can be seen by comparing the $THD_{20\,kHz}$ values.

Table 4.1.
Total Harmonic Distortions

		Current			Supply Voltage
Load type	Method	Load $THD_{2\,kHz}$	Supply $THD_{2\,kHz}$	Supply $THD_{20\,kHz}$	$THD_{2\,kHz}$
Diode rectifier + RL load	L filter	27.8 %	2.3 %	6.6 %	1.7 %
	Pass. Damp LCL	27.8 %	3.2 %	3.4 %	1.7 %
	Act. Damp LCL	27.8 %	2.1 %	3.0 %	0.8 %
Diode rectifier + RC load	L filter	71.0 %	3.6 %	7.6 %	1.8 %
	Pass. Damp LCL	65.3 %	3.7 %	4.0 %	0.8 %
	Act. Damp LCL	67.0 %	2.2 %	3.1 %	0.6 %

The active filter efficiencies presented in Fig. 4.7(a) – (b) show that the additional resistors decrease the efficiency, i.e. increase the power losses, only slightly. In the literature, the increase in the power losses has been claimed to be a drawback of the passively damped LCL filter. However, the measurements presented in Publication [P5] show that the additional losses in the passively damped LCL were only about 5 W. This is about 3 % of the total power losses of the active filter and 0.1 % of the nominal power (5 kVA) of the load to be compensated. Compared with the first-order L-type supply filter, the efficiency reduction in the nominal operating point is less than one percentage unit.

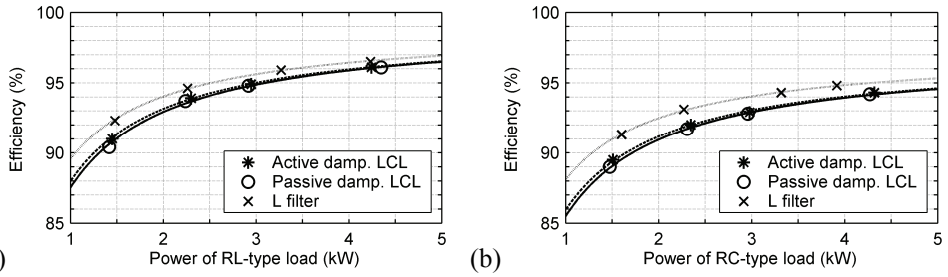

Fig. 4.7. Measured efficiencies using the passive and the active damping methods when the harmonic producing load is a diode bridge with (a) an RL-type load and (b) an RC-type load.

The active resonance damping method examined requires measurements of at least two load phase currents (i_l), two filter phase currents (i_f) and two bridge phase currents (i_{ff}); six current sensors in total. This means that the active resonance damping method requires two sensors more than the passive method which utilizes the control system originally designed for the first-order L-type supply filter. In addition to the higher number of current sensors, the control strategy of the actively damped system is more complicated: there are more controllers to be

tuned and it requires more microcontroller computing time. The benefit of all this is about one percentage unit lower harmonic distortion than that obtained with the passive damping method. However, the actively damped system can be assumed to be more robust for the external disturbances than the passively damped system. For example, if the mains voltages contain a large amount of harmonics, this would impair the performance of the passively damped system, since there is no feedback from the mains side currents in the control system.

5. Effect of SiC Diodes on Semiconductor Power Losses

In this chapter, the power loss profile of the voltage-source active filter is determined and possible benefits obtained by replacing the silicon diodes in the PWM bridge with their silicon carbide (SiC) counterparts are analyzed. This is based on Publication [P6].

Traditionally in power electronic applications, silicon (Si) diodes have been used. However, a major drawback of them is high reverse recovery current causing high switching losses. These constitute a significant proportion of the total power losses in the pulse-width-modulated semiconductor bridge. In addition to the inherent power dissipation in the diodes, the reverse recovery current causes additional turn-on losses in switching devices such as insulated gate bipolar transistors (IGBTs), MOSFETs, etc. (Elasser et al., 2003).

Publication [P6] studies the use of silicon carbide Schottky diodes in voltage-source shunt active power filter application. The conventional three-phase IGBT bridge is constructed with six Si-based IGBTs and six antiparallel Si diodes. In the study, the diodes are replaced with their SiC counterparts to determine their effect on the semiconductor bridge power losses in the active filter. The semiconductor power losses in both of the constructions are determined by calculations and the distribution of the conduction and switching losses is estimated. In the following, the results of the study are summarized.

The power dissipation in the diode consists almost solely of the turn-off losses; turn-on and on-state losses are negligible compared with these (Ozpineci and Tolbert, 2003). According to Elasser et al. (2003), the silicon devices have reached their theoretical limits in terms of reverse recovery time, and the state-of-the-art Si diodes exhibit reverse recovery times as low as 25 ns. Any reduction in the power losses, i.e. in the reverse recovery time, would require a change of material or a drastic improvement of the current technology (Elasser et al., 2003).

An attractive alternative to these so-called silicon PiN diodes are Schottky barrier diodes fabricated in wide bandgap semiconductor materials (Ozpineci et al., 2006). The most promising material candidate is silicon carbide (SiC), but gallium arsenide (GaAs) and gallium nitrate (GaN) are also being investigated (Dolny, 2005; Shen and Omura, 2007).

Power semiconductor devices made of SiC and other wide bandgap materials offer several benefits over their silicon counterparts (Dolny, 2005; Friedrichs and Rupp, 2005; Ozpineci et al., 2006; Shen and Omura, 2007). Due to the higher breakdown field strength of SiC, a thinner drift region is allowed and thus on-resistance of SiC devices is much smaller compared with their silicon counterparts. Therefore, majority-carrier devices like MOSFETs

and Schottky diodes can be used instead of minority-carrier devices such as IGBTs and PiN diodes. This results in greatly reduced switching loss, which enables the use of higher switching frequencies. Consequently, substantially smaller and cheaper passive components can be used. SiC devices can also operate at reasonably higher junction temperatures than Si devices. As a result, the weight, volume, cost, and complexity of thermal management systems can be reduced. In addition, due to the high thermal conductivity of SiC, the thermal resistance of the device die is reduced.

Although SiC offers significant performance advantages compared with Si and the first commercial SiC products, i.e. Schottky barrier diodes, were introduced in 2001 (Friedrichs and Rupp, 2005), there are both economic and technical obstacles that prevent the large-scale commercialization of SiC technology in the near future. For example, SiC substrates contain a high level of defects which limit device yields (Zolper, 2005). In addition, there exist manufacturing difficulties due to the extremely high thermal stability of SiC. Thus, typical fabrication processes are either extremely slow or require excessively high processing temperatures (Dolny, 2005). An important issue is also that PiN rectifiers are a mature product and thus their manufacturing processes are well established and the costs are low (Dolny, 2005). According to Shen and Omura (2007), the cost of SiC devices ranges currently from five to ten times that of silicon devices with the same voltage and current ratings. However, the cost ratio between SiC and silicon is estimated to decrease to three in 3 – 5 years and eventually to one in 8 – 12 years (Shen and Omura, 2007).

5.1. Power Loss Distribution

The measured distribution of power loss between the filter chokes and the semiconductors, including the dc link capacitor, have been presented in Figs. 5.1 and 5.2. The measurements were carried out with the calorimetric measurement setup described in Publication [P6] and in section 2.4.2. In the measurements, the switching frequency was 10 kHz, the dc-link voltage 725 V, and the inductance of the filter choke 5 mH. The results show that the semiconductor bridge used has only a slight effect on the total power losses, whereas the main source for losses is the supply filter.

The power loss distribution between the switching and the conduction losses is shown in Figs. 5.3 and 5.4. Since the measurement configuration did not provide the possibility to separate the switching and conduction losses, the figures illustrate estimates for the distribution. The estimates are based on the calculations presented in Publication [P6].

If we compare the power losses presented in Figs. 5.3 and 5.4, we can see that the conduction losses are almost equal in both of the bridges. Use of the SiC components reduces the switching losses, as could be expected. The reduction in the total semiconductor losses is about 20 % when the RC-type load is compensated. However, the reduction is only about 6.5 % of the total losses in the active power filter main circuit, which improves the efficiency by about 0.4 percentage units.

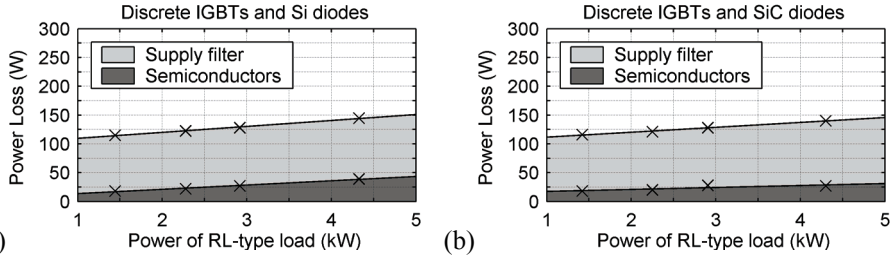

Fig. 5.1. Measured total power loss distribution when the bridge is constructed using discrete IGBTs and (a) Si diodes, (b) SiC diodes. The load to be compensated is a diode bridge with an RL load.

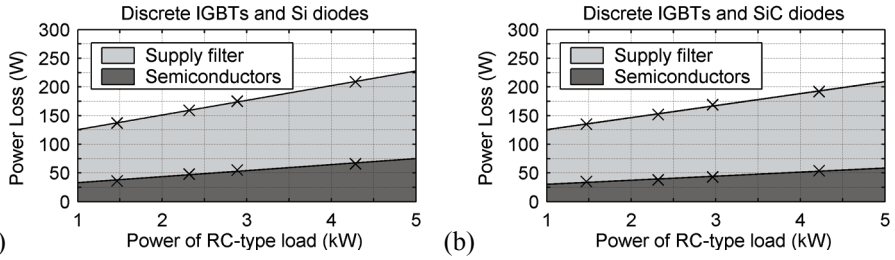

Fig. 5.2. Measured total power loss distribution when the bridge is constructed using discrete IGBTs and (a) Si diodes, (b) SiC diodes. The load to be compensated is a diode bridge with an RC load.

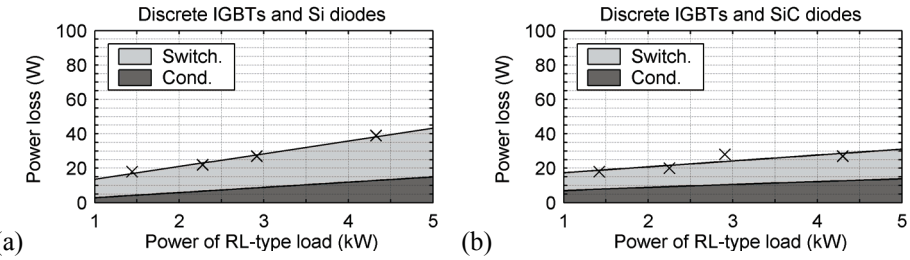

Fig. 5.3. Measured semiconductor losses and estimated power loss distribution when the bridge is constructed using discrete IGBTs and (a) Si diodes, (b) SiC diodes. The load to be compensated is a diode bridge with an RL load.

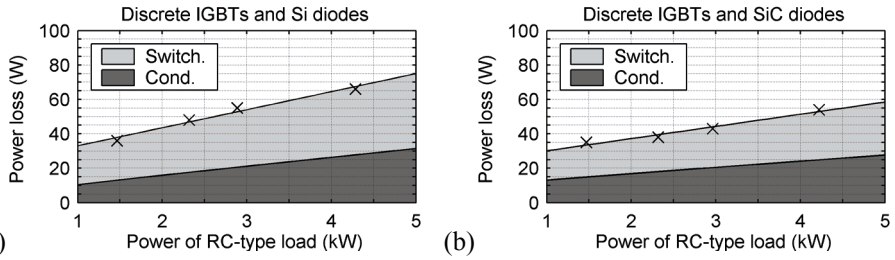

Fig. 5.4. Measured semiconductor losses and estimated power loss distribution when the bridge is constructed using discrete IGBTs and (a) Si diodes, (b) SiC diodes. The load to be compensated is a diode bridge with an RC load.

The analysis and the results presented in Publication [P6] show that SiC diodes provide a reduction in the semiconductor power losses of the active filter. A decrease in semiconductor losses is important because this would allow reducing the cooling. Furthermore, because the SiC devices can operate at higher temperatures (Ozpineci et al., 2006), also this could provide a reduction in the heatsink volume. On the other hand, the smaller power losses make it possible to increase the switching frequency, thus enabling the use of smaller active filter coils.

6. Comparison of Voltage- and Current-Source Active Power Filters

The first active filter implementations were based on the current-source inverter (Gyugyi and Strycula, 1976; Akagi, 1994), but recently research has mainly concentrated on voltage-source active filters. However, some attention has still been paid to current-source active filters (CSAPF), see e.g. (Nishida et al., 2002; Salo, 2002; To et al., 2005; Chao and Grantham, 2006; Pires and Silva, 2006). Since voltage-source PWM technology is widely used in industrial applications, this has also been more commonly used in active filters (Akagi, 1994). Furthermore, current-source technology has been said to have some drawbacks compared with voltage-source systems, such as high on-state losses in the PWM bridge and an inefficient inductive energy storage element on the dc side of the bridge. In the early 2000s, reverse-blocking IGBTs (RB-IGBTs) were introduced (Lindemann, 2001) and they would offer reduction of the on-state losses. Nevertheless, this is still quite a new device, so that its development is still not complete and its availability is limited, too.

So far, both voltage and current-source active filters have been discussed by Grady et al., (1990), Akagi (1994), Yunus and Bass (1996), and Benchaita et al. (1999). Akagi (1994) briefly introduces the main operation principles of the systems. The focus of the literature review presented by Grady et al. (1990) is not the comparison of voltage- and current-source APFs. Instead, it assesses general aspects of advantages and disadvantages of the topologies. Furthermore, the paper was published in 1990 and thus there has been development in both technologies since then. Single-phase voltage and current-source active filters are compared by Yunus and Bass (1996). The operational comparison presented in their paper is mainly based on discussion and simulations. Benchaita et al. (1999) examine three-phase active filters with analog control systems and their paper focuses on power circuit design, such as semiconductor devices, their constraints, and the design of supply filters and dc links. The functional comparison presented by Benchaita et al. (1999) is made by examining the filtering performance in the case where the harmonics are produced by a thyristor rectifier with an RL-type load.

This chapter summarizes the comparison of the digitally controlled and vector-modulated voltage-source and current-source active power filters presented in Publication [P7]. The main circuit configurations and space-vector modulation techniques used are discussed as well as the load current detection -based control systems. In addition, the filtering characteristics, power loss distribution and efficiencies of both systems are examined and compared in various operating points.

6.1. Main Circuit and Control

The main circuits for the voltage-source and current-source shunt active filters are shown in Fig. 6.1. Both of the topologies require a different kind of supply filter (L or LCL vs. LC) and energy-storage elements (capacitor vs. inductor). In addition, the PWM bridge of the voltage-source converter consists of six controllable bidirectional switches constructed using IGBTs and antiparallel diodes. Conversely, the current-source bridge is built with six controllable unidirectional switches. Because of the very low reverse voltage blocking capability of the IGBTs these are typically constructed using diodes in series with the transistors, as shown in Fig. 6.1(b). However, instead of the series connection the use of the RB-IGBTs discussed previously would also be possible. Furthermore, the switching devices of the current-source PWM bridge have to be protected against overvoltages with a separate clamp circuit. One possibility for this is shown in Fig. 6.1(b).

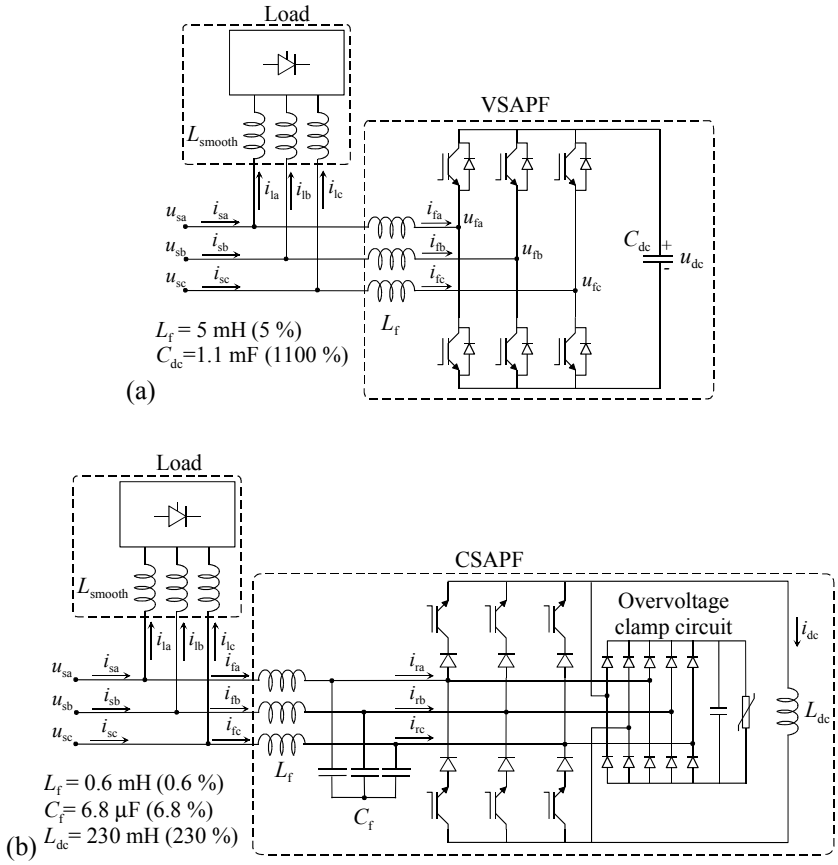

Fig. 6.1. Main circuit of (a) a voltage-source shunt APF and (b) a current-source shunt APF.

The switching vectors of the voltage-source PWM bridge are presented in Fig. 6.2(a). The bridge is controlled such that three switches are simultaneously in on-state, as discussed in Chapter 2. Since the dc voltage u_{dc} is applied over the dc link, it is possible to realize six active vectors ($\underline{u}_{f1} - \underline{u}_{f6}$) and two zero vectors ($\underline{u}_{f7} - \underline{u}_{f8}$). In contrast, the current-source PWM bridge modulates unidirectional dc current and the bridge is controlled such that one of the upper switches and one of the lower switches are in on-state at a time. This results in six possible active vectors ($\underline{i}_{r1} - \underline{i}_{r6}$) and three zero vectors ($\underline{i}_{r7} - \underline{i}_{r9}$), illustrated in Fig. 6.2(b). The

zero vectors are obtained by short-circuiting the dc-link choke by turning on both the upper and the lower switch in a phase.

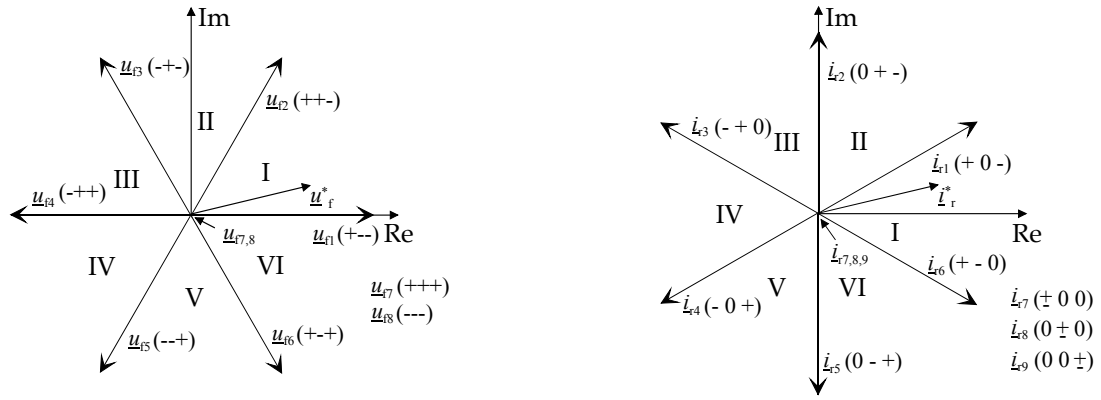

Fig. 6.2. Switching vectors for the (a) voltage-source and (b) current-source PWM bridge.

In the examination presented in Publication [P7], both of the active filters are controlled based on the load current detection method. Furthermore, the compensating current reference is generated using the computational control delay compensation presented in Publication [P1] and in (Salo, 2002; Salo and Tuusa, 2003). The block diagrams are shown in Fig. 6.3(a) – (b). The most important difference in the control structures is that due to the voltage-source nature, the VSAPF prefers closed-loop current control, while the CSAPF enables precise open-loop current control. However, because the open-loop current control may cause resonance of the LC-type supply filter, this has to be taken into account in the control. This is referred to in Fig. 6.3(b) with the block labeled "Res. Damp.". Furthermore, the block "*RG*" refers to the dc-link current reference generation. The resonance damping method and the dc-link current reference generation have been presented in (Salo, 2002; Salo and Tuusa, 2003).

6.2. Filtering Characteristic

The filtering characteristic of the voltage- and current-source active filters was compared with the prototypes built. The parameters have been presented in Appendix A.

The measurement results are shown in Figs. 6.4 – 6.5 and the total harmonic distortions of the waveforms are collected in Table 6.1. The load current waveforms and the harmonic contents are shown in Figs. 3.19(a),(c) and 3.22(a),(c). The results show that the filtering characteristics of the low-order harmonics differ only slightly. However, more important issue is the switching ripple current. The compensating current of the voltage-source APF contains substantially more switching ripple than that of the current-source APF. This is because of the supply filter structure: the second-order LC filter used in the CSAPF offers a low impedance path for the switching ripple, while the first-order L used in VSAPF does not. Thus, from the switching ripple point of view, either of the LCL filter structures discussed in Chapter 4 would be more appropriate for use in this comparison.

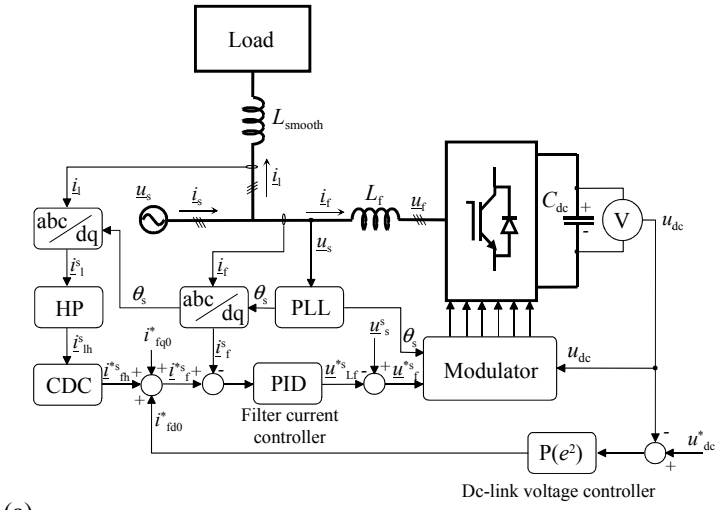

Fig. 6.3. Control system for (a) the voltage-source active power filter and (b) the current-source active power filter.

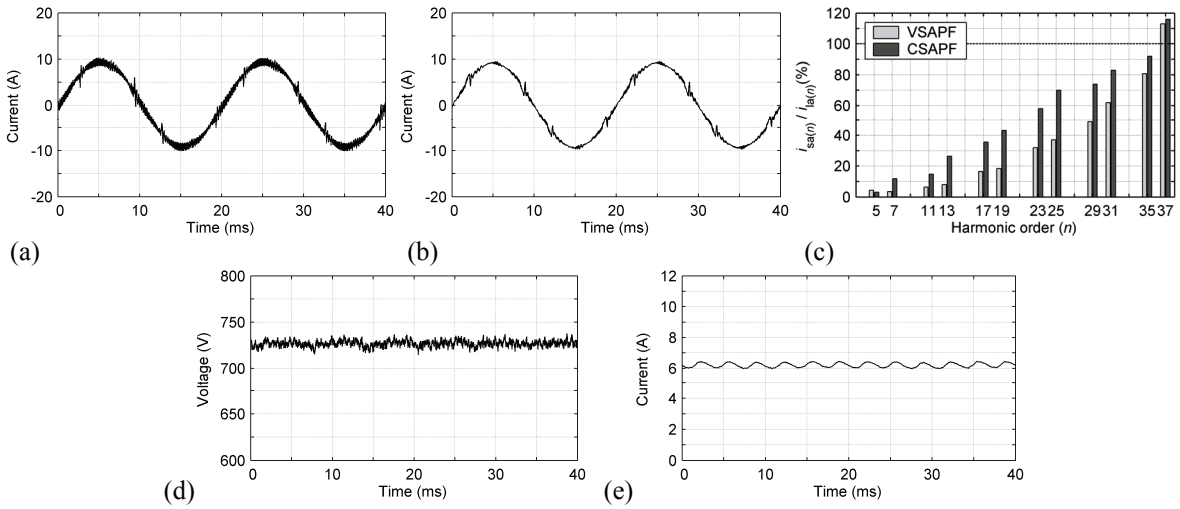

Fig. 6.4. Measurement results when the load is a diode rectifier with an RL load. Supply current with (a) VSAPF and (b) CSAPF (c) Harmonics in the supply currents versus the corresponding harmonics in the load current. (d) VSAPF dc-link voltage. (e) CSAPF dc-link current.

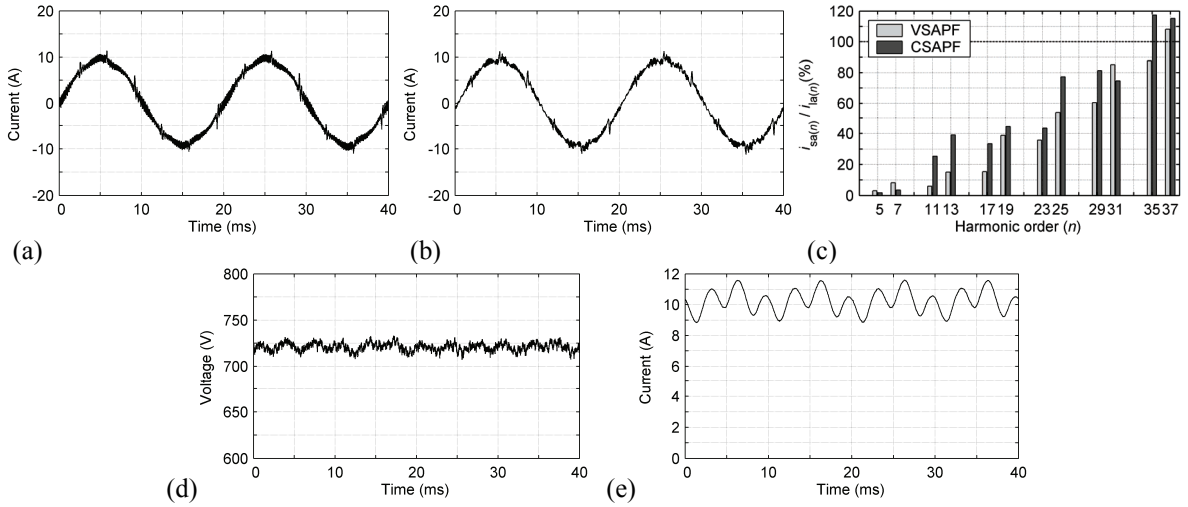

Fig. 6.5. Measurement results when the load is a diode rectifier with an RC load. Supply current with (a) VSAPF and (b) CSAPF (c) Harmonics in the supply currents versus the corresponding harmonics in the load current. (d) VSAPF dc-link voltage. (e) CSAPF dc-link current.

Table 6.1.
Total Harmonic Distortion

Load type	Method	Load $THD_{2\ kHz}$	Supply $THD_{2\ kHz}$	Supply $THD_{20\ kHz}$
Diode rectifier + RL load	VSAPF	27.6 %	2.3 %	8.2 %
	CSAPF		3.9 %	5.9 %
Diode rectifier + RC load	VSAPF	64.4 %	4.1 %	8.9 %
	CSAPF		4.9 %	7.7 %

Figure 6.6(a) – (d) presents the operation of the APFs when the power of the non-linear load changes stepwise. Load current waveforms can be found in Fig. 6.6(a) and (b), while the corresponding supply current waveforms are shown in Fig. 6.6(c) and (d) respectively. The results show that the dynamic responses of the active power filters are similar.

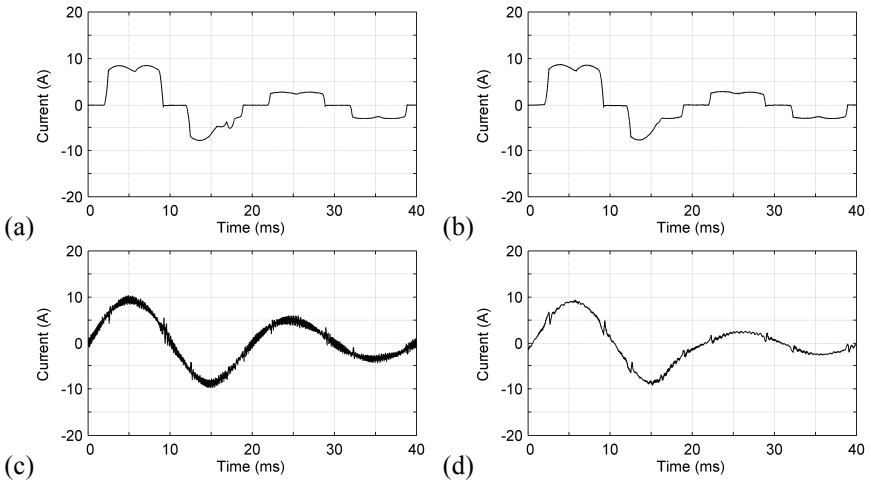

Fig. 6.6. Measurement results when the load changes stepwise. (a) and (b) Phase-a load current. (c) Supply current with VSAPF corresponding to (a). (d) Supply current with CSAPF corresponding to (b).

6.3. Power Losses

Distributions of measured power losses between main circuit components of the active filters are presented in Fig. 6.7(a) – (f), where Fig. 6.7(a) – (c) corresponds to the RL-type and Fig. 6.7(d) – (f) to the RC-type diode rectifier load. The values obtained in the measurements are shown with crosses, asterisks, and circles, while the solid lines represent approximations.

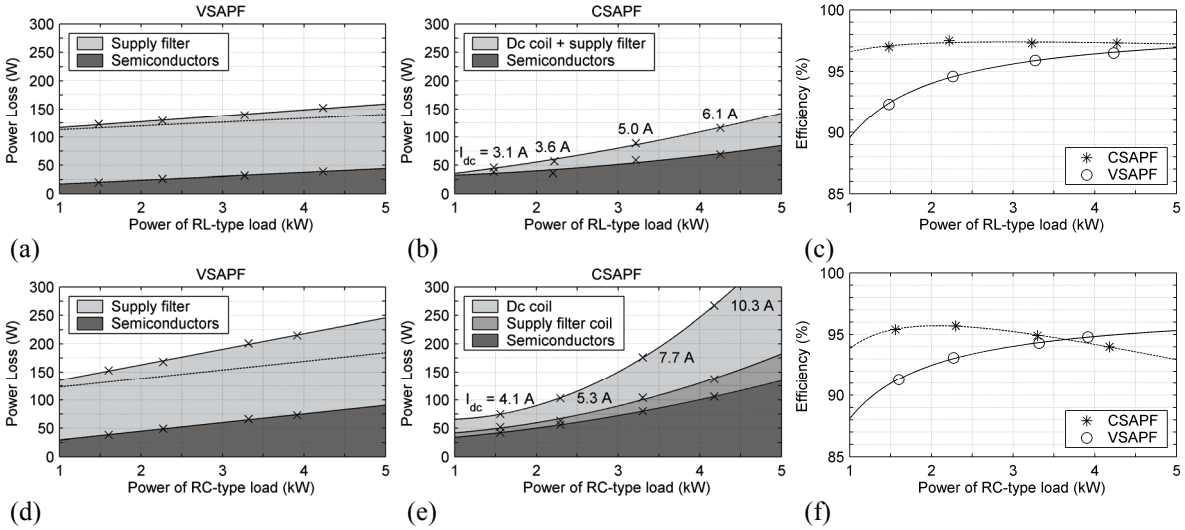

Fig. 6.7. Distribution of power loss between main circuit components and active filter efficiencies when (a) – (c) RL-type load and (d) – (f) RC-type load are compensated. Crosses, asterisks, and circles indicate values obtained and solid lines are least mean square estimations. Dashed lines approximate the divisions between the ripple current losses (below the line) and the losses caused by the harmonic compensating current (upper side). Figures (b) and (d) also include the magnitude of the dc current used in the operating point.

In the following, differences in the semiconductor power losses are discussed. Switching of the VSAPF is always hard and the switching voltage equals the dc-link voltage (725 V). In contrast, in the CSAPF some commutations take place naturally. Furthermore, the switching voltage depends on the instantaneous voltages of the supply filter capacitors and the angle of the active filter current reference vector. Thus, the maximum switching voltage in the steady state is approximately the peak value of the line-to-line voltage (565 V), whereas the average value of the switching voltage is much smaller. In addition, although the carrier frequencies used in both filters are equal, the CSAPF has lower switching frequency than the VSAPF. This is due to the modulation strategy used. Consequently, switching losses in the CSAPF are lower than in the VSAPF.

The on-state losses in the current-source APF can be expected to be higher than in the voltage-source APF, because switching devices are constructed with the series-connections of IGBTs and diodes. Consequently, the dc-link current i_{dc} flows through four semiconductor devices at any time. This increases the on-state losses compared with the VSAPF, where the three-phase compensating current $\underline{i}_f$ flows through three devices. The maximum current equals the peak of the phase current, but the average of the current is substantially lower. In Fig. 6.7(a), (b), (d), and (e) it can be deduced that the increased load power leads to an increase in compensating current. This causes a smaller increase in the semiconductor losses in the VSAPF than in the CSAPF.

The resistive power losses in the supply filter inductor ($L_f = 5$ mH) of the voltage-source active filter increase proportionally to the square of the filter current $\underline{i}_f$: the higher the harmonics to be compensated, the higher are the power losses in the filter inductor. In addition, the carrier frequency current component has a significant effect on the power losses in the supply filter. This can be seen in Fig. 6.7(a) and (d), where the dashed lines divide the filter losses into ripple current losses (below the approximation line) and losses caused by the harmonics compensating current (above the line). Since the VSAPF has a larger supply filter inductor and ripple current than the CSAPF, the losses in the filter inductor are also greater, as can be seen in Fig. 6.7(d) and (e).

The efficiencies of the VSAPF and the CSAPF as functions of the load power are shown in Fig. 6.7(c) and (f). The results show that with low power loads there are significant differences between the efficiencies, but when the load power increases towards the rated power (5 kW), the differences decrease. The main reason for the variation in the efficiency of the VSAPF is the power losses caused by the switching ripple current in the supply filter inductor L_f. When the load power is low, the proportion of the losses in the inductor is large compared with the load power. If the load is increased, the losses caused by the switching ripple remain approximately constant, since the ripple current has approximately the same absolute value at all operating points. That is, the efficiency improves with the increased load power. The reasons for the high efficiency of the current-source APF compared with the voltage-source APF at low power loads are the controlled dc-link current and the low losses in the LC supply filter.

6.4. Conclusions

The filtering characteristics of both active filters were found to be quite similar. Regardless of the type of the non-linear load, after active filtering the total harmonic distortion of the supply current calculated up to 2 kHz was below 5 %. Due to the supply filter structure, the VSAPF caused high frequency switching ripple compared with the CSAPF. Most of the losses in the VSAPF are due to the switching ripple in the supply filter, and the dc-link losses are minimal. In contrast, the power losses in the supply filter of the CSAPF are minor compared with the dc-link choke, which is a very substantial source of power loss.

Reduction of the dc-link power losses of the CSAPF has been studied by Chao and Grantham (2006). They proposed implementing a superconducting magnet as the energy storage in the dc link. The results presented in the paper show that the dc-link power losses can be reduced at least 50 %, although the power consumption of the cooling system of the magnet is included in the losses. However, the cooling increases the costs of the solution.

The efficiency measurements presented in this study showed that near to the nominal operating point, where compensating currents were high, the voltage-source active filter has higher efficiency than the current-source filter. In contrast, when the load power was low, the

current-source active filter was significantly more efficient than the voltage-source APF. The benefits and drawbacks are summarized in Table 6.2.

Table 6.2.
Benefits and Drawbacks of the Active Filters

	VSAPF	CSAPF
BENEFITS	- effective filtering of harmonics - high efficiency at nominal operating point	- effective filtering of harmonics - simple open-loop current control possible - high efficiency also with low power loads
DRAWBACKS	- switching ripple current - power losses in ac filter - low efficiency with low power loads - limited lifetime of the electrolytic dc-link capacitor	- bulky and heavy dc-inductor - high dc-link losses - overvoltage clamp circuit is needed

7. Application to Flicker Mitigation

This chapter examines a case study in which a voltage-source shunt active power filter is applied to mitigate voltage flicker problem caused by resistance spot welding. The study is presented in depth in Publication [P8].

In general, voltage fluctuations in electrical power systems can be reduced by changing the supply network, by installing compensators, or in some cases by changing the operating mode of the disturbing equipment (Ashmole, 2001). In the literature, compensator solutions are discussed e.g. in (Takeda et al., 1988; Doležal et al., 2000; Baldwin et al., 2005; Bilgin et al., 2007; Bongiorno and Svensson, 2007). Baldwin et al. (2005) present a solution in which thyristor switched capacitors (TSCs) are used to improve the voltage quality in resistance welding circuits in industrial power distribution systems. A voltage dip mitigation method incorporating a shunt-connected voltage-source converter is presented by Bongiorno and Svensson (2007). In their study, voltage dips at the point of common coupling (pcc) are compensated by injecting reactive power with the converter. Bilgin et al. (2007) propose a STATCOM based on a current-source converter. This is used to compensate reactive power of coal mining excavators. Shunt and series active filters with/without static VAr compensators are studied in (Doležal et al., 2000; Takeda et al., 1988). In these studies, the compensators are applied to compensate flicker caused by an electric arc furnace. Takeda et al. (1988) briefly present principles for compensating e.g. harmonic current, reactive power, and voltage fluctuation, and combinations of these, using a shunt active filter and a fixed reactive power compensation capacitor bank. Takeda et al. point out that by dividing the required compensation power equally between the active filter and the fixed compensator, the hybrid compensator is able to control the reactive power from 0 – 100 %. Thus, the necessary capacity of the active filter can be halved compared with stand-alone installation of the active filter.

Publication [P8] investigates a hybrid compensator solution which incorporates an active compensator and passive, fixed, reactive power compensator capacitor banks. In the paper, two control structures for the hybrid compensator are studied. Publication [P8] applies the stability analysis presented by Akagi (1997) and Malesani et al. (1998b) to the hybrid compensator presented by Takeda et al. (1988) and examines issues related to the stability of the compensator. Furthermore, in Publication [P8] the compensation characteristics of the solutions are considered comprehensively using simulation and practical measurement results. In addition, the resulting flicker severity indices are assessed.

7.1. Disturbing Load

The source of the flicker of lighting i.e. illumination changes investigated is voltage fluctuation caused by a resistance spot welding machine. Figure 7.1 shows the location of the machine in the distribution network. The block "Weld." represents the welding machine and the other electrical loads used in the industrial plant, while the block "Comp." is the compensator studied. From the point of view of the electrical network, a typical spot welding process can be considered to involve a controlled intermittent short-circuit fault, where a high-reactance welding transformer limits the current (Baldwin et al., 2005).

Figure 7.2(a) shows the behavior of the root-mean-square values of the measured three-phase voltages at the point of common coupling in the low-voltage bus ($u_{s,LVpcc}$) when the welding machine operates without compensation. The rms voltages are calculated from the sampled waveforms as

$$U(k) = \sqrt{\frac{1}{N}\sum_{i=0}^{N-1} u^2(k-i)}\,, \tag{7.1}$$

where $U(k)$ is the rms voltage at discrete time instant k, N is the number of samples in the fundamental (50 Hz) period, and $u(k)$ is the voltage at discrete time instant k. Two voltage drops can be seen in Fig. 7.2(a) during the examination period. Because of these, other customers connected to the same distribution system suffer from impaired power quality. Figure 7.2(b) presents the measured phase currents of the welding process and Fig. 7.2(c) and (d) the resulting three-phase instantaneous active and imaginary powers, respectively.

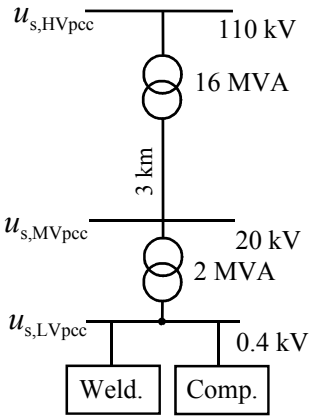

Fig. 7.1. Location of the process in the distribution system.

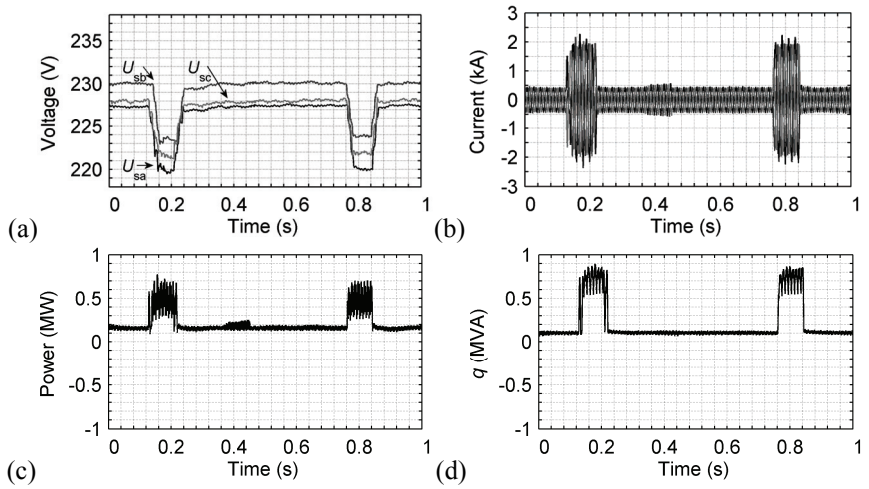

Fig. 7.2. (a) Rms of the measured mains phase voltages u_{sa}, u_{sb}, and u_{sc} at the low-voltage side of the transformer, (b) three-phase welding currents, (c) instantaneous active power, and (d) instantaneous imaginary power.

The main reason for the voltage fluctuations seen in Fig. 7.2(a) are the rapid variations in the reactive power, as discussed in Publication [P8]. Attempts have earlier been made to utilize a solution in which TSCs were adopted to mitigate the flicker, but the results have not been satisfactory. This is because the control of the TSCs introduces delays and thus the system has not been fast enough to react to sudden reactive power changes. As a result, the TSC may

instantaneously over- or under-compensate the reactive power. Although voltage drops can be significantly reduced, voltage fluctuations have still been too disturbing.

7.2. Hybrid Compensator

The solution examined in Publication [P8] is the use of an active compensator together with a so-called fixed detuned filter. The main circuit of this hybrid compensator as well as the measurements needed by the control system are shown in Fig. 7.3. The control of the active filter is based on the load current detection method and the compensation current reference is generated either using the sum current $\underline{i}_\mathrm{l}$ consisting of the passive compensator and the welding currents or using the welding current $\underline{i}_\mathrm{weld}$. In Fig. 7.3 the alternatives are presented with dashed lines.

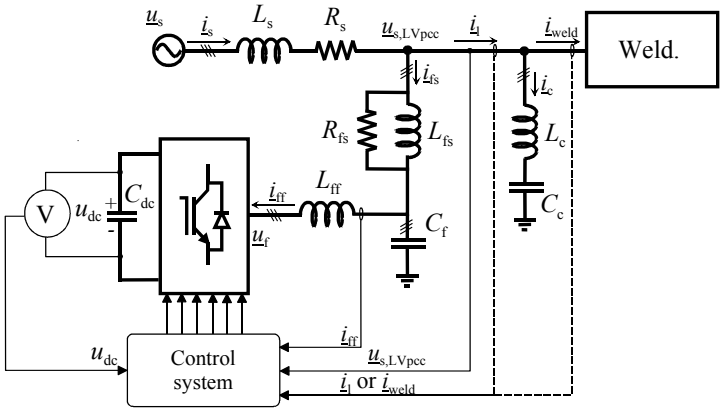

Fig. 7.3. Main circuit configuration of the compensator system.

The compensation operates as follows. During the welding cycles the reactive power drawn by the welding machine is compensated jointly by the active and passive compensators. On the other hand, during the idle periods, the active compensator keeps the mains reactive power at zero by compensating the excessive reactive power. The active part offers fast responses to welding current changes while the passive part provides a reduction of the ratings of the active compensator, as proposed also in (Takeda et al., 1988). Since the maximum reactive power drawn by the load is about 800 kVAr, the appropriate ratings for the active and passive compensators are 400 kVA each.

A capacitive element located on the load side of the active filter may lead to instability, as presented e.g. by Akagi (1997), Malesani et al. (1998b), and Wu et al. (2007b). On the basis of an analysis similar to that made in (Akagi, 1997; Malesani et al., 1998b), it is found in Publication [P8] that the compensator in which the compensating current reference is generated using the current $\underline{i}_\mathrm{l}$ may cause instability. To avoid this problem, in Publication [P8] an alternative control structure is also studied. In the alternative control structure, the compensating current reference is generated using the welding current $\underline{i}_\mathrm{weld}$ instead of the current $\underline{i}_\mathrm{l}$ which contains the passive compensator current $\underline{i}_\mathrm{c}$. This structure leads to a stable solution, as presented in (Wu, 2007b) and [P8]. However, Wu et al. (2007b) state that in this case, harmonics of the mains voltage may excite the series resonance.

7.3. Simulation Model

The simulations have been carried out using the Matlab Simulink program. In the simulations the control system involving the computational control delay compensation method presented in Publication [P1] has been used. The simulation model is shown in Fig. 7.4. The space-vector model for the main circuit has been derived with the help of the single-phase equivalent circuit illustrated in Fig. 7.5. In the Simulink model, the mains has been modeled with sinusoidal voltage sources with constant amplitudes and the supply network as a series connection of inductance L_s and resistance R_s. Furthermore, the load has been assumed to be a current source that is independent of the supplying voltage. Hence, instead of modeling the welding machine, actual welding currents recorded at the industry plant have been used in the simulations.

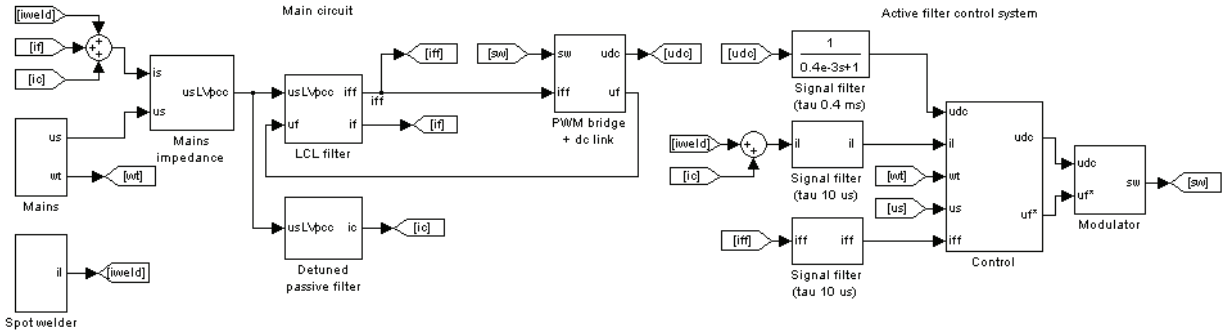

Fig. 7.4. Simulink model of the hybrid compensator.

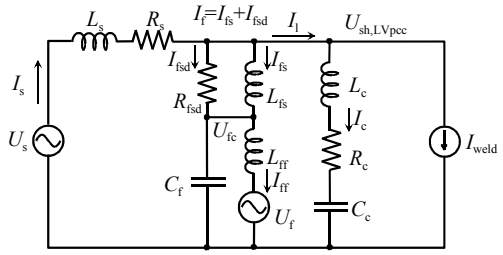

Fig. 7.5. Single-phase circuit for the hybrid compensator.

In the following, the equations used in the Simulink model are presented. According to Fig. 7.5, the supply current is

$$\underline{I}_s = \underline{I}_{weld} + \underline{I}_c + \underline{I}_f . \tag{7.2}$$

The voltage at the point of common coupling can be calculated as

$$\underline{U}_{s,LVpcc} = \underline{U}_s - (sL_s + R_s)\underline{I}_s . \tag{7.3}$$

However, since pure derivation is a problem in the numerical simulation software, instead of (7.3) the following approximation is used in the block “Mains impedance” (Fig. 7.4):

$$\underline{U}_{s,LVpcc} \approx \underline{U}_s - \left(\frac{sL_s}{s\tau_s + 1} + R_s \right) \underline{I}_s . \tag{7.4}$$

The block “Detuned passive filter” calculates the current drawn by the passive compensator as

$$\underline{I}_c = \frac{1}{sL_c} \left(\underline{U}_{s,LVpcc} - R_c \underline{I}_c - \frac{1}{sC_c} \underline{I}_c \right) . \tag{7.5}$$

The simulation model has been simplified by ignoring the frequency dependence of the LCL filter chokes. This can be done since the objective of the simulations has been to predict the flicker of the voltage supplying the welding process and the flicker is mainly due to the low frequency voltage fluctuations. Thus, the LCL-filter chokes are modeled simply as series-connection of a constant inductance and a resistance. The simplification affects especially the frequency characteristics of the chokes above several hundred hertz.

The following equations are solved in the block "LCL filter":

$$\underline{I}_{\mathrm{fs}} = \frac{1}{sL_{\mathrm{fs}}}\left(\underline{U}_{\mathrm{s.LVpcc}} - \underline{U}_{\mathrm{fc}} - R_{\mathrm{fs}}\underline{I}_{\mathrm{fs}}\right) \tag{7.6}$$

$$\underline{I}_{\mathrm{fsd}} = \frac{\underline{U}_{\mathrm{s,LVpcc}} - \underline{U}_{\mathrm{fc}}}{R_{\mathrm{fsd}}} \tag{7.7}$$

$$\underline{I}_{\mathrm{f}} = \underline{I}_{\mathrm{fs}} + \underline{I}_{\mathrm{fsd}} \tag{7.8}$$

$$\underline{U}_{\mathrm{fc}} = \frac{1}{sC_{\mathrm{f}}}\left(\underline{I}_{\mathrm{f}} - \underline{I}_{\mathrm{ff}}\right) \tag{7.9}$$

$$\underline{I}_{\mathrm{ff}} = \frac{1}{sL_{\mathrm{ff}}}\left(\underline{U}_{\mathrm{c}} - \underline{U}_{\mathrm{f}} - R_{\mathrm{ff}}\underline{I}_{\mathrm{ff}}\right). \tag{7.10}$$

The block "PWM bridge and dc-link" is based on (2.24), (2.38), and (2.39), while "Modulator" is implemented based on (2.26) – (2.29). The control algorithm applied in the simulations is the load current detection -based system with the computational control delay compensation, presented in Section 3.2. The simulation parameters have been presented in Appendix D. The measurement signals led to the control system ("Control") in Fig. 7.4 are filtered with signal filters implemented with first-order low-pass filters. Their time constants are presented in the figure and referred to with the term "tau".

Network parameters (inductance L_{s} and resistance R_{s}) used in the simulations were estimated by examining the behavior of the measured mains voltages at the point of common coupling in the low voltage bus ($\underline{u}_{\mathrm{s,LVpcc}}$) under different loading conditions. Then the resulting voltage $\underline{u}_{\mathrm{s,LVpcc}}$ was simulated using the measured currents and the estimated network parameters. The simulation result was compared with the measured voltage $\underline{u}_{\mathrm{s,LVpcc}}$ and the parameters were modified iteratively so that both the simulated and measured behavior of $\underline{u}_{\mathrm{s,LVpcc}}$ was practically identical. Finally, the network model was validated with separate measurement data by comparing simulated voltage behavior in various situations.

7.4. Results

The performance of the hybrid compensator was examined both with simulations and measurements. Since the maximum reactive power drawn by the load was about 800 kVAr, the chosen combination to mitigate the flicker was a 400 kVA active filter and a 400 kVAr passive compensator. However, for test setup purposes only a 210 kVA active power filter (consisting of three parallel-connected 70 kVA active filters) and a 500 kVAr fixed detuned filter were available. Thus, the performance of the chosen combination (400 kVA/400 kVAr)

was examined through simulations, but the simulation model was validated with measurements and simulations made using the combination 210 kVA/500 kVAr. The results are presented in Publication [P8]. Figures 7.6 – 7.8 show the simulation results obtained using the optimal combination. Figure 7.9(a) – (d) illustrates root-mean-squares of the phase-a voltage at the low-voltage bus in the measured and simulated operating points.

The results presented in Figs. 7.6 – 7.8 show that the hybrid compensator compensates completely the variations in the reactive power drawn by the welding process. This results in the reduced voltage fluctuations, as seen in Fig. 7.9. Furthermore, since the simulation and measurement results presented are in good agreement with each other, the simulation model can be stated to be valid.

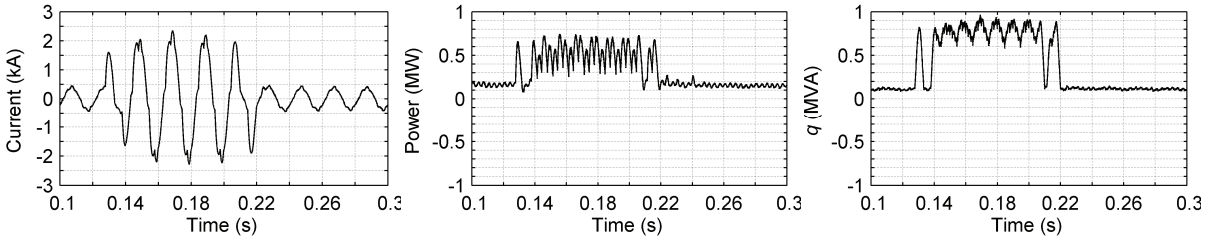

Fig. 7.6. Measured (a) phase-a welding current, (b) instantaneous active power, and (c) instantaneous imaginary power of the welding process.

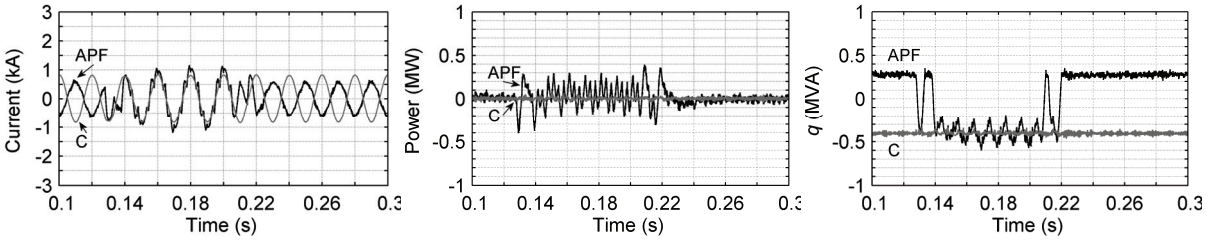

Fig. 7.7. Simulated active filter and passive compensator (a) phase-a currents, (b) instantaneous active, and (c) imaginary powers. Active filter current reference generation using $\underline{i}_{\text{weld}}$ (APF 400 kVA and C 400 kVAr).

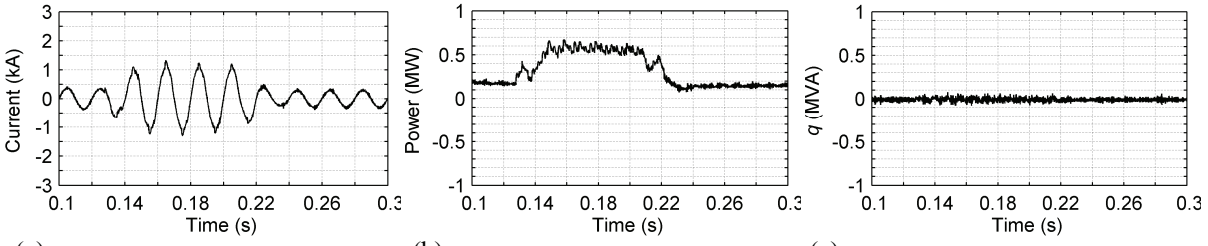

Fig. 7.8. Simulated (a) phase-a supply current, (b) instantaneous active, and (c) imaginary power drawn from the mains. Active filter current reference generation using $\underline{i}_{\text{weld}}$ (APF 400 kVA and C 400 kVAr).

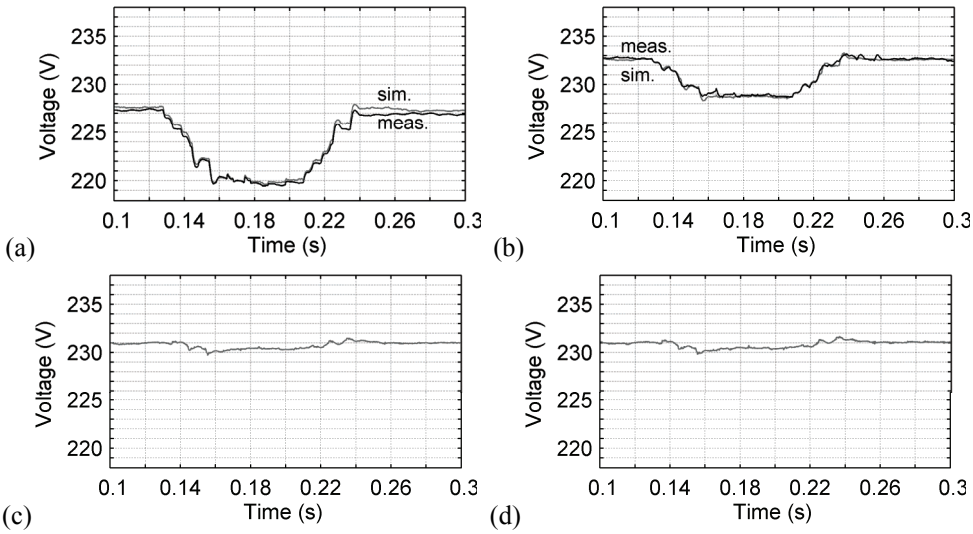

Fig. 7.9. Rms of the phase-a voltage at the point of common coupling in the low-voltage bus ($u_{sa,LVpcc}$). (a) Simulated and measured voltages, no compensation. (b) Simulated and measured voltages, current reference generation using $\underline{i}_l$ (APF 210 kVA and C 500 kVAr). (c) Simulated voltage, current reference generation using $\underline{i}_l$ (APF 400 kVA and C 400 kVAr). (d) Simulated voltage, current reference generation using $\underline{i}_{weld}$ (APF 400 kVA and C 400 kVAr).

7.4.1. Flicker Assessment

Flicker severity is the intensity of flicker annoyance defined by the UIE-IEC flicker measuring method. It is evaluated by the following quantities: short-term severity indices (Pst) measured over a period of ten minutes and long-term severity indices (Plt) calculated from a sequence of 12 Pst values over a two-hour interval (IEEE Std. 1453-2004, 2005).

During the network experiments made, the flicker levels were measured over several 10-minute periods with a power quality analyzer (IEC 61000-4-30 class A). Since the examination of the compensator solution contained both simulations and measurements, and furthermore since the properly rated combination of the compensators was not available for the measurements, the flicker levels of both simulated and measured voltages were evaluated. The evaluation procedure is presented in Fig. 7.10.

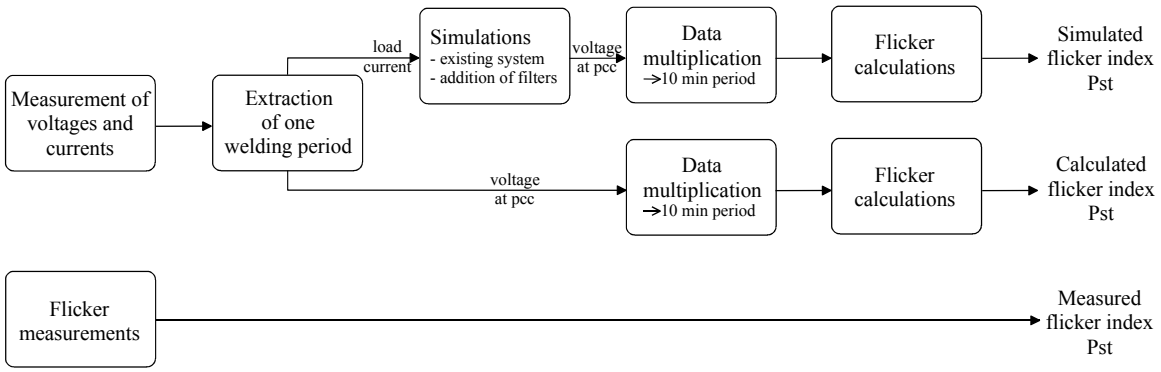

Fig. 7.10. Procedures for evaluation of flicker indices.

Short-term flicker indices in different situations are shown in Table 7.1. Here ‘Simul.’ means that voltage changes are first simulated and then the Pst values are calculated, ‘Calc.’ that the

Pst values are calculated on the basis of the measured instantaneous voltage values, and 'Meas.' that the values are measured with the power quality analyzer at medium voltage (MV) during the network experiments. The measured values vary slightly, since unlike in simulations, the consecutive welding periods are not similar in practice. In addition, in the real industrial plant there are also time periods lasting a couple of minutes during which the welding process is not on. The measured flicker severity indices are in moderate agreement with the calculated values and thus the results validate the simulation model and the calculation procedure. The results presented show that by using the hybrid compensator, the flicker levels can be greatly reduced.

Table 7.1.
Short-term flicker indices

Compensator	Simul. (LV, 0.4 kV)	Calc. (LV, 0.4 kV)	Simul. (MV, 20 kV)	Meas. (MV, 20 kV)
No compensation	5.47	5.78	1.61	1.2 – 1.4
APF 207 kVA and C 500 kVAr	2.94	2.81	0.91	0.8 – 0.9
APF 400 kVA and C 400 kVAr	0.60		0.27	
Modified structure (400 kVA/400kVAr)	0.64		0.27	

8. Summary and Conclusions

8.1. Summary and Scientific Contribution of the Publications

Publication [P1]

Publication [P1] examines the application of a computational control delay compensation method to the voltage-source shunt active power filter. The method was originally proposed for the current-source active power filter by co-author Mika Salo in (Salo, 2002) and (Salo and Tuusa, 2003). *The main contribution of Publication [P1] is the frequency domain analysis for the computational control delay compensation method and the application of the method to the voltage-source shunt active power filter.* The analysis and experimental results presented in Publication [P1] show that the method improves filtering of the low-order harmonics.

Publication [P2]

The main contribution of Publication [P2] is to propose the space-vector-based current reference generation method that combines two different approaches to compensate delays caused by the digital control system. If the load is of predictable type and the load current is distorted only by harmonics, the load current at the next sampling instant is predicted on the basis of the data stored in the memory in the previous period, similarly to Lindgren and Svensson (1998). Conversely, if the load current behavior cannot be predicted, e.g. in the case of interharmonics or load change, the prediction is turned off. However, in this case the computational control delay compensation examined in Publication [P1] is used. The experimental results presented in Publication [P2] verify the theory and demonstrate effective filtering both in stationary and dynamic state of the load.

In Publication [P2], the voltage-source shunt active power filter efficiency with RL- and RC-type loads has been estimated by assuming a symmetrical three-phase system and measuring the average power only in the a-phase. Since even a slight asymmetry of the supply voltages causes unsymmetrical distribution of the powers between the phases, especially in the case of the RC-type load, the active filter efficiencies presented in Publication [P2] are incorrect and should be ignored.

Publication [P3]

Publication [P3] proposes current-sensorless space-vector control of the voltage-source active power filter with the modified main circuit structure. The filtering performance and power losses are examined in laboratory measurements and the results are compared with a conventional shunt active filter. The measurement results show that the proposed system has a

wider harmonic filtering bandwidth than the conventional filter. However, it is also noted that the produced pulse-width-modulated voltages set restrictions on the type of load to be compensated. The efficiency measurements show that the losses in the active filter bridge and in the supply filter choke are lower than the losses in the conventional shunt active filters. In the paper, the effects of the parameter mismatches of the proposed open-loop control are also analyzed. These are found to have a slight effect on the system operating point. It is also noted that the mains voltage sensing should be accurate. *To the best of the author's knowledge, Publication [P3] and Related Publication [RP5] are the first publications presenting current-sensorless harmonic compensation with active power filters.*

Publication [P4]

The scientific contribution of Publication [P4] is to propose an improved current-sensorless control method for the active power filter with the modified main circuit structure. The control method proposed in Publication [P3] is based on the steady state equations and Publication [P4] concentrates on analyzing the transient state operation. This is found to cause dc components in the supply currents. Publication [P4] proposes an improved control method that is based on a dynamic model of the system. The performance of the system is examined in simulations and laboratory tests.

Publication [P5]

Publication [P5] presents a comparison of an active and a passive method for LCL filter resonance damping, assesses their suitability for the active power filter application, and presents their benefits and drawbacks. The comparison is carried out using transfer function models and a laboratory prototype. The results presented show that both topologies filter the harmonics effectively and the switching ripple is attenuated. The active filter with an actively damped LCL filter requires more current sensors and there are more controllers to be tuned than in the passively damped system. A simple control system, originally designed for the first-order L-type filter, can without changes be applied to the passively damped LCL filter, but the system requires additional damping resistors. The results presented in Publication [P5] show that the additional resistors increase the power losses only slightly. However, the actively damped system can be assumed to be more robust in the case of external disturbances than the passively damped system. *To the best of the author's knowledge, Publication [P5] is the first publication to present a comparison of the actively and passively damped LCL filters in active power filter application.*

Publication [P6]

Publication [P6] studies the use of silicon carbide Schottky diodes in the voltage-source shunt active power filter. The Si diodes of the conventional three-phase bridge are replaced with their SiC counterparts to determine their effect on the semiconductor bridge power losses. The power losses are first determined by calculations, and the distribution of the conduction and switching losses is estimated. Finally, measurements are performed to confirm the results. On the basis of the examination presented, it can be assumed that SiC diodes provide a reduction

in the semiconductor power losses of the active filter. A decrease in the semiconductor losses is important because this allows reducing the cooling. Furthermore, because the SiC devices can operate at higher temperatures, also this could provide a reduction in the heatsink volume. On the other hand, the smaller power losses make it possible to increase the switching frequency, thus making it possible to use smaller active filter chokes. *To the best of the author's knowledge, Publication [P6] is the first publication to examine the use of SiC semiconductor devices in the active power filter application. An additional scientific contribution is that the paper presents estimates for the distribution of the conduction and switching losses in the active filter semiconductor bridge.*

Publication [P7]

Publication [P7] presents a comparison of the voltage-source and current-source shunt active filters controlled with similar harmonic compensation algorithm. First, the main circuits and space-vector modulation techniques used are studied and the digital control systems are presented. The filtering performances of the systems with different kinds of non-linear load are examined and finally the power losses of the active filters are studied. The current-source active filter requires a bulky and heavy dc choke. In addition, the main circuit is found to be slightly more complicated, since an overvoltage clamp is needed. The drawback of the voltage-source topology is the electrolytic capacitors in the dc link, because their lifetime is limited. The operational performances and efficiencies of the active filters are studied through measurements. The filtering performances of both active filters are quite similar. Power loss distributions of the main circuit components were presented at various operating points. The major part of the power losses in the voltage-source active filter is due to the switching ripple current in the supply filter choke. Conversely, in the current-source active filter the dc-link losses are found to be important. *The main contribution of Publication [P7] is the comparison using state-of-the-art voltage-source and current-source shunt active power filters with similar compensation algorithms. To the best of the author's knowledge, Publication [P7] is the first publication to present detailed estimates for power loss distributions of the main circuit components in both of the active filter topologies.*

Publication [P8]

Publication [P8] presents an application of the active power filter to mitigate the voltage flicker problem caused by a resistance spot welding process. The paper examines two control structures for the hybrid compensator incorporating an active part and a passive detuned filter. Publication [P8] applies the stability analysis presented by Akagi (1997) and Malesani et al. (1998b) to the hybrid compensator presented by Takeda et al. (1988) and analyzes the stability issues of the compensator. The compensation characteristics of the systems are considered comprehensively using simulation and practical measurement results. In addition, the flicker severity indices obtained after compensation are also assessed. The first compensator structure, in which the welding process and a detuned passive filter are considered as a load of the active compensator, is found to yield a reduction of the voltage drops causing the flicker, but in some cases the structure may be unstable. The second

configuration is found to be more independent of the system parameters. The main advantage of the solution is that the system offers fast responses to changes in the need for compensation. In addition, by combining an active and passive reactive power compensator, the ratings of the active compensator can be halved compared with the situation where the active compensator is used alone. A drawback of the system is the increased complexity of the compensator and possible instability problems. *The contribution of Publication [P8] is to present application issues concerning flicker mitigation using an active compensator and a fixed detuned filter, stability analysis of the system, simulations, and validating experimental tests from the point of view the flicker severity indices*.

8.2. Conclusions

Active filters are controlled current or voltage sources that are used to compensate the harmonics, interharmonics, and the reactive component of the current or voltage distortion and fluctuations. They can solve almost all of the problems that exist with conventional passive filters. In addition, they are small in size and offer, for example, a wide and/or selectable filtering bandwidth. However, their main drawback is high cost. Since active filters are constructed with several components and their operation depends on complicated control, passive filters may be considered more reliable.

In this thesis a digitally controlled three-phase three-wire voltage-source shunt active power filter was examined. One of the main objectives of this work was to improve the current compensation characteristics of the voltage-source shunt active power filter by compensating and minimizing effects caused by control delays. First, a computational control delay compensation method proposed originally for a current-source active power filter was applied and analyzed in a voltage-source active filter [P1]. Second, a method utilizing previously measured data to generate the compensating current reference in the stationary state, or the CDC method in unpredictable situations, was proposed [P2]. The third examined system was a modified main circuit structure and two current-sensorless control methods were proposed, analyzed, and tested [P3], [P4]. The CDC method was found to improve the filtering of the low-order harmonics, but the harmonics above 1.5 kHz were increased compared with the basic method. The prediction-based current reference generation improved the filtering characteristics over a wide frequency band. Effective compensation behavior was also found when the modified main circuit structure and the current-sensorless control were used. However, because of the non-ideal characteristics of the PWM bridge, the filtering of the low-order harmonics was slightly affected. The power loss measurement results presented in Publication [P3] showed that the losses in the active filter bridge and in the supply filter choke of the modified main circuit structure were lower than the losses in the conventional shunt active filters. However, a drawback found was that the PWM voltage produced with the active filter increases the power losses in the smoothing inductor installed in front of the load. A solution for this could be to use a multilevel PWM bridge instead of the two-level bridge. In this way, the additional power losses caused by the switching ripple current could be reduced, but also the supply filter coil could be reduced.

The second main objective of the thesis was to compare an active and a passive method for LCL filter resonance damping and assess the suitability of the LCL filters for active power filter application. This was presented in Chapter 4, which contained a summary of [P5]. The results presented showed that efficient current ripple attenuation and fast dynamic responses required in using the active power filter can be achieved with both of the methods. In addition, it was found that in contrast to what is often stated in the literature, the passive damping increased the power losses only slightly. The active resonance damping method examined was observed to require more current sensors and more complicated control than the passively damped system, and slightly better harmonic compensation characteristics were found. The actively damped system can be assumed to be more robust in the case of external disturbances, such as harmonics in the mains voltages, than the passively damped system.

The third main objective was to determine the active filter power loss profile and to examine the application of SiC-based power diodes in the active filter main circuit. These were studied in Publication [P6] in calculations and measurements and the study was summarized in Chapter 5. The results showed that by using SiC diodes the semiconductor losses could be decreased by about 20 %. Although the semiconductors account for only a minor proportion of the total power losses of the active power filter, the decrease in the semiconductor losses is important because this allows reducing the cooling. Furthermore, because the SiC devices can operate at higher temperatures, also this could provide a reduction in the heatsink volume. On the other hand, the smaller power losses make it possible to increase the switching frequency, thus making possible the use of smaller active filter coils. In Publication [P6] only technical aspects were examined. However, the economic viewpoints such as main circuit component cost, availability of the SiC devices, would be very important factors in practice.

Comparison of voltage-source and current-source active power filters was the fourth main objective of the thesis. This is presented in [P7] and summarized in Chapter 6. First, the main circuits and space-vector modulation techniques used were studied and the digital control systems presented. The current-source active filter was noticed to require a bulky and heavy dc choke. In addition, the main circuit was found to be slightly more complicated, since an overvoltage clamp is needed. The drawback of the voltage-source topology was found to be the electrolytic capacitors in the dc link, because their lifetime is limited. The operational performances of the topologies and main circuit power losses were studied in measurements. The filtering characteristics were found to be similar. Power loss distributions of the main circuit components were presented at various operating points. Most of the power losses in the voltage-source active filter were due to the switching ripple current in the supply filter choke. Conversely, in the current-source active filter the dc link losses were found to be important.

The fifth main objective of the thesis was to examine application of the shunt active power filter to mitigate the voltage flicker problem. This study was presented in Chapter 7, which

was a summary of [P8]. In the examination, two hybrid compensator structures incorporating an active part and a passive detuned filter were analyzed and examined. The main idea in both of the structures was that the active filter provides fast compensation dynamics, while the use of the passive filter provides a reduction in the active filter ratings. Similarly, also investment costs can be greatly reduced. The first compensator structure examined was found to offer a great reduction in the voltage drops causing the flicker, but in some cases the structure may be unstable. The second configuration was found to obtain similar compensation characteristics, but it was more robust with respect to time delays and system parameters. In addition to the system analysis, a simulation model enabling off-line evaluation of the flicker indices resulting from the installation of the compensator was developed. The simulation model was validated with practical measurements.

Methods examined in Publications [P1] and [P2] have been applied also in other studies. Computational control delay compensation examined in Publication [P1] is applied to a hybrid compensator in [RP2] and [RP3]. Furthermore, the prediction-based current reference generation proposed in Publication [P2] is extended to be used in the four-wire active power filter in Related Publication [RP6], while Related Publication [RP7] proposes the control of the Vienna I rectifier with active filter function. In addition, based on Publication [P2] a 50-kVA prototype for a shunt active power filter was tested and reported in (Happonen, 2005), while in (Parkatti et al., 2007) the active filter at 690-V mains voltage level is examined.

Important topics for future research are the detailed analysis of the effects of the supply voltage and of the supply network on the active filter control and filtering characteristics. These are not assessed in this thesis. The operation of the active filter in the case of distorted and/or unbalanced mains is another important topic for the future as well as operation with loads producing other types of interharmonics than flicker. Also the study about issues considering electromagnetic interference (EMI) caused by active filter, and effects e.g. of SiC diodes, is important issue for further research. In addition, the distribution of power losses in the LCL-type supply filter and the optimization of the filter taking into account also the economic aspects should be studied.

References

Aburto, V., Schneider, M., Morán L., Dixon, J. (1997) "An active power filter implemented with a three-level npc voltage-source inverter," in *Conference Record of the 28th Annual IEEE Power Electronics Specialists Conference (PESC '97)*, St. Louis, MO, USA, June 22– 27, vol. 2, pp. 1121 – 1126.

Akagi, H., Kanazawa, Y., Nabae, A. (1984) "Instantaneous reactive power compensators comprising switching devices without energy storage components," *IEEE Transactions on Industry Applications*, vol. IA-20, no. 3, pp. 625 – 630, May/June 1984.

Akagi, H. (1994) "Trends in active power line conditioners," *IEEE Transactions on Power Electronics,* vol. 9, no. 3, pp. 263 – 268, May 1994.

Akagi, H. (1997) "Control strategy and site selection of a shunt active filter for damping of harmonic propagation in power distribution systems," *IEEE Transactions on Power Delivery*, vol. 12, no. 1, pp. 354 – 363, January 1997.

Akagi, H., Fujita, H., Keiji, W. (1999) "A shunt active filter based on voltage detection for harmonic termination of a radial power distribution line," *IEEE Transactions on Industry Applications*, vol. 35, no. 3, pp. 638 – 645, May/June 1999.

Akagi, H., Srianthumrong, S., Tamai, Y. (2003) "Comparisons in circuit configuration and filtering performance between hybrid and pure shunt active filters," in *Conference Record of the 2003 IEEE Industry Applications Conference, 38th IAS Annual Meeting*, Salt Lake City, UT, USA, October 12 – 16, pp. 1195 – 1202.

Akagi, H., Watanabe, E.H., Aredes, M. (2007a) *Instantaneous power theory and applications to power conditioning*, IEEE Press, Piscataway, NJ, USA, 393 p.

Akagi, H. (2007b) "A transformerless hybrid active filter for integration into a medium-voltage motor drive with a passive front end," in *Proceedings of the 7th International conference on power electronics (ICPE'07)*, Daegu, Korea, October 22–26, pp. 1 – 8.

Arrillaga, J., Watson, N.R. (2003) *Power system harmonics*, second edition, John Wiley & Sons Ltd., Chichester, United Kingdom, 399 p.

Ashmole, P., Amante, P. (1997) "System flicker disturbances from industrial loads and their compensation," *Power Engineering Journal*, vol. 11, issue 5, pp. 213 – 218, October 1997.

Ashmole, P. (2001) "Quality of supply – voltage fluctuations, part 2," *Power Engineering Journal*, vol. 15, issue 2, pp. 108 – 114, April 2001.

Asiminoaei, L., Lascu, C., Blaabjerg, F., Boldea, I. (2007a) "Performance improvement of shunt active power filter with dual parallel topology," *IEEE Transactions on Power Electronics,* vol. 22, no. 1, pp. 247 – 259, January 2007.

Asiminoaei, L., Blaabjerg, F., Hansen, S. (2007b) "Detection is key - harmonic detection methods for active power filter applications," *IEEE Industry Applications Magazine*, vol. 13, no. 4, pp. 22 – 33, July/August 2007.

Bajnica, N., Naunin, D. (2005) "Two degree of freedom resonant structure for robust current control and active filtering," in *Proceedings of the 11th European Conference on Power Electronics and Applications (EPE 2005)*, Dresden, Germany, September 11 – 14, 10 p.

Baldwin, T.L., Hogans, Jr., T., Henry, S.D., Renovich, Jr., F., Latkovic, P.T. (2005) "Reactive-power compensation for voltage control at resistance welders," *IEEE Transactions on Industry Applications*, vol. 41, no. 6, pp. 1485 – 1492, November/December 2005

Benchaita, L., Saadate, S., Salem nia, A. (1999) "A Comparison of Voltage Source and Current Source Shut Active Filter by Simulation and Experimentation," *IEEE Transactions on Power Systems*, vol. 14, no. 2, pp. 642 – 647, May 1999.

Bendre, A., Divan, D., Kranz, W., Brumsickle, W.E. (2006) "Are voltage sags destroying equipment? Equipment failures caused by power quality disturbances," *IEEE Industry Applications Magazine*, vol. 12, no. 4, pp. 12 – 21, July/August 2006.

Bilgin, H.F., Ermis, M., Kose, K.N., Cetin, A., Cadirci, I., Acik, A., Demirci, T., Terciyanli, A., Kocak, C., Yorukoglu, M. (2007) "Reactive-power compensation of coal mining excavators by using a new-generation STATCOM," *IEEE Transactions on Industry Applications*, vol. 43, no. 1, pp. 97 – 110, January/February 2007.

Bojrup, M., Karlsson, P., Alaküla, M., Gertman, L. (1999) "A multiple rotating integrator controller for active filters," in *Proceedings of the 8th European Conference on Power Electronics and Applications (EPE'99)*. Lausanne, Switzerland, September 7 – 9, 9 p.

Bollen, M.H.J. (2000) *Understanding power quality problems: voltage sags and interruptions*, IEEE Press, Piscataway, NJ, USA, 543 p.

Bolsens, B., De Brabandere, K., Van den Keybus, J., Driesen, J., Belmans, R. (2005) "Three-phase observer-based low distortion grid current controller using an LCL output filter," in *Proceedings of the 36th Annual Power Electronics Specialists Conference (PESC'05)*, Recife, Brazil, June 12–16, pp. 1705 – 1711.

Bongiorno, M., Svensson, M. (2007) "Voltage dip mitigation using shunt-connected voltage source converter," *IEEE Transactions on Power Electronics*, vol. 22, no. 5, pp. 1867 – 1874, September 2007.

Borisov, K., Ginn, H., Chen, G. (2007) "A computationally efficient RDFT based reference signal generator for active compensator," in *Proceedings of the 38th Annual Power Electronics Specialists Conference (PESC'07)*, Orlando, FL, USA, June 17–22, pp. 1092 – 1098.

van der Broeck, H.W., Skudelny, H.-C., Stanke, G.V. (1988) "Analysis and realization of a pulsewidth modulator based on voltage space vectors," *IEEE Transactions on Industry Applications,* vol. 24, no. 1, pp. 142 – 150, January/February 1988.

Buso, S., Malesani, L., Mattavelli, P. (1998) "Comparison of current control techniques for active filter applications," *IEEE Transactions on Industrial Electronics*, vol. 45, no. 5, pp. 722 – 729, October 1998.

Chao, C., Grantham, C. (2006) "Design considerations of a high-temperature superconducting magnet for energy storage in an active power filter," *IEEE Transactions on Applied Superconductivity*, vol. 16, no. 2, pp. 612 – 615, June 2006.

Chaoui, A., Gaubert, J.-P., Krim, F., Rambault, L. (2007) "Direct power control of shunt active filter," in *Proceedings of the 12th European Conference on Power Electronics and Applications (EPE 2007)*, Aalborg, Denmark, September 2 – 5, 11 p.

Choe, G.-H., Park, M.-H. (1988) "A new injection method for ac harmonic elimination by active power filter," *IEEE Transactions on Industrial Electronics*, vol. 35, no. 1, pp. 141–147, February 1988.

Cichowlas, M., Malinowski, M., Kazmierkowski, M.P., Sobczuk, D.L., Rodríguez, P., Pou, J. (2005) "Active filtering function of three-phase PWM boost rectifier under different line voltage conditions," *IEEE Transactions on Industrial Electronics*, vol. 52, no. 2, pp. 410 – 419, April 2005.

Corradini, L., Stefanutti, W., Mattavelli, P. (2007) "Analysis of multi-sampled current control for active filters", in *Conference Record of the 2007 IEEE Industry Applications Conference, 42nd IAS Annual Meeting.* New Orleans, LA, USA, September 23 – 27, pp. 1608 – 1615.

Czarnecki, L.S. (2004) "On some misinterpretations of the instantaneous reactive power p-q theory," *IEEE Transactions on Power Electronics*, vol. 19, no. 3, pp. 828 – 836, May 2004.

Czarnecki, L.S. (2006) "Instantaneous reactive power p-q theory and power properties of three-phase systems," *IEEE Transactions on Power Delivery*, vol. 21, no. 1, pp. 362 – 367, January 2006.

Dahono, P. K. (2002) "A control method to damp oscillation in the input LC filter of AC-DC PWM converter," in *Proceedings of the 33rd Annual Power Electronics Specialists Conference (PESC'02)*, Cairns, Australia, June 23 – 27, vol. 4, pp. 1630 – 1635.

Das, J.C. (2004) "Passive filters – potentialities and limitations," *IEEE Transactions on Industry Applications*, vol. 40, no. 1, pp. 232 – 241, January/February 2004.

Dixon, J.W., Tepper, S., Morán, L. (1994) "Analysis and evaluation of different modulation techniques for active power filters," in *Proceedings of the 9th Annual Applied Power Electronics Conference and Exposition (APEC'94)*, Orlando, FL, USA, February 13 – 17, vol. 2, pp. 894 – 900.

Dixon, J.W., Contardo, J.M., Morán L.A. (1999) "A fuzzy-controlled active front-end rectifier with current harmonic filtering characteristics and minimum sensing variables," *IEEE Transactions on Power Electronics*, vol. 14, no. 4, pp. 724 – 729, July 1999.

Doležal, J., Castillo, A.G., Tlustý, J., Valouch, V. (2000) "Topologies and control of active filters for flicker compensation," in *Proceedings of the 2000 IEEE International Symposium on Industrial Electronics (ISIE 2000)*, Cholula, Puebla, Mexico, December 4 – 8, vol. 1, pp. 90 – 95.

Dolny, G.M. (2005) "High-voltage semiconductor devices: status and trends", *Proceedings of the Bipolar/BiCMOS Circuits and Technology Meeting*, Santa Barbara, CA, USA, October 9 – 11, pp. 78 – 85.

Dumitrescu, A.-M., Griva, G., Bostan, V., Magureanu, R. (2007) "Design of current controllers for active power filters using Naslin polynomial technique," n *Proceedings of the 12th European Conference on Power Electronics and Applications (EPE 2007)*, Aalborg, Denmark, September 2 – 5, 7 p.

Elasser, A., Kheraluwala, M.H., Ghezzo, M., Steigerwald, R.L., Evers, N.A., Kretchmer, J., Chow, T.P. (2003) "A comparative evaluation of new silicon carbide diodes and state-of-the-art silicon diodes for power electronic applications," *IEEE Transactions on Industry Applications*, vol. 39 no. 4, pp. 915 – 921, July/August 2003.

Etxeberria-Otadui, I., de Heredia, A.L., Gaztañaga, H., Bacha, S., Reyero, M.R. (2006) "A single synchronous frame hybrid (SSFH) multifrequency controller for power active filters," *IEEE Transactions on Industrial Electronics*, vol. 53, no. 5, pp. 1640 – 1648, October 2006.

Ferrero, A., Superti-Furga, G. (1991) "A new approach to the definition of power components in three-phase systems under nonsinusoidal conditions," *IEEE Transactions on Instrumentation and Measurement*, vol. 40, no. 3, pp. 568 – 577, June 1991.

Friedrichs, P., Rupp. R. (2005) "Silicon carbide power devices – current developments and potential applications," *Proceedings of the 11th European Conference on Power Electronics and Applications (EPE 2005)*, Dresden, Germany, September 11 – 14, 11 p.

Fukuda, S., Imamura, R. (2005) "Application of a sinusoidal internal model to current control of three-phase utility-interface converters," *IEEE Transactions on Industrial Electronics*, vol. 52, no. 2, pp. 420 – 426, April 2005.

García-Cerrada, A., Pinzón-Ardila, O., Feliu-Batlle, V., Roncero-Sánchez, P., García-González, P. (2007) "Application of a repetitive controller for a three-phase active power filter," *IEEE Transactions on Power Electronics*, vol. 22, no. 1, pp. 237 – 246, January 2007.

George, S., Agarwal V. (2007) "A DSP based optimal algorithm for shunt active filter under nonsinusoidal supply and unbalanced load conditions," *IEEE Transactions on Power Electronics*, vol. 22, no. 2, pp. 593 – 601, March 2007.

González, S.A., García-Retgui, R., Benedetti, M. (2007) "Harmonic computation technique suitable for active power filters," *IEEE Transactions on Industrial Electronics*, vol. 54, no. 5, pp. 2791 – 2796, October 2007.

Grady, W. M., Samotyj, M. J., Noyola, A. H. (1990) "Survey of Active Power Line Conditioning Methodologies," *IEEE Transactions on Power Delivery*, vol. 5, no. 3, pp 1536 – 1542, July 1990.

Griñó, R., Cardoner, R., Costa-Castelló, R., Fossas, E. (2007) "Digital repetitive control of a three-phase four-wire shunt active filter," *IEEE Transactions on Industrial Electronics*, vol. 54, no. 3, pp. 1495 – 1503, June 2007.

Gutiérrez, E.I., Durán-Gómez, J.L. (2006) "Power quality improvement of a current-pulsed power supply based on a three-level NPC PWM VSI scheme as an active power filter," in *Proceedings of the 10th IEEE International Power Electronics Congress (CIEP 2006)*, Puebla, Mexico, October 16 – 18, 6 p.

Gyugyi, L., Strycula, E.C. (1976), "Active ac power filters," in *Conference Records of the IEEE-IAS Annual Meeting*, Chicago, IL, USA, October 12th, pp. 529 – 535.

Halkosaari, T. (1999) *Evaluation of power losses and conducted emissions in current source PWM frequency converter (Virtavälipiirillisen PWM taajuudenmuuttajan tehohäviöiden ja johtuvien häviöiden tarkastelu)*, Thesis for the degree of Licentiate of Technology, Department of Electrical Engineering, Tampere University of Technology, Tampere, Finland, 96 p. (in Finnish)

Halpin, S.M., Singhvi, V. (2007) "Limits for interharmonics in the 1 – 100-Hz range based on lamp flicker considerations," *IEEE Transactions on Power Delivery*, vol. 22, no. 1, pp. 270 – 276, January 2007.

Han, B.-M., Bae, B.-Y., Ovaska, S.J. (2005) "Reference signal generator for active power filters using improved adaptive predictive filter," *IEEE Transactions on Industrial Electronics*, vol. 52, no. 2, pp. 576 – 584, April 2005.

Happonen, T. (2005) *Implementation and testing of a 50 kVA active power filter (50 kVA:n aktiivisuodinprototyypin rakentaminen ja testaus)*. Master of Science thesis, Department of Electrical Engineering, Tampere University of Technology, Tampere, Finland, 87 p. (in Finnish)

Harashima, F., Inaba, H., Tsuboi, K. (1976) "A closed-loop control system for the reduction of reactive power required by electronic converters," *IEEE Transactions on Industrial Electronics and Control Instrumentation*, vol. IECI-23, no. 2, pp. 162 – 166, May 1976.

Hayashi, Y., Sato, N., Takahashi, K. (1991) "A novel control of a current-source active filter for ac power system harmonic compensation," *IEEE Transactions on Industry Applications*, vol. 27, no. 2, pp. 380 – 385, March/April 1991.

Heydt, G.T. (1998) "Electric power quality: a tutorial introduction," *IEEE Computer Applications in Power*, vol. 11, no. 1, pp. 15 – 19, January 1998.

Ho, W.-J., Lio, J.-B., Feng, W.-S. (1997) "A line-interactive UPS structure with built-in vector controlled charger and PFC," in *Proceedings of the 1997 International Conference on Power Electronics and Drive Systems*, Singapore, May 26 – 29, vol. 1, pp. 127 – 132.

Holtz, J. (1992) "Pulsewidth modulation – a survey," *IEEE Transactions on Industrial Electronics*, vol. 39, no. 5, pp. 410 – 420, October 1992.

Holmes, D.G., Lipo, T.A. (2003) *Pulse width modulation for power converters: principles and practice*. IEEE Press, Piscataway, New Jersey, USA, 724 p.

Hsieh, G.-C., Hung, J.C. (1996) "Phase-locked loop techniques – a survey," *IEEE Transactions of Industrial Electronics*, vol. 46, no. 6, pp. 609 – 615, December 1996.

Huaijun, Z., Wei, L., Zongming, Q. (2005) "A new control algorithm for compensation of harmonics and reactive power and its implementation based on DSP," in *Proceedings of the 8th International Conference on Electical Machines and Systems (ICEMS 2005)*, Nanjing, China, September 27 – 29, vol. 2, pp. 1387 – 1390.

IEEE Interharmonic Task Force and the Cigré 36.05/CIRED 2 CC02 Voltage Quality Working Group (1997) "Interharmonics in power systems," 9 p.

Itoh, S., Fukuda, S. (1988) "Basic characteristics of active power filter using current-source converter," in *Official Proceedings of the First International Power Conversion Conference (PCIM '88)*, Tokyo, Japan, December 8 – 10, pp. 443 – 452.

Itoh, J.-I., Tamada, S. (2007) "A novel engine generator system with active filter and UPS functions using a matrix converter," n *Proceedings of the 12th European Conference on Power Electronics and Applications (EPE 2007)*, Aalborg, Denmark, September 2 – 5, 10 p.

Jeong, S.G., Woo, M.-H. (1997) "DSP-based active power filter with predictive current control," *IEEE Transactions on Industrial Electronics*, vol. 44, no. 3, pp. 329 – 326, June 1997.

Jin, T., Smedely, K.M. (2006) "Operation of one-cycle controlled three-phase active power filter with unbalanced source and load," *IEEE Transactions on Power Electronics*, vol. 21, no. 5, pp. 1403 – 1412, September 2006.

Joos, G., Morán, L., Ziogas, P. (1991) "Performance analysis of a PWM inverter VAr compensator," *IEEE Transactions on Power Electronics*, vol. 6 no. 3, pp. 380 – 391, July 1991.

Kawahira, H., Nakamura, T., Nakazawa, S., Nomura, M. (1983) ”Active power filter,” *Conference Record of the International Power Electronics Conference (IPEC ’83)*, Tokyo, Japan, March 27 – 31, 1983, pp. 981 – 992.

Kazmierkowski, M.P., Krishnan, R., Blaabjerg, F. (edit.) (2002) *Control in power electronics; selected problems*. Academic Press, San Diego, CA, USA, 518 p.

Kovács, K.P., Rácz, I. (1959) *Transiente Vorgänge in Wechselstrommaschinen*, *Band I*, Verlag der Ungarischen Akademie der Wissenschaften, Budapest, Hungary, 514 p.

Kwon, B.-H., Youm, J.-H., Lim, J.-W. (1999) “A line-voltage-sensorless synchronous rectifier,” *IEEE Transactions on Power Electronics*, vol. 14 no. 5, pp. 966 – 972, September 1999.

Lascu, C., Asiminoaei, L., Boldea, I., Blaabjerg, F. (2007) “High performance current controller for selective harmonic compensation in active power filters,” *IEEE Transactions on Power Electronics*, vol. 22, no. 5, pp. 1826 – 1835, September 2007.

de Leon, F., Semlyen, A. (1993) “Time domain modeling of eddy current effects for transformer transients,” *IEEE Transactions on Power Delivery*, vol. 8, no. 1, pp. 271 – 280, January 1993.

Limongi, L.R., Bojoi, R., Pica, C., Profumo, F., Tenconi, A. (2007) “Analysis and comparison of phase locked loop techniques for grid utility applications,” in *Proceedings of the Fourth Power Conversion Conference (PCC ’07)*, Nagoya, Japan, April 2 – 5, pp. 674 – 681.

Lindgren, M., Svensson, J. (1998) “Control of a voltage-source converter connected to the grid through an LCL-filter – application to active filtering,” in *Proc. 29th Annu. Power Electron. Spec. Conf. (PESC’98)*, Fukuoka, Japan, May 17–22, vol. 1, pp. 229 – 235.

Lindemann, A. (2001) “A new IGBT with reverse blocking capability,” in *Proceedings of the 9th European Conference on Power Electronics and Applications (EPE 2001)*, Graz, Austria, August 27 – 29, 7 p.

Liserre, M., Dell’Aquila, A., Blaabjerg, F. (2004) “Genetic algorithm-based design of the active damping for an LCL-filter three-phase active rectifier,” *IEEE Transactions on Power Electronics*, vol. 19, no. 1, pp. 76 – 86, January 2004.

Liserre, M., Blaabjerg, F., Hansen, S. (2005) “Design and control of an LCL-filter-based three-phase active rectifier,” *IEEE Transactions on Industry Applications*, vol. 41, no. 5, pp. 1281 – 1291, September/October 2005.

Liu, H., Liu, G., Shen, Y. (2006) “A novel harmonics detection method based on wavelet algorithm for active power filter,” in *Proceedings of the 6th World Congress on Intelligent Control and Automation*, Dalian, China, June 21 – 23, pp. 7617 – 7621.

Liu, J., Wang, X., Yuan, C., Wang, Z. (2007) “On the control of active power filters,” in *Proceedings of the 7th International Conference on Power Electronics (ICPE’07)*, Daegu, Korea, October 22–26, pp. 33 – 42.

Loh, P. C., Holmes, D. G. (2005) “Analysis of multiloop control strategies for LC/CL/LCL-filtered voltage-source and current-source inverters,” *IEEE Transactions on Industry Applications*, vol. 41, no. 2, pp. 644 – 654, March/April 2005.

Malesani, L., Mattavelli, P., Tomasin, P. (1996) “High-performance hysteresis modulation technique for active filters,” in *Proceedings of the 11th Annual Applied Power Electronics Conference and Exposition (APEC’96)*, San Jose, CA, USA, March 3 – 7, vol. 2, pp. 939 – 946.

Malesani, L., Mattavelli, P., Buso, S., ”Dead-beat current control for active filters,” in *Proceedings of the 24th Annual Conference of the IEEE Industrial Electronics Society (IECON ’98)*, Aachen, Germany, August 31 – September 4, 1998, vol. 3, pp. 1859 – 1864.

Malesani, L., Mattavelli, P., Buso, S. (1998) “On the applications of active filters to generic loads,” in *Proceedings of the 8th International Conference on Harmonics and Quality of Power (ICHQP’98)*, Athens, Greece, October 14 – 16, vol. 1, pp. 310 – 319.

Malesani, L., Mattavelli, P., Buso, S. (1999) “Robust dead-beat current control for PWM rectifiers and active filters,” *IEEE Transactions on Industry Applications*, vol. 35, no. 3, pp. 613 – 620, May/June 1999.

Marks, J.H., Green, T.C. (2002) “Predictive transient-following control of shunt and series active power filters,” *IEEE Transactions on Power Electronics*, vol. 17, no. 4, pp. 574 – 584, July 2002.

Marconi, L., Ronchi, F., Tilli, A. (2003) “Robust control of shunt active filter based on the internal model principle,” in *Proceedings of the 2003 American Control Conference (ACC 2003)*, Denver, CO, USA, June 4 – 6, vol. 5, pp. 3943 – 3948.

Mattavelli, P. (2001) “A closed-loop selective harmonic compensation for active filters,” *IEEE Transactions on Industry Applications*, vol. 37, no. 1, pp. 81 – 89, January 2001.

Mattavelli, P., Marafão, F.P. (2004) “Repetitive-based control for selective harmonic compensation in active power filters,” *IEEE Transactions on Industrial Electronics*, vol. 51, no. 5, pp. 1018 – 1024, October 2004.

Maza Ortega, J.M., Perales Esteve, M., Burgos Payán, M., Gómez Expósito, A., García Franquelo, L. (2005) “Reference current computation methods for active power filters: accuracy assessment in the frequency domain,” *IEEE Transactions on Power Electronics*, vol. 20, no. 2, pp. 446 – 456, March 2005.

Mendalek, N., Al-Haddad, K. (2000) “Modeling and nonlinear control of shunt active power filter in the synchronous reference frame,” in *Proceedings of Ninth International Conference on Harmonics and Quality of Power*, Orlando, FL, USA, October 1 – 4, vol. 1, pp. 30 – 35.

Mendalek, N., Al-Haddad, K., Fnaiech, F., Dessaint, L.A (2002a) “Sliding mode control of 3-phase shunt active filter in the d-q frame,” in *Proceedings of the 33rd Annual Power Electronics Specialists Conference (PESC’02)*, Cairns, Australia, June 23 – 27, vol. 1, pp. 369 – 375.

Mendalek, N., Fnaiech, F., Al-Haddad, K., Dessaint, L.-A. (2002b) “A non-linear optimal predictive control of a shunt active power filter,” in *Conference Record of the 2002 IEEE Industry Applications Conference, 37th IAS Annual Meeting*, Pittsburgh, PA, USA, October 13 – 18, vol. 1, pp. 70 – 77.

Mohan, N., Undeland, T.M., Robbins, W.P. (1995) *Power electronics – converters, applications, and design*, second edition, John Wiley & Sons, New York, USA, 802 p.

Morcos, M.M., Gomez, J.C. (2002) “Flicker sources and mitigation,” *IEEE Power Engineering Review*, vol. 22, issue 11, pp. 5 – 10, November 2002.

Munduate, A., Garcerá, G., Figueres, E. (2006) “Robust control of a shunt active power filter for the medium voltage range based on a three-level neutral point clamped converter,” in *Proceedings of the 32nd Annual Conference on IEEE Industrial Electronics (IECON 2006)*, Paris France, November 7 – 10, pp. 2162 – 2167.

Nascimento, C.F., Oliveira Jr., A.A., Silva, I.N., Monteiro, J.R.B.A. (2007) "Harmonic detection based on artificial neural networks for current distortion compensation," in *Proceedings of the 2007 IEEE International Symposium on Industrial Electronics*, Vigo, Spain, June 4 – 7, pp. 2864 – 2869.

Newman, M.J., Zmood, D.N., Holmes, D.G. (2002) "Stationary frame harmonic reference generation for active filter systems," *IEEE Transactions on Industry Applications*, vol. 38, no. 6, pp. 1591 – 1599, November/December 2002.

Nishida, K., Konishi, Y., Nakaoka, M. (2002) "Current control implementation with deadbeat algorithm for three-phase current-source active power filter," *IEE Proceedings Electric Power Applications*, vol. 149, no. 4, pp. 275 – 282, July 2002.

Nishida, K., Rukonuzzaman, M., Nakaoka, M. (2005) "Digital control three-phase shunt active power filter with a new harmonic-current-extraction process," *IEE Proceedings Generation, Transmission & Distribution*, vol. 152, no. 4, pp. 529 – 538, July 2005.

Novotny, D.W, Lipo, T.A. (1996) *Vector control and dynamics of ac drives*, Oxford University Press, Oxford, UK, 440 p.

Ollila, J. (1993) *Analysis of PWM-converters using space vector theory – application to a voltage source rectifier*. Doctoral dissertation. Tampere University of Technology, Tampere, Finland, 179 p.

Ortúraz, M.E., Carmi, R.E., Dixon, J.W., Morán, L. (2006) "Voltage-source active power filter based on multilevel converter and ultracapacitor dc link," *IEEE Transactions on Industrial Electronics*, vol. 53, no. 2, pp. 477 – 485, April 2006.

Oum, J.H., Lim, Y.-C., Jung, Y.-G. (2007) "Z-source active power filter with a fuel cells source," in *Proc. 7th International conference on power electronics (ICPE'07)*, Daegu, Korea, October 22–26, pp. 467 – 471.

Owen, E.L. (1998) "A history of harmonics in power systems," *IEEE Industry Applications Magazine*, vol. 4, no. 1, pp. 6 – 12, January/February 1998.

Ozpineci, B., Tolbert, L.M. (2003) "Characterization of SiC Schottky diodes at different temperatures," *IEEE Power Electronics Letters*, vol. 1 no. 2, pp. 54 – 57, June 2003.

Ozpineci, B., Chinthavali, M., Tolbert, L.M., Kashyap, A., Mantooth, H.A. (2006) "A 55 kW three-phase inverter with Si IGBTs and SiC Schottky diodes," in *Proceedings of the 21st Annual IEEE Applied Power Electronics Conference and Exposition (APEC'06)*, Dallas, TX, USA, March 19 – 23, 7 p.

Pan, Z., Peng, F.Z., Wang, S. (2005) "Power factor correction using a series active filter," *IEEE Transactions on Power Electronics,* vol. 20, no. 1, pp. 148 – 153, January 2005.

Park, R.H. (1929) "Two-reaction theory of synchronous machines - generalized method of analysis, part I," *AIEE Transactions*, vol. 48, pp. 716 – 730, July 1929.

Parkatti, P., Routimo, M., Tuusa, H. (2007) "Modification of a commercial frequency converter to an active power filter in 690 V power system," in *Proceedings of the International Exhibition & Conference for Power Electronics, Intelligent Motion and Power Quality, PCIM 2007 Europe*, Nuremberg, Germany, May 22 – 24, 2007, 6 p.

Pecharanin, N., Sone, M., Mitsui, H. (1994) "An application of neural network for harmonic detection in active filter," in *Proceedings of IEEE International Conference on Neural Networks (ICNN '94)/IEEE World Congress on Computational Intelligence*, Orlando, FL, USA, June 28 – July 2, vol. 6, pp. 3756 – 3760.

Pfaff, G., Weschta, A., Wick, A.F. (1984) "Design and experimental results of a brushless ac servo drive," *IEEE Transactions on Industry Applications*, vol. IA-20, no. 4, pp 814 – 821, July/August 1984.

Pires, V.F., Silva, J.F. (2006) "A current source active power filter controlled by a sliding mode approach," in *Proceedings of the 12th International Power Electronics and Motion Control Conference (EPE-PEMC 2006)*, Portorož, Slovenia, August 30 – September 1, pp. 1654 – 1659.

Qiao, C., Jin, T., Smedley, K.M. (2001) "Unified constant-frequency integration control of three-phase active-power-filter with vector operation," in *Proc. IEEE 32nd Annual Power Electronics Specialists Conference (PESC'01)*. Vancouver, Canada, June 17 – 21, pp. 1608 – 1614.

Qiao, C., Smedley, K.M. (2002) "Three-phase bipolar mode active power filters," *IEEE Transactions on Industry Applications*, vol. 38, no. 1, pp. 149 – 158, January/February 2002.

Radulovic, Z., Sabanovic, A. (1994) "Active filter control using a sliding mode approach," in *Proceedings of the 25 Annual IEEE Power Electronics Specialists Conference (PESC '94)*, Taipei, Taiwan, June 20 – 25, vol. 1, pp. 177 – 182.

le Roux, W., van Wyk, J.D. (2000) "The effect of signal measurement and processing delay on the compensation of harmonics by PWM converters," *Transactions on Industrial Electronics*, vol. 47, no. 2, pp. 297 – 304, April 2000.

le Roux, W., van Wyk, J.D. (2001) "Modeling of distortion compensation ineffectivity in filters for nonactive power," *IEEE Transactions on Industrial Electronics*, vol. 48, no. 1, pp. 91 – 100, February 2001.

Routimo, M. (2002) *Microcontroller based control of a voltage-source active power filter (Jännitevälipiirillisen aktiivisuodattimen mikrokontrolleripohjainen säätö)*. Master of Science thesis, Department of Electrical Engineering, Tampere University of Technology, Tampere, Finland, 89 p. (in Finnish)

Routimo, M. (2005) *Improving the current compensation of a digitally controlled active power filter (Digitaalisesti säädetyn rinnakkaisaktiivisuotimen virtakompensoin-nin parantaminen)*. Thesis for the degree of Licentiate of Technology, Department of Electrical Engineering, Tampere University of Technology, Tampere, Finland, 112 p. (in Finnish)

Salo, M. (2002) *Microcontroller based control of current-source PWM converter applications*. Doctoral dissertation. Tampere University of Technology, Tampere, Finland, 150 p.

Salo, M., Tuusa, H. (2003) "A novel open-loop control method for a current-source active power filter," *IEEE Transactions on Industrial Electronics*, vol. 50, no. 2, pp. 313 – 321, April 2003.

Sasaki, H., Machida, T. (1971) "A new method to eliminate ac harmonic currents by magnetic flux compensation – considerations on basic design," *IEEE Transactions on Power Apparatus and Systems*, vol. PAS-90, no. 5, pp. 2009 – 2019, September 1971.

Sasaki, H., Machida, T. (1974) "Transient analysis of harmonic current elimination method by magnetic flux compensation," *IEEE Transactions on Power Apparatus and Systems*, vol. PAS-93, no. 2, pp. 669 – 675, March 1974.

Saetieo, S., Devaraj, R., Torrey, D.A. (1995) "The design and implementation of a three-phase active power filter based on sliding mode control," *IEEE Transactions on Industry Applications*, vol. 31, no. 5, pp. 993 – 1000, September/October 1995.

Serpa, L. A., Kolar, J. W., Ponnaluri, S., Barbosa, P. M. (2005) "A modified direct power control strategy allowing the connection of three-phase inverter to the grid through LCL filters," in *Conference Record of the 2005 IEEE Industry Applications Conference, 40th IAS Annual Meeting*, Hong Kong, October 2 – 6, 2005, vol. 1, pp. 565 – 571.

Shen, Z.J., Omura, I. (2007) "Power semiconductor devices for hybrid, electric, and fuel cell vehicles," *Proceedings of the IEEE*, vol. 95, no. 4, pp. 778 – 789, April 2007.

Smedely, K.M., Ćuk, S. (1995) "Once-cycle control of switching converters," *IEEE Transactions on Power Electronics*, vol. 10, no. 6, pp. 625 – 633, November 1995.

Smedley, K.M., Zhou, L., Qiao, C. (2001) "Unified constant-frequency integration control of active power filters – steady-state and dynamics," *IEEE Transactions on Power Electronics*, vol. 16, no. 3, pp. 428 – 436, May 2001.

Sozanski, K.P. (2004) "Non-causal current predictor for active power filter," in *Nineteenth Annual IEEE Applied Power Electronics Conference and Exposition (APEC'04)*, Anaheim, CA, USA, February 22 – 26, vol. 3, pp. 1470 – 1474.

Sozanski, K., Jarnut, M. (2005) "Three-phase active power filter using the sliding DFT control algorithm," in *Proceedings of the 11th European Conference on Power Electronics and Applications (EPE 2005)*, Dresden, Germany, September 11 – 14, 10 p.

Srianthumrong, S., Akagi, H. (2003) "A medium-voltage transformerless ac/dc power conversion system consisting of a diode rectifier and a shunt hybrid filter," *IEEE Transactions on Industry Applications*, vol. 39, no. 3, pp. 874 – 882, May/June 2003.

Stones, J., Collinson, A. (2001) "Power quality," *Power Engineering Journal (IEE)*, vol. 15, no. 2, pp. 58 – 64, April 2001.

Van de Sype, D.M., De Gussemé, K., Vand den Bossche, A.P., Melkebeek, J.A. (2004) "Small-signal Laplace-domain analysis of uniformly-sampled pulse-width modulators," in *Proceedings of the IEEE 35th Annual Power Electronics Specialists Conference*, *PESC'04*, Aachen, Germany, June 20 – 25, vol. 6, pp. 4292 – 4298.

Takeda, M., Ikeda, K., Tominaga, Y., (1987) "Harmonic current compensation with active filter," in *Conference records of the IEEE-IAS Annual Meeting*, Atlanta, GA, USA, October, pp. 808 – 815.

Takeda, M., Ikeda, K., Teramoto, A., Aritsuka, T. (1988) "Harmonic current and reactive power compensation with an active filter," in *Proceedings of the 19th Annual IEEE Power Electronics Specialists Conference (PESC'88)*, Kyoto, Japan, April 11 – 14, vol. 1, pp. 1174 – 1179.

Tangtheerajaroonwong, W., Hatada, T., Akagi, H. (2007) "A transformerless hybrid active filter using a three-level diode-clamped PWM converter," in *Proceedings of the Fourth Power Conversion Conference (PCC '07)*, Nagoya, Japan, April 2 – 5, pp. 667 – 673.

Tarkiainen, A. (2005) *Power quality improving with virtual flux-based voltage source line converter*, Doctoral dissertation. Lappeenranta University of Technology, Lappeenranta, Finland, 140 p.

Timbus, A., Teodorescu, R., Blaabjerg, F., Liserre, M., (2005) "Synchronization Methods for Three Phase Distributed Power Generation Systems. An Overview and Evaluation," in *Proceedings of the 36th Annual Power Electronics Specialists Conference (PESC'05)*, Recife, Brazil, June 12–16, pp. 2474 – 2481.

To, H.-P., Rahman, F., Grantham, C. (2005) "Time delay compensation for a current-source active power filter using state-feedback controller," in *Conference Record of the 2005 IEEE Industry Applications Conference, 40th IAS Annual Meeting*, Hong Kong, October 2 – 6, vol. 2, pp. 1213 – 1219.

Tong, L., Qian, Z., Kuang, N., Lingxiao, X., Peng, F.Z. (2007) "Optimal design of synchronous reference frame harmonic detection method," in *Proceedings of the 38th Annual Power Electronics Specialists Conference (PESC'07)*, Orlando, FL, USA, June 17–22, vol. 1, pp. 1071 – 1076.

Twining, E., Holmes, D. G. (2003) "Grid current regulation of a three-phase voltage source inverter with an LCL input filter," *IEEE Transactions on Power Electronics*, vol. 18, no. 3, pp. 888 – 895, May 2003.

Vas, P. (1992) *Electrical machines and drives: a space-vector theory approach*, Oxford University Press, Oxford, UK, 808 p.

Vas, P. (1998) *Sensorless vector and direct torque control*, Oxford University Press, Oxford, UK, 729 p.

Viitanen, T. (2005) *Space vector modulation of boost-type three-phase, three-switch and three-level unidirectional PWM rectifier – analysis and implementation*. Doctoral dissertation. Tampere University of Technology, Tampere, Finland, 150 p.

Väliviita, S., Ovaska, S.J. (1998) "Delayless method to generate current reference for active filters," *IEEE Transactions on Industrial Electronics*, vol. 45, no. 4, pp. 559 – 567, August 1998.

Wang, X., Liu, J., Hu, J., Meng, Y., Yuan, C. (2007) "Frequency characteristics of the d-q synchronous-frame current reference generation methods for active power filter," in *Proc. 7th International conference on power electronics (ICPE'07)*, Daegu, Korea, October 22–26, pp. 945 – 950.

Williams, S.M., Hoft, R.G. (1991) "Adaptive frequency domain control of PWM switched power line conditioner," *IEEE Transactions on Power Electronics*, vol. 6, no. 4, pp. 665 – 670. October 1991.

Wu, J.-C. (1995) "A new UPS scheme provides harmonic suppression and input power factor correction," *IEEE Transactions on Industrial Electronics*, vol. 42 no. 6, pp. 629 – 635, December 1995.

Wu, L., Zhuo, F., Zhang, P., Li, H., Wang, Z. (2007) "Study on the influence of supply-voltage fluctuation on shunt active power filter," *IEEE Transactions on Power Delivery*, vol. 22, no. 3, pp. 1743 – 1749, July 2007.

Wu, L., Zhuo, F., Li, H., Wang, Z. (2007) "Stability analysis and controller design of hybrid compensation system with parallel active power filter and parallel capacitors," in *Proceedings of the 38th Annual Power Electronics Specialists Conference (PESC'07)*, Orlando, FL, USA, June 17–22, pp. 1105 – 1111.

Xiao, C., Chen, G., Odendaal, W.G.H. (2007) "Overview of power loss measurement techniques in power electronic systems," *IEEE Transactions on Industry Applications*, vol. 43, no. 3, pp. 657 – 664, May/June 2007.

Xie, B., Dai, K., Xiang, D., Fang, X., Kang, Y. (2006) "Application of moving average algorithm for shunt active power filter," in *Proceedings of the IEEE International Conference on Industrial Technology (ICIT 2006)*. Mumbai, India, December 15–17, pp. 1043 – 1047.

Xu, Y., Tolbert, L.M., Kueck, J.D. (2007) "Voltage and current unbalance compensation using a parallel active filter," in *Proceedings of the 38th Annual Power Electronics Specialists Conference (PESC'07)*, Orlando, FL, USA, June 17–22, pp. 2919 – 2925.

Yunus, H. I., Bass, R. M. (1996) "Comparison of VSI and CSI topologies for single-phase active power filters," in *Proceedings of the 27th Annual Power Electronics Specialists Conference (PESC'96)*, Baveno, Italy, June 23–27, vol. 2, pp. 1892 – 1898.

Zhang, Z., Fahmi, N.R., Norris, W.T. (2001) "Flicker analysis and methods for electric arc furnace flicker (EAF) mitigation (a survey)," in *Proceedings of the 2001 IEEE Porto Power Tech Conference*, Porto, Portugal, September, 10 – 13, vol. 1, 6 p.

Zolper, J.C. (2005) "Emerging silicon carbide power electronics components," *Proceedings of the 20th Annual IEEE Applied Power Electronics Conference and Exposition (APEC'05)*, Austin, TX, USA, March 6 – 10, vol. 1, pp. 11 – 17.

Åström, K.J., Wittenmark, B. (1997) *Computer-controlled systems: theory and design*, third edition, Prentice Hall, Upper Saddle River, NJ, USA, 557 p.

Åström, K.J., Hägglund, T. (2006) *Advanced PID control*, ISA – Instrumentation, Systems, and Automation Society, Research Triangle Park, North Carolina, USA, 460 p.

Özkaya, H., Sentürk, O.S., Hava, A.M. (2007) "Performance enhancement and comparison of discrete time current regulators for parallel active filters," in *Proceedings of the 12th European Conference on Power Electronics and Applications (EPE 2007)*, Aalborg, Denmark, September 2 – 5, 10 p.

Standards and Technical Reports

CEI/IEC 61000-3-2:2000+A1:2001+A2:2004 (2004) *International standard: Electromagnetic compatibility – (EMC) – part 3-2: limits – limits for harmonic current emissions (equipment input current ≤ 16 A per phase)*, edition 2.2.

CEI/IEC 61000-3-4:1998 (1998) *Technical report: Electromagnetic compatibility (EMC) – part 3-4: limits – limitation of emission of harmonic currents in low-voltage power supply systems for equipment with rated current greater than 16 A*, first edition.

CEI/IEC 61000-3-12:2004 (2004) *International standard: Electromagnetic compatibility (EMC) – limits – limits for harmonic currents produced by equipment connected to low-voltage systems with input current >16 A and ≤75 A per phase*, first edition.

IEEE Std. 100-2000 (2000) *The authoritative dictionary of IEEE standard terms*, *7th edition*. The Institute of Electrical and Electronics Engineers, Inc., New York, NY, USA.

IEEE Std. 519-1992 (1993) *IEEE recommended practices and requirements for harmonic control in electrical power systems*, Institute of Electrical and Electronics Engineers, Inc., New York, NY, USA.

IEEE Std. 1453-2004, (Adoption of CEI/IEC 61000-4-15:1997+A1:2003) (2005) *IEEE Recommended Practice for Measurement and Limits of Voltage Fluctuations and Associated Light Flicker on AC Power Systems*, Institute of Electrical and Electronics Engineers, Inc., New York, NY, USA.

Appendix A

Active Filter Prototypes

The active filter prototypes used in Publications [P1] – [P7] operate at the switching frequency of 10 kHz and they were designed according to a 5 kVA rated power. In this thesis, the prototypes were used to compensate the harmonics and the fundamental reactive power of the non-linear load of 5 kVA nominal power. In Publications [P1] – [P5], and [P7], short-circuit power of the supplying network measured at the point where the test setups were connected was about 0.60 MVA. In Publication [P6] this was about 0.69 MVA.

Voltage-Source Shunt Active Filter

The PWM bridge used in Publications [P1] – [P7] was constructed with a Semikron SKM40GD123D module containing all of the IGBTs and the antiparallel-connected diodes (rated current 40 A and voltage 1200 V) of the three-phase bridge. In addition, discrete IGBTs IRG4PH40U (rated current 40 A, voltage 1200 V) and Si diodes HFA30PB120PbF (rated current 30 A, voltage 1200 V) manufactured by International Rectifier, and SiC diodes CSD202120 (rated current 20 A, voltage 1200 V) made by Cree were also used in Publication [P6]. The PWM bridge gate drivers were manufactured by Vacon PLC.

The active filter dc link consists of three electrolytic capacitors (Aerovox ALS31C) connected in series. The rated capacitance for each of them is 3300 μF (±20 %) and the maximum voltage 450 V. The filter chokes used were manufactured by Trafomik. Their rated current is 10 A (50 Hz) and they consist of three-phase inductors which were made of separate laminated iron cores with separate windings, i.e. one single-phase choke per phase. The wye-connected ac capacitors used in the LCL filter in Publication [P5] are Arcotronics MKP C.4BT polypropylene capacitors with a capacitance of 5 μF (±5 %) each and the rated voltage 700 V.

Figures A.1 – A.3 illustrate the block diagrams of the microcontroller implementations of the prototypes. The active filter control systems were implemented with a Motorola MPC555 microcontroller. The microcontroller board was designed in the Institute of Power Electronics at Tampere University of Technology. In addition to the microcontroller, the board contains auxiliary circuits such as overcurrent and overvoltage sensing and protection, a logic circuit for modulation signal generation, and measurement signal processing circuits.

The current measurements required by the control system were realized with LEM LA55-P current transducers. On the microcontroller board, the current signals produced by the current transducers are transformed to the voltage signals (0 – 5 V) and led to the AD converters. The

resolution of the measurement is about 50 mA. The dc-link voltage is obtained via the AD converter and a differential mode measurement in the microcontroller board. The resolution of the measurement is 0.82 V.

The parameters of the prototype main circuits have been collected in Tables A.1 – A.2. Figures A.4 – A.5 show the photographs of the prototypes. No photograph of the current-sensorless active power filter is given, since apart from the wiring it is similar to Fig. A.4.

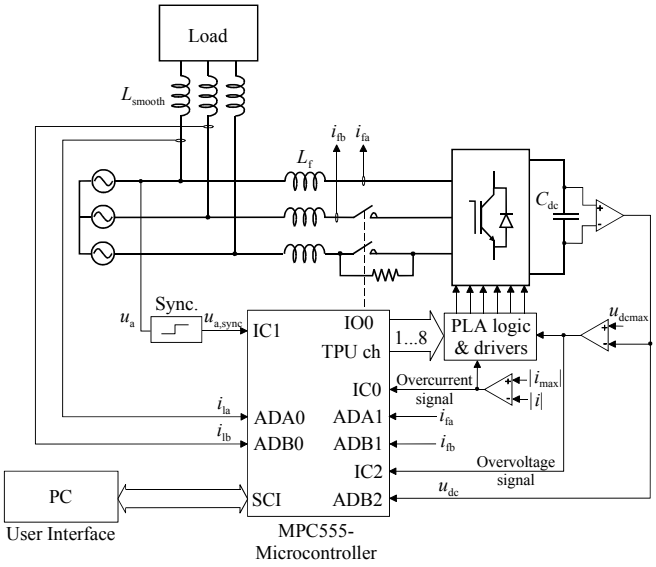

Fig. A.1. Block diagram of shunt active filter prototype implementation showing measured quantities and corresponding connections to microcontroller input ports.

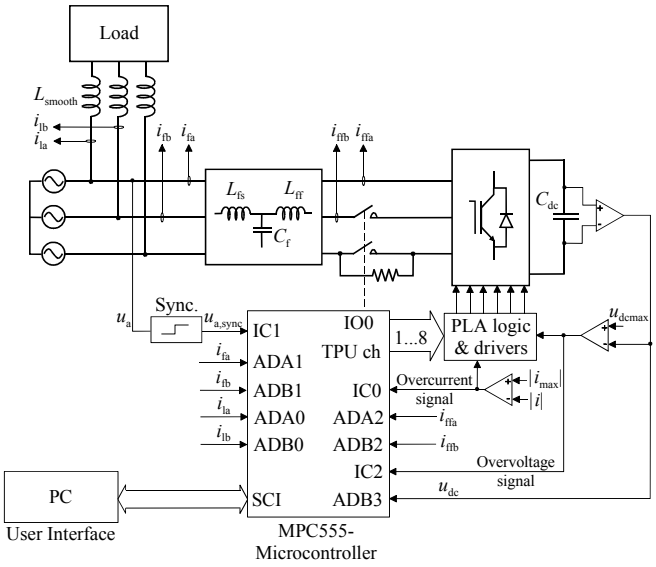

Fig. A.2. Block diagram of shunt active filter prototype implementation with LCL-type supply filter showing measured quantities and corresponding connections to microcontroller input ports.

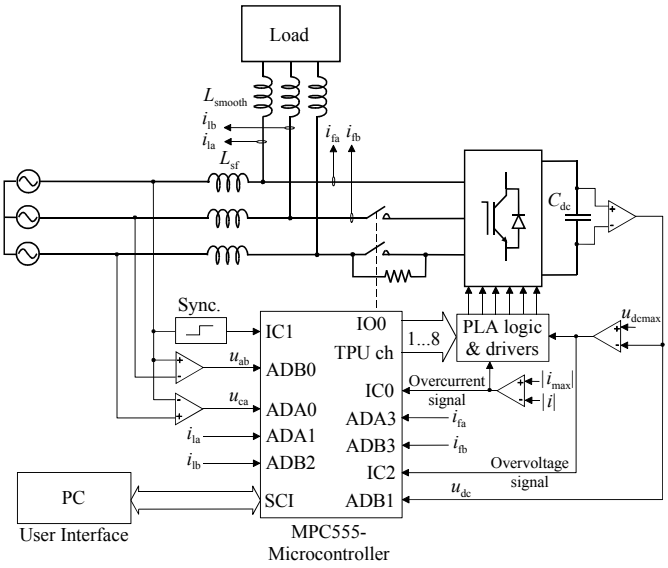

Fig. A.3. Block diagram of implementation of active filter with modified main circuit structure showing measured quantities and corresponding connections to microcontroller input ports.

Table A.1.
Main circuit parameters of the voltage-source shunt active filter

	VSAPF	
Rated power S_{nom}	5 kVA	1.00 p.u.
Mains phase voltage U_s	230 V	1.00 p.u.
Mains frequency f_s	50 Hz	1.00 p.u.
L filter inductor L_f	5 mH	0.05 p.u.
LCL filter inductor L_{fs}	0.6 mH	0.006 p.u.
LCL filter capacitor C_f	5 μF	0.05 p.u.
LCL filter inductor L_{ff}	4 mH	0.04 p.u.
Damping resistor R_d	33 Ω	1.04 p.u.
Dc-link capacitor C_{dc}	1.1 mF	11.00 p.u.
Dc-link voltage u_{dc}	725 V	
PWM carrier frequency f_{sw}	10 kHz	
Dead time t_d	~1 μs	
Inductor L_{smooth}	2.3 mH	0.023 p.u.

Table A.2.
Main circuit parameters of the modified main circuit structure

	VSAPF	
Rated power S_{nom}	5 kVA	1.00 p.u.
Mains phase voltage U_s	230 V	1.00 p.u.
Mains frequency f_s	50 Hz	1.00 p.u.
Filter inductor L_{sf}	10 mH	0.10 p.u.
Dc-link capacitor C_{dc}	1.1 mF	11.00 p.u.
Dc-link voltage u_{dc}	620 V	
PWM carrier frequency f_{sw}	10 kHz	
Dead time t_d	~1 μs	
Inductor L_{smooth}	2.3 mH	0.023 p.u.

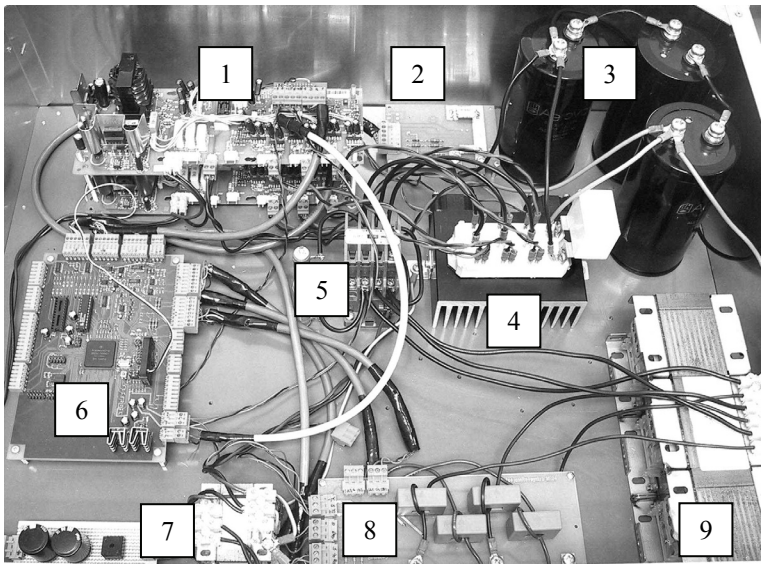

Fig. A.4. Photograph of voltage-source shunt active filter prototype with L-type supply filter. 1 gate driver boards, 2 dc-link voltage measuring board, 3 dc-link capacitors, 4 IGBT bridge, 5 charging circuit 6 microcontroller board, 7 auxiliary power circuit, 8 current transducers, 9 supply filter choke L_f.

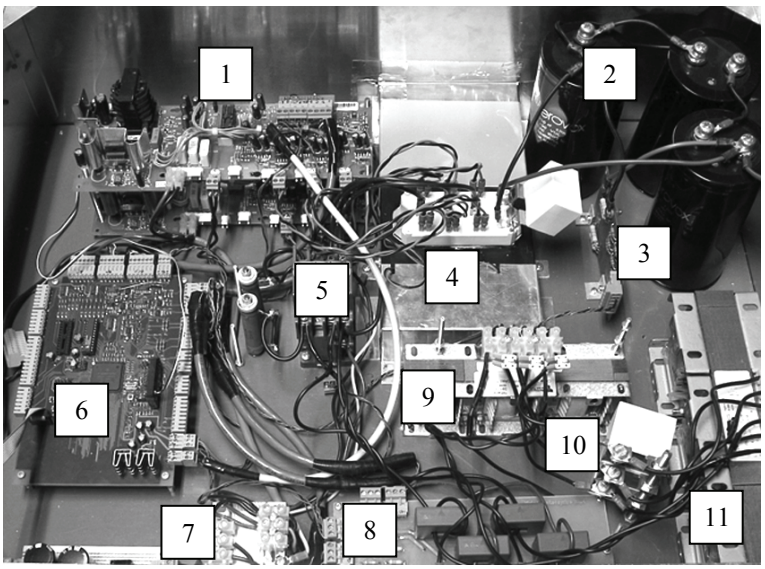

Fig. A.5. Photograph of voltage-source shunt active filter prototype with LCL-type supply filter. 1 gate driver boards, 2 dc-link capacitors, 3 dc-link voltage measuring board, 4 IGBT bridge, 5 charging circuit 6 microcontroller board, 7 auxiliary power circuit, 8 current transducers, 9 filter choke L_{fs}, 10 filter capacitors C_f, 11 filter choke L_{ff}.

Current-Source Shunt Active Filter

The control system of the current-source shunt active power filter used in Publication [P7] was implemented with a similar microcontroller board as discussed above. The PWM bridge was constructed using Semikron IGBT modules SKM50GB123D (rated current 50 A and voltage 1200 V) and serial diodes STTA9012TV2 (rated current 45 A, voltage 1200 V) made by STMicroelectronics. The gate driver boards used were designed in the Institute of Power Electronics at Tampere University of Technology.

The dc link was constructed as a series connection of one 30 mH dc inductor (10 A) and two 100 mH inductors originally designed for ac current (10 A/50 Hz). The ac filter chokes are similar to those used in the voltage-source active filter prototype. The wye-connected ac capacitors were Arcotronics MKP C.4B capacitors with a capacitance of 6.8 μF (±5 %) each and the rated voltage 600 V. A more detailed presentation of the current-source shunt active power filter prototype can be found in (Salo, 2002).

The parameters of the prototype main circuits have been collected in Table A.3. Figure A.6 shows the photographs of the prototypes.

Table A.3.
Main circuit parameters of the current-source active filter

	CSAPF	
Rated power S_{nom}	5 kVA	1.00 p.u.
Mains phase voltage U_s	230 V	1.00 p.u.
Supply frequency f_s	50 Hz	1.00 p.u.
Filter inductor L_f	0.6 mH	0.006 p.u.
Filter capacitor C_f	6.8 μF	0.068 p.u.
Dc inductor L_{dc}	230 mH	2.30 p.u.
Dc resistance of dc inductor	1.3 Ω	
Max. dc-link current i_{dc}	11 A	
PWM carrier frequency f_{sw}	10 kHz	
Overlapping time t_{ol}	~1 μs	
Inductor L_{smooth}	2.3 mH	0.023 p.u.

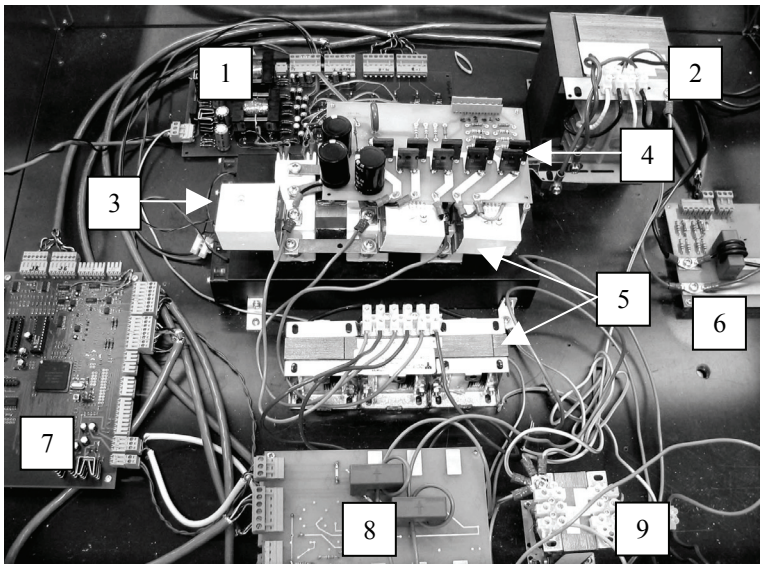

Fig. A.6. Photograph of current-source shunt active filter prototype. 1 gate driver boards, 2 part of dc-link inductor, 3 PWM bridge, 4 overvoltage clamp, 5 LC filter 6 dc current measuring board, 7 microcontroller board, 8 ac current transducers, 9 auxiliary power.

Appendix B

Control System Parameters

Table B.1.
CDC – controller parameters

	RL-type load			RC-type load		
	Current control		Voltage control	Current control		Voltage control
	d-axis	q-axis		d-axis	q-axis	
T_{cc}	50 µs	50 µs	–	50 µs	50 µs	–
T_{vc}	–	–	3750 µs	–	–	3750 µs
P	75	62,5	0,00095	50	62,5	0,00095
T_I	∞	∞	–	∞	∞	–
T_D	16.6 µs	30 µs	–	25 µs	30 µs	–
τ_c	$2T_{cc}$	$2T_{cc}$	–	$2T_{cc}$	$2T_{cc}$	–
u_{dc}^*	–	–	750 V	–	–	750 V

Table B.2.
Prediction-based method – controller parameters

	RL-type load			RC-type load		
	Current control		Voltage control	Current control		Voltage control
	d-axis	q-axis		d-axis	q-axis	
T_{cc}	50 µs	50 µs	–	50 µs	50 µs	–
T_{vc}	–	–	3750 µs	–	–	3750 µs
P	75	62,5	0,00095	62,5	62,5	0,000285
T_I	∞	∞	–	∞	∞	–
T_D	25 µs	20 µs	–	30 µs	20 µs	–
τ_c	$2T_{cc}$	$2T_{cc}$	–	$2T_{cc}$	$2T_{cc}$	–
u_{dc}^*	–	–	750 V	–	–	750 V

Table B.3.
Current-sensorless – controller parameters

	Basic version PI(e^2)	Improved version PI
u_{dc}^*	620 V	620 V
T_{vc}	1 ms	1 ms
P	0.0006	0.08
$\widetilde{P}_{min}$	0.005	–
$\widetilde{P}_{max}$	0.2	–
T_i	21.8 ms	50 ms
τ_c	–	10 ms

Table B.4.
LCL filter with active damping and prediction based method – controller parameters

	RL-type load			RC-type load		
	Current control		Voltage control	Current control		Voltage control
	d-axis	q-axis		d-axis	q-axis	
T_{cc}	50 µs	50 µs	–	50 µs	50 µs	–
T_{vc}	–	–	3750 µs	–	–	3750 µs
P_{ic}	36.6	36.6		36.6	36.6	
P	1.2	1.2	0,00095	1.2	1.2	0,000285
T_I	1 ms	1 ms	–	1 ms	1 ms	–
T_D	2.54 µs	2.54 µs	–	2.54 µs	2.54 µs	–
τ_c	$2T_{cc}$	$2T_{cc}$	–	$2T_{cc}$	$2T_{cc}$	–
u_{dc}^*	–	–	750 V	–	–	750 V

Table B.5.
LCL filter with passive damping and prediction based method – controller parameters

	RL-type load			RC-type load		
	Current control		Voltage control	Current control		Voltage control
	d-axis	q-axis		d-axis	q-axis	
T_{cc}	50 µs	50 µs	–	50 µs	50 µs	–
T_{vc}	–	–	3750 µs	–	–	3750 µs
P	30.5	30.5	0,00095	30.5	30.5	0,000285
T_I	1 ms	1 ms	–	1 ms	1 ms	–
T_D	7.5 µs	7.5 µs	–	7.5 µs	7.5 µs	–
τ_c	$2T_{cc}$	$2T_{cc}$	–	$2T_{cc}$	$2T_{cc}$	–
u_{dc}^*	–	–	750 V	–	–	750 V

Appendix C

Parameters of the Inductor Models

The frequency-dependent choke models were approximated on the basis of the measurement results presented by Halkosaari (1999). First, the inductances of the chokes used in this thesis were determined at 50 Hz. Then the measured frequency characteristics of chokes presented in (Halkosaari, 1999) were used to approximate the characteristics of the chokes used in this thesis.

The nominal inductances of the chokes used in the prototypes built were 5 mH, 4 mH, and 0.6 mH (at 50 Hz, 10 A). The measured inductance for the 5 mH choke at 50 Hz was about 4.9 mH. However, the measurements showed that the actual inductance of the 4-mH choke was also about 5 mH at 50 Hz. Thus, the same Foster model parameters were used for both of the chokes. Furthermore, the measured inductance of the choke with the rated inductance of 0.6 mH at 50 Hz was about 1 mH. The parameters of the third-order series Foster model are presented in Table C.1 and the frequency characteristics of the models are shown in Figs. C.1 – C.2.

Table C.1.
Third-order Series Foster Model Parameters

Nominal Value of the Filter Choke	Foster Model						
	L_1	L_2	L_3	R_{dc}	R_1	R_2	R_3
5 mH (50 Hz, 10 A)	0.40 mH	1.8 mH	3.0 mH	0.074 Ω	0.13 Ω	9.0 Ω	426 Ω
4 mH (50 Hz, 10 A)	0.40 mH	1.8 mH	3.0 mH	0.074 Ω	0.13 Ω	9.0 Ω	426 Ω
0.6 mH (50 Hz, 10 A)	0.18 mH	0.31 mH	0.59 mH	0.037 Ω	0.063 Ω	2.1 Ω	112 Ω

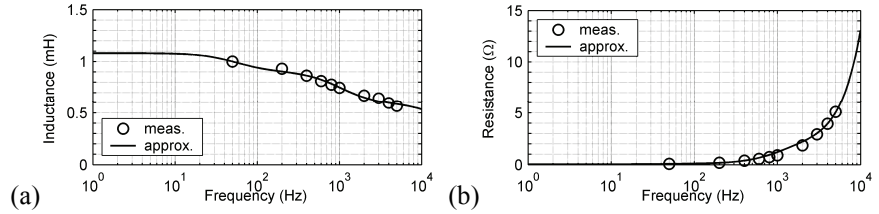

(a) (b)

Fig. C.1. Measured and approximated frequency characteristics of (a) the inductance and (b) the resistance of the choke with 0.6 mH nominal inductance.

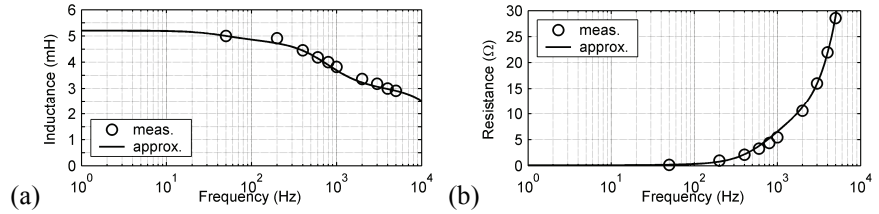

(a) (b)

Fig. C.2. Measured and approximated frequency characteristics of (a) the inductance and (b) the resistance of the chokes with 4 mH and 5 mH nominal inductances.

Appendix D

Parameters for the Hybrid Compensator

Table D.1.
Main circuit parameters for the hybrid compensator

			Hybrid compensator		
Mains	Mains phase-a voltage	U_{sa}	231.2 V		1.005 p.u.
	Mains phase-b voltage	U_{sb}	234 V		1.017 p.u.
	Mains phase-c voltage	U_{sc}	232 V		1.009 p.u.
	Mains frequency	f_s	50 Hz		1.00 p.u.
	Mains inductance	L_s	18 µH		
	Time constant	τ_s	31.83 µs		
	Mains resistance	R_s	1.2 mΩ		
Detuned filter	Rated reactive power	Q_{nom}	400 kVAr	500 kVAr	1.00 p.u.
	Capacitance	C_c	7.4 mF	9.25 mF	0.922 p.u.
	Blocking reactor	L_c	95.9 µH	76.7 µH	0.076 p.u.
	Resistance	R_c	3.8 mΩ	3.0 mΩ	0.0095 p.u.
Active filter	Rated compensating power	S_{nom}	210 kVA	400 kVA	1.00 p.u.
	LCL filter inductor	L_{fs}	33.4 µH	17.3 µH	0.014 p.u.
	Resistance of inductor L_{fs}		6.0 mΩ	4.7 mΩ	0.008 p.u.
	Damping resistor	R_{fs}	3.34 Ω	1.725 Ω	4.35 p.u.
	LCL filter inductor	L_{ff}	167 µH	86.25 µH	0.068 p.u.
	Resistance of inductor L_{ff}		13.3 mΩ	9.7 mΩ	0.017 p.u.
	LCL filter capacitor	C_f	13.2 µF	25.5 µF	0.0095 p.u.
	Switching frequency	f_{sw}	10 kHz	10 kHz	
	Dc-link voltage	u_{dc}	700 V	700 V	
	Dc-link capacitor	C_{dc}	24.7 mF	47.1 mF	5.87 p.u.

Appendix E

Base Values

In this thesis, the following base values were used:
Frequency $f_B = 50$ Hz
Angular frequency $\omega_B = 2\pi f_B \approx 314.2$ rad/s
Voltage $U_B = 230$ V

The base values for impedance, resistance, inductance, and capacitance wree calculated depending on the rated power P_B as $R_B = 3U_B^2/P_B$, $Z_B = 3U_B^2/P_B$, $L_B = Z_B/\omega_B$, and $C_B = 1/(\omega_B Z_B)$, respectively. For the rated powers used in this thesis, the base values are shown in Table A1.1. Rated power of 5 kVA was used in prototypes presented in Publications [P1] – [P7], while in Publication [P8] the rated power of the compensator is 210 kVA, 400 kVA, or 500 kVA.

Table E.1.
Base values

Rated power	P_B	5 kVA	210 kVA	400 kVA	500 kVA
Current	I_B	7.25 A	304.34 A	579.7 A	724.6 A
Impedance and resistance	$Z_B = R_B$	31.74 Ω	755.7 mΩ	396.8 mΩ	0.3174 Ω
Inductance	L_B	101.0 mH	2.406 mH	1.263 mH	1.010 mH
Capacitance	C_B	100.3 µF	4.212 mF	8.023 mF	10.03 mF

Publications

Publication [P1]

Routimo, M., Salo, M., and Tuusa, H.

A control delay compensation method for voltage source active power filter

Proceedings of the Ninth European Power Quality Conference, PCIM 2003 Europe, Nürnberg, Germany, May 20 – 22, 2003, pp. 93 – 97.

Publication [P2]

Routimo, M., Salo, M., and Tuusa, H.

A novel simple prediction based current reference generation method for an active power filter

Proceedings of the IEEE 35th Annual Power Electronics Specialists Conference, PESC,'04, Aachen, Germany, June 20 – 25, 2004, vol. 4, pp. 3215– 3220.

Errata:

i Page 3220, Section IV.A Efficiency: The efficiency of the voltage-source shunt active power filter compensating RL- and RC-type loads has been estimated by assuming symmetrical three-phase system and measuring the average power only in the a-phase. Since even a slight asymmetry of the supply voltages causes unsymmetrical distribution of the powers between the phases, especially in the case of the RC-type load, the active filter efficiencies presented are incorrect. Thus, the section IV.A should be ignored.

Publication [P3]

Routimo, M., Salo, M., and Tuusa, H.

Voltage-source active power filter with a current sensorless control

International Review of Electrical Engineering

IREE by Praise Worthy Prize, vol. 2, no. 3, May-June 2007, pp. 346 – 358.

Errata:

i Page 357, Section VII. Conclusions, last paragraph, first sentence:
There is: "…are lower than the losses in the convention shunt active filters…"
Should be: "…are lower than the losses in the conventional shunt active filters…"

Publication [P4]

Routimo, M., Salo, M., and Tuusa, H.

Control method to improve the transient performance of a current sensorless active power filter

Proceedings of the Nordic Workshop on Power and Industrial Electronics, Norpie'06, Lund, Sweden, June 12 – 14, 2006, 6 p.

Publication [P5]

Routimo, M. and Tuusa, H.

LCL type supply filter for active power filter – comparison of an active and passive method for the resonance damping

Proceedings of the IEEE 38th Annual Power Electronics Specialists Conference, PESC'07, Orlando, FL, USA, June 17 – 21, 2007, pp. 2939 – 2945.

Errata:

i Page 2940, Fig. 1(a): An arrow on the right side of the block "PLL" should point to right, to the block "abc/dq", not to left as shown if the figure.

ii Page 2941, left column, below Eq (7):
There is: "…we can write the equations according to Figs. 1a and b."
Should be: "…we can write the following equations according to Figs. 1a and b."

iii Page 2941, Fig. 4(b):
There is: "Signal"
Should be: "Signal filters"

iv Page 2943, Section III.B. Control System, last paragraph:
There is: "However, the overall performance of the simulated system is in agreement with the simulations."
Should be: "However, the overall performance of the simulated system is in agreement with the measurements."

Publication [P6]

Routimo, M. and Tuusa, H.

Effect of SiC diodes on power losses of the voltage-source shunt active power filter

International Review of Electrical Engineering

IREE by Praise Worthy Prize, vol. 2, no. 6, November-December 2007, pp. 803 – 813

Publication [P7]

Routimo, M., Salo, M., and Tuusa, H.

Comparison of voltage-source and current-source shunt active power filters

IEEE Transactions on Power Electronics

TPEL, vol. 22, no. 2, March 2007, pp. 636 – 643.

Publication [P8]

Routimo, M., Mäkinen, A., Salo, M., Seesvuori, R., Kiviranta, J., and Tuusa, H.

Flicker mitigation with a hybrid compensator

IEEE Transactions on Industry Applications

TIA, vol. 44, no. 4, July-August 2008, pp. 1227 – 1238.

Errata:

i Page 1232, Fig. 8(c) and (d): There is confusion in Figure 8. Figure labelled as Fig. 8(d) should be labelled as Fig. 8(c), and vice versa. The figure captions are correct.